Retrieval of Surface Microwave Emissivity Using Multisensor Satellite Measurements

Hala Khalid Al-Jassar

A thesis submitted in fulfillment of the requirements
for the degree of PhD

Mullard Space Science Laboratory
Department of Space and Climate Physics
University College London

June 1995

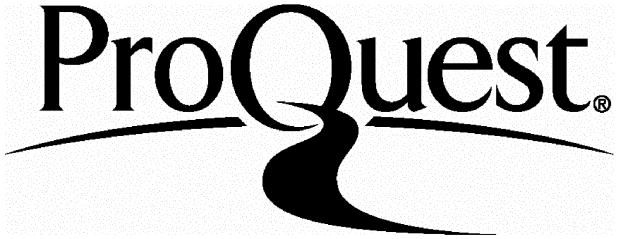

Abstract

This thesis concerns the development and validation of a technique to measure the microwave emissivity of the Earth's surface from space. The dependence of microwave emissivity upon various surface geophysical parameters is discussed. The role of these geophysical parameters in the global climate system together with the importance of satellite remote sensing are also discussed. The physics of microwave emission and the models used to predict the microwave emission of the Earth's surface are described, including the assumptions made and constraints that apply. The atmospheric contribution to the microwave signal from space is investigated and found to be a major source of errors.

A new technique is developed to correct the apparent microwave emissivity as seen by the radiometer from space for both atmospheric absorption and direct and reflected emission due to water vapour using radiometer data in both the microwave and infrared regions. Validation study of this new technique over the ocean surface is performed using simultaneous data from the Along Track Scanning Radiometer (ATSR) and the Microwave sounder (ATSR/M). The technique is applied to the soil moisture retrieval from space by performing a case study over the Simpson Desert in Australia using near-contemporaneous data from the Advanced Very High Resolution Radiometer (AVHRR) and TOPEX microwave sounder. Results obtained from the satellite data are compared with contemporaneous ground data. Analysis of errors and error sources is discussed. Constraints on the accuracy of emissivity measurement are set out and recommendations are suggested for future application.

Contents

Figures

Tables

Acknowledgements

Many people deserve thanks for the help and support they have provided during the coarse of this research. Firstly, I am grateful to my supervisor Professor Chris Rapley for his encouragement, guidance, morale support, and for his concerns and helpful comments even after his departure and his leadership of the IGBP. I thank Dr. Andy Harris for devising the concept of correction based on my original simulation study and for the very interesting discussions and expertise regarding the atmospheric problem to satellite data in general. Dr. Jeff Ridley deserves particular thanks for providing an invaluable source of criticism, encouragement, and expertise in microwave emission theory and I am very grateful for his sustained interest in my research. I am also indebted to Dr. Fiona Strawbridge, who helped supervise my research during the first two years, and for the concerns and helpful comments even after her departure from MSSL. I thank Dr. Ian Mason for his helpful comments and encouragement. Thanks also to other members of the MSSL for providing a stimulating environment to work in.

I must also acknowledge the contributions of several outside institutions towards the work presented in this thesis.

I acknowledge the following for providing satellite microwave data: Dr. Laurence Eymard from CETP in France for providing ATSR/M data, CNES for TOPEX/TMR data. I also acknowledge the following for providing satellite infrared data: RAL in UK for ATSR and CSIRO in Australia for AVHRR data. RAL provided the atmospheric infrared radiative transfer model used in this study.

I thank Dr. AbdulKarim Henaidi (Director of Climate and Scientific Documentation Centre) from MEPA in Saudi Arabia for providing the radiosonde data. I also acknowledge NOAA in USA, and Alice Springs meteorological station in Australia for providing the radiosonde data.

Last but not least, thanks to Kuwait University who provided the funding for me.

The work presented in this thesis is my own, unaided work, except where otherwise acknowledged.

TO MY FAMILY,
WHOSE LOVE AND SUPPORT HAS ALWAYS KEPT ME GOING

Chapter 1

Climate and Satellite Remote Sensing

In recent years, international concern has arisen regarding the impact of human activities, principally the increase in carbon dioxide (CO_2) and other greenhouse gases on global temperatures. Other human activities have caused desertification and deforestation which affect climate by changing the albedo (reflectivity) of land. An increase in sulphate aerosols as a consequence of fossil fuel combustion, can modify cloud characteristics which in turn may influence the climate. Depletion of ozone in the stratosphere due to Chlorofluorocarbons (CFCs) may also influence the climate.

Thus human activities may cause significant changes to the climate system, and consequently international programs such as the World Climate Research Programme (WCRP) and the International Geosphere-Biosphere Programme (IGBP) were established to study the likely consequences. The WCRP and IGBP are two of the largest co-ordinated scientific enterprises man has tackled this century. The objectives of the WCRP are to determine: (a) to what extent the climate can be predicted and (b) the extent of man's influence on climate. Three streams of research in the WCRP have been identified, namely (1) long-range weather predictions over periods of several weeks, (2) interannual variability of the global atmosphere and the tropical oceans over periods of several years, (3) longer-term variations. The IGBP is a major project that is attempting to integrate a wide variety of disciplines and areas of study within a global environmental research programme. Particular emphasis is placed on the need for development of an adequate global data and information system (Barrett and Curtis, 1992). The IGBP and WCRP each have a number of ongoing research programmes (IPCC, 1990). For these, modelling efforts and global observations, especially from satellites, of all components of the climate system are required (Houghton and Morel, 1984).

1.1 The Earth's Climate

A simple definition of climate is an average of appropriate components of the weather over a period from a few years to a few centuries (IPCC, 1990). For example, a description of the climate over any period involves the average of appropriate components of the weather over that period, together with the statistical variations of those components. Historically, fluctuations of climate have occurred over many time scales due to natural processes. In recent years, much concern has been caused by the change in climate due to human activities.

Commonly, the variables which are used to determine climate fluctuations are concerned mainly with the atmosphere. Actually, processes in the atmosphere are strongly coupled to the land surface, ocean, cryosphere, and biosphere. These components together form the climate system.

1.1.1 The Climate System

The climate system is complex and consists of many components. These components are the following, see figure 1.1:

- Atmosphere

  This is the most variable component. The lower atmosphere possesses a characteristic thermal response time to imposed changes of hours up to about one month.

- Oceans

  The oceans represent a large heat reservoir as they absorb most of the incident solar radiation. The upper layers of the oceans interact with the overlaying atmosphere or ice on time scales of months to years while the deeper oceans have thermal adjustment times of the order of centuries.

- Cryosphere

  The cryosphere consists of continental ice, mountain glaciers, surface snow and sea ice. Sea ice and snow show large seasonal variations from days to years while land ice change is much slower, between 100 to 10000 years.

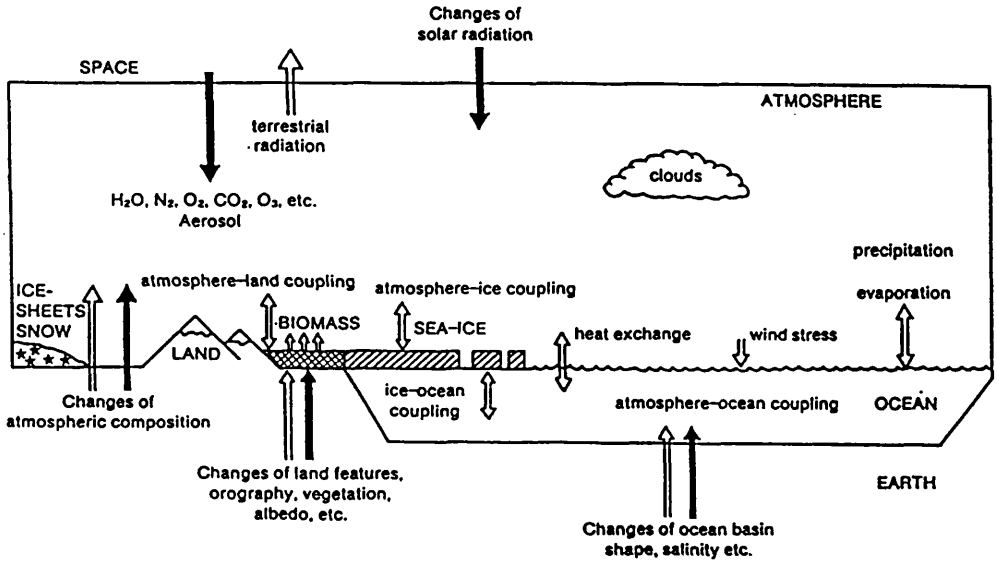

Figure 1.1 Schematic illustration showing the components of the climate system (coupled atmosphere-ocean-ice-land) (from Houghton and Morel, 1984)

- Geosphere

  The land surface consists of the lakes, rivers, soil (i.e. soil moisture), and ground water. All of these are of importance to the hydrological cycle. The time for changes varies from days up to months.

- Biosphere

  The vegetation and other living systems on the land and in the ocean control the magnitude of the fluxes of several greenhouse gases including CO_2 and methane. The biosphere reacts on time scales of hours (e.g. plankton growth) up to centuries (tree-growth).

The various components of the climate system interact principally through:

- Exchange of heat. This occurs through different physical processes including absorption and emission of radiation, convection and conduction, and exchange of latent heat via evaporation and condensation.

- Exchanges of water and minor chemical constituents (e.g. CO_2) between land, ice or ocean surface which occur continuously.

1.1.2 Factors Affecting Climate

About one third of the incoming solar energy is reflected by the Earth, the rest being absorbed by different Earth components (e.g. atmosphere, ocean, ice, land). When the earth is in thermal equilibrium, the energy received by the Earth from the sun (in short wavelengths) is balanced by outgoing radiation at thermal (long wavelengths). The effective temperature of the Earth is chiefly determined by the amount of outgoing terrestrial radiation into space and is described by Stefan-Boltzmann law (see chapter 2). The effective temperature of the Earth 253 K, while the actual averaged surface temperature is 288 K. One of the most important factors which affect the outgoing thermal energy from earth to space is the greenhouse effect. Naturally, greenhouse gases are necessary to keep the Earth's warm. Figure 1.2 shows the fundamental process which the global climate system is heated by incoming short-wave solar radiation and cooled by long-wave infrared radiation into space. But by adding more of these gases (e.g. CO_2 , CFCs), mankind is capable of raising the global-averaged annual mean surface-air temperature. This is known as global warming.

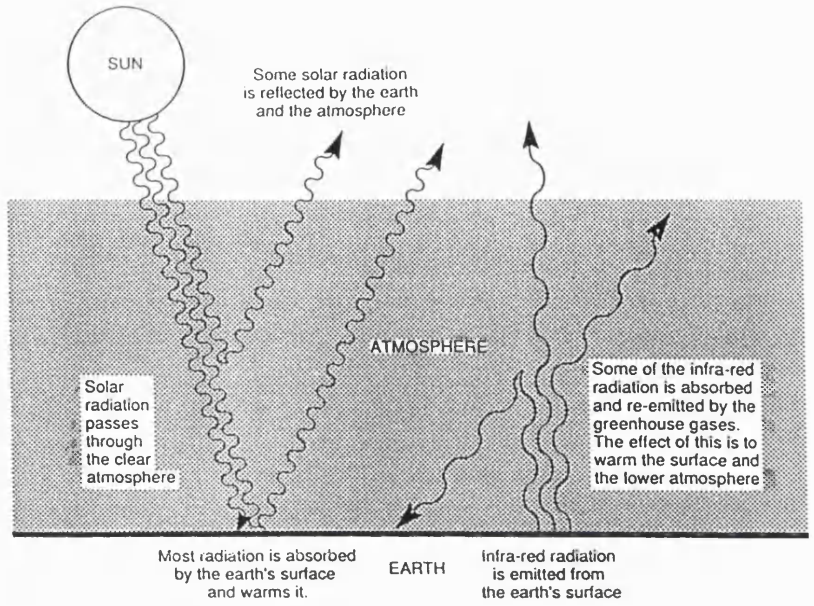

Figure 1.2 A simplified diagram illustrating the greenhouse effect (IPCC 1990)

There are several other factors which can change the balance between the energy absorbed and that emitted, some of which have been mentioned above. These factors include natural and human activities and are known as climate forcing agents. The most obvious natural forcing agent is the change in the output energy from the sun on long (~100,000 years) and short (~ the 22 years solar cycle) time scales. Aerosols in the atmosphere can also affect climate because they can reflect solar radiation and absorb thermal radiation. Aerosols are released either naturally (e.g. volcanic eruptions) or by human activities (e.g. burning fossil fuel). Also, any change in the albedo (reflectivity) of land due to desertification or deforestation and urbanisation will affect the amount of solar energy absorbed.

1.1.3 Climate Feedbacks

As components of the Earth's system start to warm, factors called positive and negative feedbacks can play an important role in determining the degree of global warming. Positive feedbacks can amplify the warming, while negative feedbacks can reduce the warming but can not produce global cooling. Important examples are (e.g. Houghton and Morel 1984; IPCC 1990):

1. Ice-albedo positive feedback. As the global warming occurs, ice melts. As ice reflects away nearly all solar radiation incident on it, any decrease in ice cover will lead to greater absorption of solar radiation as a result of the less reflective planet. The resultant warming of the surface will lead to further melting.

2. Water-vapour-radiation positive feedback. An increase in atmospheric temperature will lead to an increase in water vapour emission. The increased water vapour will act as a radiation blanket over the surface because of its opacity to thermal infrared energy. Thus result with a further increase of the surface temperature.

3. Cloud-radiation positive and negative feedbacks. The feedbacks related to clouds are extremely complex (e.g. IPCC, 1990; IPCC, 1992) and a full demonstration of cloud feedback is beyond the scope of this thesis. In summary, clouds may contribute to the greenhouse warming of the climate system, but also to cooling through the reflection and reduction in solar radiation due to their high albedo. For example when global warming occurs, clouds may be displaced to higher altitudes. As higher clouds are colder than lower clouds, they will emit less radiation and so they serve to enhance the greenhouse effect. Clouds in this case will act as a positive feedback. Clouds also contribute a negative feedback through the reflection of incoming solar radiation and consequent reduction in absorption of solar radiation at the surface.

1.1.4 Climate Modelling

In order to forecast changes in the climate system, numerical models have been developed. These models simulate different feedback mechanisms and the interactions between different components of the climate system.

Global prediction models concentrate on the circulation of the atmosphere. Therefore these models are called Atmospheric General Circulation Models (AGCMs). AGCMs were originally derived from weather forecast models and are generally run coupled with simple representations of the thermal behaviour of the upper ocean. A comprehensive representation of all main components in the climate system has been developed by very few models due to lack of computer resources.

The validation of climate models requires the availability of appropriate observed data, in particular those obtained from satellites. In the mean time the validation of a number of atmospheric model variables is handicapped by limitations in the available observed and model data (e.g. precipitation , evaporation, soil moisture, snow depth).

1.1.5 Global Climate Change

All models show substantial changes in climate when CO_2 concentrations are doubled. However, in their current state of development, there are considerable uncertainties in the predictions of global climate change. Improved prediction of global climate change requires better treatment of processes affecting the distribution and properties of clouds, ocean-atmosphere interactions, convection, sea ice and transfer of heat and moisture from surface (IPCC 1990). Increased model resolution will allow more realistic predictions of global and regional climate change.

Different scenarios for predicting the climate have been developed under the IPCC working group. Under the IPCC Business-as-Usual (Scenario A), the energy supply is coal and only modest efficiency (improvements in energy use) are achieved. Carbon dioxide controls are modest and deforestation continues until the tropical forests are depleted. In scenario B, the energy supply mix shifts toward lower carbon fuels (e.g. natural gas). Large efficiency increases are achieved, and deforestation is reversed. In Scenario C, a shift towards renewable and nuclear energy takes place in the second half of the next century while in Scenario D the shift takes place in the first half. Observations and predictions of the increase of global mean temperature from 1850 to 2100 for all Scenario are shown in figure 1.3. Model estimates of sea level rise due to thermal expansion of the oceans and melting of the glaciers are shown in figure 1.4.
Although some climate change is unavoidable, much uncertainty exists in the prediction of global climate properties such as temperature and rainfall. Greater uncertainties exist in predictions of regional climate change and in sea level and ecosystem. International co-ordinated research in which the goal is to improve our capability to observe, model, and understand the global climate system is necessary in order to reduce the current scientific uncertainties.

1.1.6 Observational Requirements

In addition to observations from ground measurements such as ships, buoys, and meteorological stations, satellite observations in particular are needed for global climate studies. The general specification of the observational requirements of the three streams

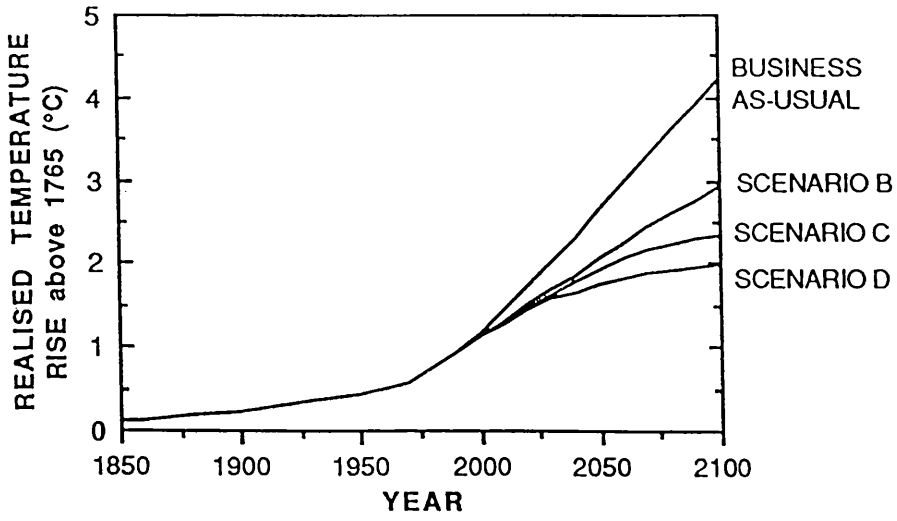

Figure 1.3 Simulations of the increase in global mean temperature from 1850 to 1990 due to observed increases in greenhouse gases, and prediction of the rise between 1990 and 2100 resulting from IPCC Scenarios. (from IPCC 1990)

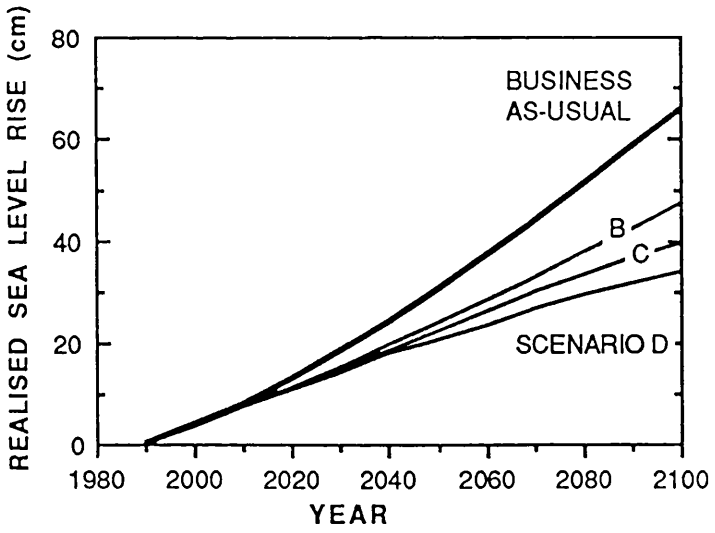

Figure 1.4 Showing the model estimates of sea-level rise from 1990-2100 due to all four Scenarios. (IPCC 1990)

of the WCRP mentioned at the beginning of this chapter are the following (Houghton and Morel 1984):

A. For the long-range forecasting (the first stream):

1 Global network of meteorological observations, including complete coverage around the equator by geostationary satellites and continuous observations from polar orbiting satellite. Sea surface temperature is an important requirement for describing the surface forcing anomalies which may account for the predictable variability of weather on time scales of several weeks. Very high accuracy of sea surface temperature (better than 0.5K) is needed in monitoring the ocean surface by satellite.

2 More refined interpretation of observations of clouds from satellite images.

3 More refined interpretation of satellite observations of the land surface in terms of quantities that describe the surface fluxes of heat and water vapour.

B. For the second stream, adequate coverage over the tropical ocean can be made by satellite observations. For example: satellite passive microwave radiometers can provide coverage of sea ice and radar altimetery to determine surface topography.

C. For the third stream, global observation of the ocean surface are required (same as the second stream). A further requirement is accurate measurement from satellites to determine the net energy input and its distribution at the top of the atmosphere, and to provide information required for the estimation of energy fluxes at the ocean surface and of heat transport within the oceans.

All these satellite measurements for the three streams need to be made not only with good coverage but also with high accuracy.

1.2 The role of Satellite Remote Sensing in Climate Studies

Historically, the capability of satellites to provide important information about the climate has been recognised since 1959 when Explorer 7 (a meteorological satellite) was launched. Since then satellites operated by United States, Soviet Union, Europe, China, Japan, and India have grown in numbers. Many of these satellites provide valuable information about the atmosphere, land and ocean components of the climate

system. Table 1.1 shows the current and planned satellite systems that provide critical data for the climate system from 1990-2010.

The increasing complexity of climate models and their global character means that many of the data needs can only be met comprehensively using remote sensing from satellites (Rowntree, 1993). The reasons are: their ability to sample the globe with high spatial and temporal resolution, the ability of satellites to measure critical climate variables, and an operational system that will ensure long term measurements which is a crucial condition for observing and understanding the climate (Gruber and Arkin, 1992).

Satellite observations contribute to our understanding of the Earth's climate by improving initial and boundary conditions for climate models, validation of climate models, and detecting changes in the global climate. Rowntree (1993) has categorised the role of satellite data for global climate studies under three main headings:

A. Data to define those characteristics of land surface which are not predicted.

B. Data to:

1. validate climate simulations,
2. initialise forecast models,
3. develop parameterization.

C. Data to define environmental changes (e.g. tropical deforestation). These are needed as input data for model experiments to estimate the response of climate to such changes.

Group A includes those features of land surface which are not predicted and so must be prescribed. For example, some early climate models specified soil moisture and how it affects evaporation, whereas today's models usually simulate it (Rowntree, 1993).

The variables in group B combine validation of climate models and initialisation of forecast models. For example, winds, temperatures, humidity in the atmosphere, snow cover, and soil moisture are simulated by climate models but short-period forecast models should use such data as are available in the initialisation stage (Rowntree, 1993).

Table 1.1

Earth observation Satellites from 1990 to 2010 (Gruber and Arkin, 1992)

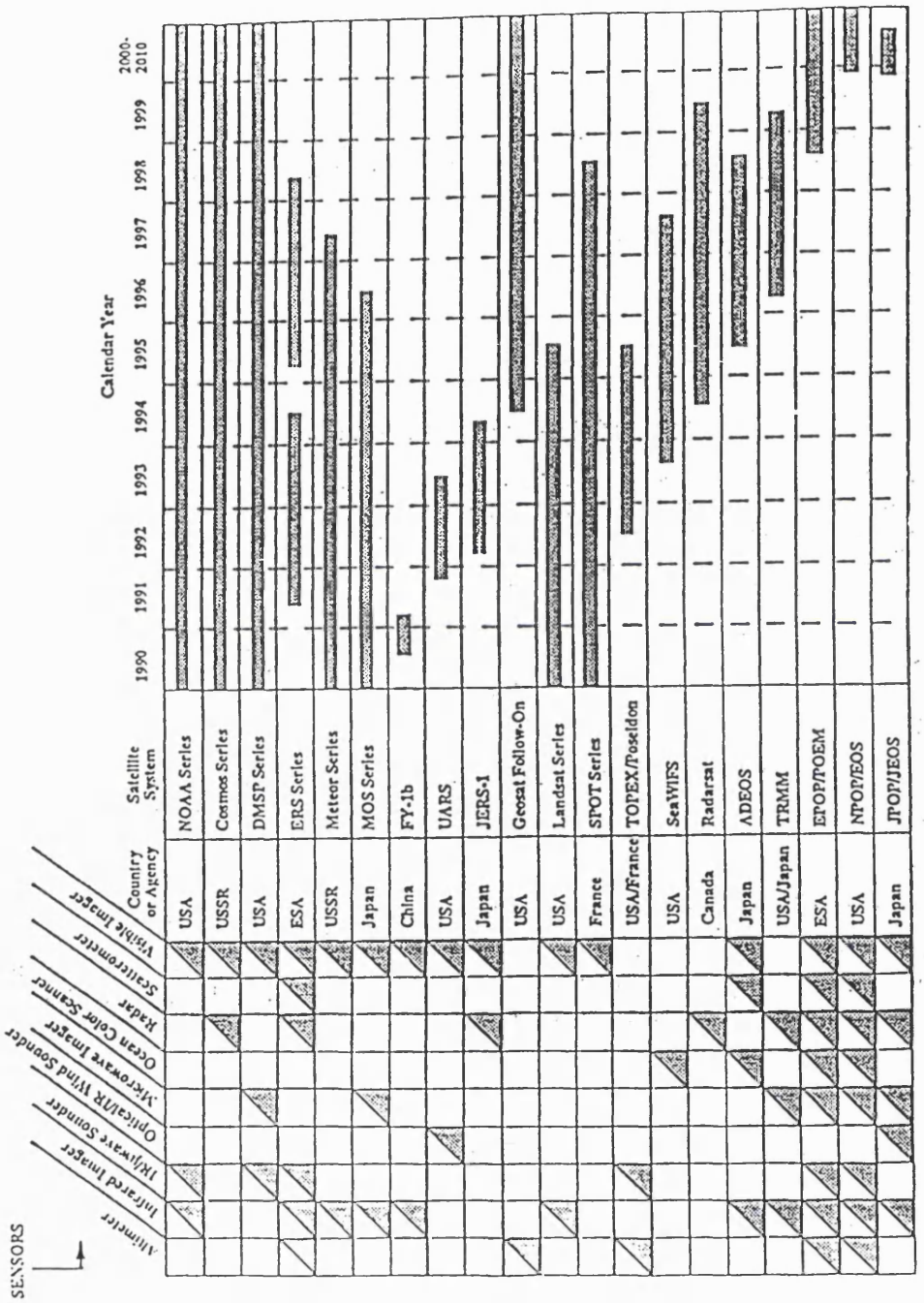

1.2.1 Passive Microwave Remote Sensing

The climate related parameters for which usable satellite climate products currently exist use observations in the visible and infrared atmospheric windows. Potentially valuable windows in the microwave portion of the spectrum are only beginning to be exploited (Gruber and Arkin, 1992). The use of microwaves for remote sensing has many capabilities which make them attractive to the studies of global climate. These capabilities are :

- Cloud penetration. For example, ice clouds have almost no effect at any microwave frequencies (see Ulaby et al. 1981). Water clouds have very small effects, even at shorter wavelengths (Ulaby et al. 1981). Choudhury et al. (1992) pointed out that at 37 GHz, clouds have almost no effect and it is mostly water vapour which affects the microwave surface emission.

- Passive microwave sensors are capable of gathering data at night as well as during the day since they are concerned with emitted radiation rather than reflected solar radiation, (Cracknell and Hayes, 1991).

- The geophysical information provided by the microwave signal is related to geometric and bulk dielectric properties of the surface or volume while that provided by visible or near infrared region is determined by molecular resonance in the surface layer (Ulaby et al. 1981). Therefore the information available from microwave remote sensing is different and complementary to that available at infrared or visible wavelengths.

- The microwave emission from the surface can penetrate through vegetation cover, depending on the moisture content and density of vegetation as well as on the wavelength. Also, the microwave emission has the capability to represent the bulk properties of the ground depending on the wavelength used and on the dryness of the soil.

Microwave radiometers: past, present and future

The first microwave radiometer observations of the Earth from space were made by the Russian satellite Cosmos 243 in 1968. Since then, microwave radiometers have been carried by many spacecrafts including Cosmos 384; Nimbus 5, 6, 7; Skylab; TIROS; Seasat, DMSP, ERS-1 and TOPEX (table 1.2). The early microwave radiometers were mainly used for looking through clouds to retrieve atmosphere (temperature profiles,

water vapour, liquid water content) and surface parameters (sea surface temperature, wind speed, ice classifications, snow cover and soil moisture). But the radiometers have been of limited spatial resolution on the ground, and consequently it has been difficult to relate their measurements to a single land surface parameter.

A new generation of microwave radiometers is being planned for launch during the next decade, table (1.2). An example of these are AMSR and ESTAR which are planned for launch in the late 1990s. These instruments are part of a system which is called HMMR. Working together with AMSU-A and AMSU-B (on NOAA polar orbiting satellites) these systems will form an Earth Observing System (EOS) to provide the information needed to better understand the fundamental global-scale processes which govern the Earth's environment (NASA 1987). The HMMR represents a major step in obtaining better radiometric resolution and reaching the spatial resolution needed for observing the fundamental geophysical processes driving the Earth's environment.

1.2.2 The Importance of Microwave Emissivity for the Retrieval of Climate Parameters

The microwave emissivity of material is defined as the ratio of the radiant flux from material to that of a blackbody (chapter 2). Microwave emissivity is an important parameter since the radiant flux from material depends on the surface geometry and dielectric and extinction properties. Therefore the interpretation of many geophysical parameters such as soil moisture, vegetation, and sea ice are dependent on knowledge of the true microwave surface emissivity (e.g. Choudhury, 1993; Comiso, 1983). Knowledge of the true microwave surface emissivity is also important for classification of geophysical parameters (Ferraro et al. 1986; Grody 1988).

Theoretical and empirical studies of various surface types have revealed the dependence of microwave emissivity upon many geophysical parameters. The sensitivity of these parameters is different at different microwave frequencies. Table 1.3 shows some of the important parameters which can be measured by the microwave portion of the spectrum. The frequencies shown in this table are generic in the sense that the measurements can generally be made over broad range of frequencies and engineering considerations will likely determine the specific choice. For example, although the low frequencies shown in this table are necessary for soil moisture measurements as they are less sensitive to vegetation and surface roughness, the exact frequency is not particular important as it is usually determined by considerations other than soil physics, such as the requirements of antenna size (for a given spatial resolution the antenna size increases

Table 1.2
Earth's Satellite Microwave Radiometers Past & Future

Year of Launch	Spacecraft/ Instrument element	Frequencies GHz	Smallest-resolution km
1968	Cosmos 243	3.5, 8.8 22.2, 37	13
1970	Cosmos 384		
1972	Nimbus 5/ ESMR	19.3	25
	NEMS	22.2, 31.4, 53.6 54.9, 58.8	200
1973	Skylab/ S193	13.9	180
	S194	1.4	
1974	Meteor	37	
1975	Nimbus 6/		
	ESMR	37	20x43
	SCAMS	22.2, 31.6, 52.8 53.8, 55.4	150
1978	DMSP/ SSM/T	50.5, 53.2, 54.3 54.9, 58.4, 58.8, 59.4	175
1978	Tiros-N/ MSU	50.3, 53.7 55.0, 57.9	110
1978	Nimbus-7/ SMMR	6.6, 10.7 18, 21, 37	18x27
1978	Seasat 1/ SMMR	6.6, 10.7 18, 21, 37	14x21
1987	DMSP/ SSM/I	19.35, 22.22, 37 85.5	16x14
1991	ERS-1/ATSR/M	23.8, 36.5	19.1
1992	TOPEX/MWR	18, 21, 37	23.5
1996+	AMSU/A AMSU/B	Temperature Sounding Humidity Sounding	
1997+	MIMR	6, 10, 19 24, 37, 90	8x5
1997+	EOS/		
	ESTAR	1.4	10
	AMSR	6.6, 10.65,18.7 23.8, 36.5, 90	1.5

Adapted from NASA (1987) & Ulaby et al. (1981)

Table 1.3

Geophysical Parameters and Microwave Frequencies at Which the Measurements are Preferred

Parameter Observable	Necessary (GHz)	Important (GHz)	Helpful (GHz)
Soil Moisture	1.4		6
Snow	18, 37	90	6, 10
Sea Ice			
Extent	18, 37		90
Type	18, 37	10, 90	6
Wind Speed (sea surface)	10	18	21, 37

Adapted from NASA (1987)

linearly as frequency decreases, see chapter 3) (NASA, 1987).

Over the land, many different studies have shown that microwave emissivities at different frequencies are sensitive to critical climatic parameters such as soil moisture, surface roughness, and vegetation which are reviewed in chapter 2 and snow cover. Over the ocean, the microwave emissivity depends strongly on significant climate parameters such as wind speed and sea surface temperature (chapter 2). The following are some of the geophysical parameters which are required by the climate studies and in which the microwave satellite radiometers can provide useful datasets.

- Soil moisture

  Soil moisture is one of the most important indicators of the effects of increased greenhouse gases on the climate, (Rowntree 1993). One example of the effect of increase in CO_2 on climate is summer aridity (represented by soil moisture) in the great plains area of North America in the late 1980's. Model simulations showed that changes of soil moisture can have a significant impact on cloud cover, rainfall (Rowntree and Bolton, 1983). However the data available to validate climate models are very limited and the only data that exist are ground based data for Asia, Vinnikov and Yeserkepova (1991). The accuracy needed for soil moisture measurement for climate studies is 0.02 with a spatial resolution of 100 km (Rowntree, personal communication).

- Snow cover

  Snow is a climatically significant parameter because of its high reflectivity of solar radiation (albedo) and because of its possible involvement in a feedback with temperature (IPCC 1990). Snow cover influences the global climate, and even small areas in mid-latitude mountains may be sensitive indicators of climate change (NASA, 1987). Snow microwave emissivities depend on snow properties , although the dielectric properties of snow is not well understood (NASA 1987).

  Passive microwave radiometers have the capability of measuring two important snow parameters for climate studies: snow water equivalent (the depth of water produced if snow were to melt) and snow-covered area.

- Sea ice

  Ice is also of great significance to the climate system when it occurs in the form of ice covering permanent water, whether oceans or lakes. Formation, destruction or

movement of such ice can be associated with very large changes in the surface albedo. Two measurements are crucial to understand the role of sea ice in the climate system: (1) the extent and concentration of the polar sea ice cover. (2) distribution of sea ice thickness (NASA 1987). The interpretation of sea ice requires a knowledge of microwave emissivity of sea ice which depends on age, thickness, salinity, composition and surface characteristics (Ulaby et al. 1986 ; Comiso, 1984). Passive microwave observations of sea ice have great potential due to the sharp contrast between the microwave emissivities of sea ice and open water (NASA 1987).

1.2.3 The Atmospheric Correction Problem

Earth remote sensing from space implies that information received by the satellite sensor must be transferred from the surface through the earth's atmosphere. Accordingly, the travelled radiation through the atmosphere has suffered absorption, emission, and scattering in the course of that journey.

Adequate corrections for atmospheric interference are required for accurate quantitative measurements of climate parameters from remote sensing data, and for any other application where accurate parameter retrieval is essential.

There are several different approaches to the applications of atmospheric corrections to the satellite data. These approaches were described by Cracknell and Hayes (1991):

1. Ignore atmospheric effects completely. In some applications this is an acceptable approach.

2. Calibration with in situ measurements of geophysical parameters. Many examples of this approach are found in the visible and infrared channels. For example, calibration of AVHRR data using results from buoys, ships (see Cracknell and Hayes, 1991 and references therein) for sea surface temperature. Although this method gives quite accurate results, it suffers from problems such as variations in the atmospheric condition from day to day, significant variations in the atmospheric conditions even within a given scene at any one time.

3. The use of a model atmosphere with parameters determined from historic data. This method is successful for low spatial resolution satellite instruments such as microwave radiometers as local spatial irregularities and rapid temporal variations are likely to cancel out (see Cracknell and Hayes, 1991 and references therein).

This method is relatively successful whenever the magnitude of atmospheric correction is relatively small compared with the signal from the surface.

4. The use of a model atmosphere with parameters determined from simultaneous meteorological data.

5. The elimination of atmospheric effects. For example by using a multi-look approach or two different satellite channels. Instruments such as the Along Track Scanning Radiometer (ATSR) on ERS-1 is an infrared red radiometer which provides dual view (forward vertical) and is used to eliminate atmospheric effect (Harris et al. 1995). One can also eliminate atmospheric effects by using two different satellite channels (e.g. McMillan 1975; Harris and Mason 1992; Franca and Cracknell 1994) or a multi-channel approach (e.g. Dechamps and Phulpin 1980; Ho et al. 1986).

In the microwave region, the effect of the atmosphere was generally assumed to be small for window regions and for frequencies less than 37 GHz (Wang et al. 1992). However, few studies have investigated the effect of the atmosphere at frequencies lower than 37GHz (e.g. Wang et al. 1992). Wang et al. (1992) used multiple-channel microwave radiometric measurements for aircraft (near 90 and 183 GHz) and satellite data (SSM/I) at 37 and 85 GHz to study the effect of atmospheric absorption on the estimation of snow depth. They showed that the radiometric correction for the effect of the atmosphere is important even at 37 GHz for a reliable estimate of snow depth.

Choudhury et al. (1992) studied the atmospheric effect on the polarization difference at 37GHz and found that the atmosphere introduce significant seasonal variations of polarization difference due to rather significant seasonal variations of perceptible water vapour. They used a radiative transfer model for 37 GHz together with meteorological data derived from satellite and surface observations in performing the atmospheric correction. Choudhury et al. (1992) found that the effect of water vapour is more important than that of clouds in accounting for atmospheric effects in an analysis of SMMR 37 GHz. Choudhury (1993) used an approximation of a radiative model and perceptible water vapour (calculated from daily mean surface vapour pressure) and surface air temperature data collected at the time of SSM/I observations to calculate the surface reflectivities from satellite observations .

In this study the microwave emissivity is retrieved using simultaneous measurements from infrared and microwave radiometers. However, the exact measurement of microwave emissivity of the Earth's surface from space is difficult due to the presence

of the atmosphere which causes errors due to the effect of water vapour (e.g. Choudhury, 1993; Comiso, 1983; Grody, 1988).

In the microwave region and in the absence of clouds, the microwave radiation leaving the Earth's surface and then received by the satellite microwave radiometer suffers from three different atmospheric effects (chapters 2): (1) Attenuation of the atmosphere, which depends mostly on the microwave frequency and water vapour content. (2) Upward emission from the atmosphere which depends mostly on the water vapour and frequency of the radiation. (3) Downwelling reflected atmospheric emission and this depends mostly on surface emissivity as well as on water vapour and the frequency used (chapter 4).

A new technique to correct the apparent microwave emissivity for both atmospheric absorption and direct and reflected atmospheric emission due to water vapour using radiometer data in both the microwave and infrared regions is presented in this study (Al Jassar et al. 1995). Radiative transfer simulations using microwave atmospheric model incorporating atmospheres covering different seasons are used to generate coefficients of corrections. A correction to the surface emissivity is made in two steps: the first is to correct the emissivity effect. The essence of this correction is that the relationship between the apparent microwave emissivity (as seen by the satellite) and the true surface emissivity is linear and the difference between them is proportional to the apparent microwave emissivity.(see simulations in chapter 4). The second step is to correct the water vapour effect using two microwave channels of which one is close to the water vapour resonance frequency.

The proposed technique provides an independent method in correcting microwave satellite data without the need to have a priori-knowledge of simultaneous atmospheric parameters. This technique is shown to give very encouraging accurate surface microwave emissivities. However, the corrected emissivity from satellite measurements is limited by the noise from the microwave radiometer and spatial resolution specified by the radiometer design (chapter 3). The technique is validated using simultaneous data from the Along Track Scanning Radiometer (ATSR) and the Microwave sounder (ATSR/M) over the ocean surface around the British Isles in chapter 5. One application of this technique, to improve the accuracy of soil moisture retrieval from microwave emission, is demonstrated in chapter 6.

1.3 Summary

The motivations for pursuing the retrieval of microwave emissivity in this study have been:

- General concern has increased in recent years regarding the impact of mankind on global climate. Global data for the validation of climate models are needed (e.g. data on soil moisture and snow depth) (Rowntree, 1993). In the mean time the validation of a number of model variables is handicapped by limitations in the available observed and model data (e.g. precipitation, evaporation, soil moisture, snow depth). Therefore, the validation of climate models requires the availability of appropriate global observed data, in particular those obtained from satellites.

- The interpretation of many climatic parameters (e.g. soil moisture, snow cover, wind speed and sea ice) depend on the knowledge of the true surface microwave emissivity.

- This study is motivated by the capabilities and potentials of microwave radiometry in providing critical geophysical parameters which are of interest for global climate studies.

The aims of this study are:

- To develop a technique to correct the apparent microwave emissivity for both atmospheric absorption and direct and reflected atmospheric emission due to water vapour using satellite radiometric microwave and infrared data

- To improve the accuracy of correcting the microwave surface emissivity. This will have an impact on the accuracy of the retrieval of geophysical parameters.

- To study and investigate the atmospheric effect due to water vapour content on different ranges of emissivities and for different atmospheres.

- To perform a validation study of the new technique and to apply the atmospheric correction technique over land in order to improve the accuracy of soil moisture retrieval as one of the important climatic parameters (Rowntree, 1993).

Chapter 2

Terrestrial microwave emission and the effect of the atmosphere

2.1 Introduction

This research is concerned with the measurement of terrestrial surface microwave emissivity from space. The emissivity depends upon various surface geophysical parameters which are of interest from the point of view of global climate studies (see chapter 1). This chapter provides a necessary understanding of the basic physics of microwave emission in general (section 2.2) including the assumptions made and the constraints applied in this work. Sections 2.3 and 2.4 review the sensitivity of microwave emissivity to various geophysical properties for soil and ocean. The soil is of interest, in this work, because of the dependence of emissivity on soil moisture which is retrieved in chapter 6, while the ocean is of interest as the validation of the atmospheric correction technique is applied over the ocean surface in chapter 5. The soil and ocean surface microwave emission models used in this study are reviewed in sections 2.3 and 2.4 respectively.

Finally, the effect of attenuation of the microwave surface emission by the atmosphere as well as the emission from the atmosphere itself is studied through the theory of radiative transfer in section 2.5. The review considers the physical processes of both absorption and emission under clear sky conditions.

2.2 Basic physics of microwave emission

Most of the energy received by earth is in the form of solar radiation. Part of the energy is scattered and absorbed by the earth's atmosphere, and the remainder is transmitted to the earth's surface in which some of this portion is scattered and the remainder is absorbed. Electromagnetic energy absorbed by matter is transformed into thermal energy, which is accompanied by a rise in the thermometric temperature. The temperature is determined by the balance between the absorbed solar radiation and radiation emitted by the earth's surface and its atmosphere. The physics of the thermal emission is described by the radiation laws.

2.2.1 Radiation Laws

All matter with temperatures above absolute zero radiates electromagnetic energy. Under thermodynamic equilibrium, a material absorbs and radiates energy at the same rate. The radiation laws use the concept of a perfect absorber and emitter. These laws are:

Planck's Black body law

A black body is defined as an idealised, perfectly opaque material that absorbs all incident radiation at all frequencies, reflecting none (Ulaby et al, 1981). It is important to understand this concept, as black bodies represent a reference against which the emission of real materials is measured.

Planck's radiation law describes the relationship between the temperature and the radiative properties of a black body:

$$B_V = \frac{2hv^3}{c^2} \left[\frac{1}{e^{hv/kT} - 1} \right] \qquad (2.1)$$

where
B_V = Black body radiant energy in $Wm^{-2}\ sr^{-1}\ Hz^{-1}$
h = Planck's constant = 6.63×10^{-34} joule.sec
v = frequency, Hz
k = Boltzmann, constant = 1.38×10^{-23} Joule K^{-1}
T = absolute temperature, K
c = speed of light = $3 \times 10^8\ ms^{-1}$

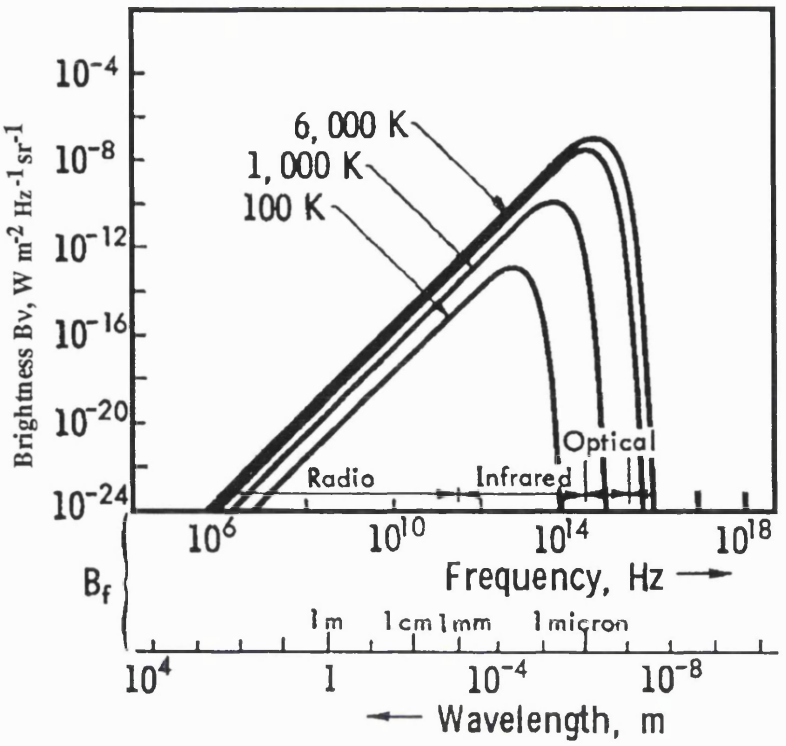

Figure 2.1 Black body radiation according to Planck's function. Adapted from Ulaby et al (1981).

Figure 2.1 shows the Planck radiation law curves as a function of wavelength as well as frequency for different temperatures. From these curves, we can see that as the temperature T increases, the brightness for the overall curve increases, and the frequency at which the B_ν is maximum increases with T. In other words hotter bodies emit more radiation at higher frequencies than cooler bodies do.

Rayleigh-Jeans' law

For low frequencies, in the microwave region, hv/kT << 1. Therefore Planck's function in equation (2.1) may be approximated by using Taylor expansion:

$$e^x - 1 = (1 + x + \frac{x^2}{2} + ...) - 1 \approx x \qquad for\ x << 1 \qquad (2.2)$$

and (2.1) becomes:

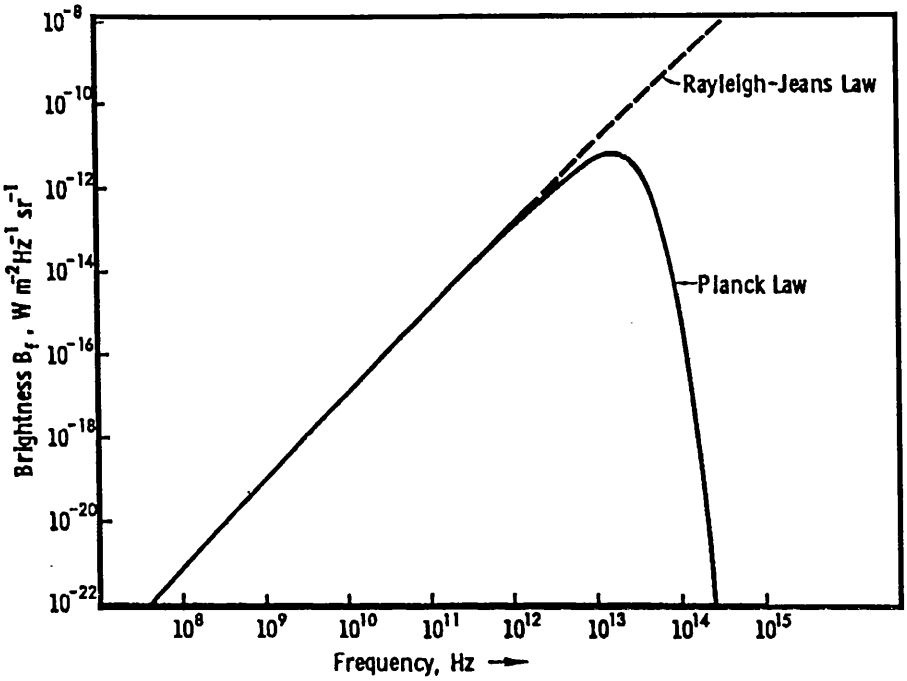

Figure 2.2 Rayleigh-Jeans approximation law for high frequencies compared to Planck's law. Adapted from Ulaby et al (1981).

$$B_\nu = \frac{2\nu^2 kT}{c^2} \tag{2.3}$$

The Rayleigh-Jeans approximation for the microwave region is shown in figure 2.2.

Stefan-Boltzmann Law

This law states that the total radiation emitted from a blackbody over all wavelengths per square metre is proportional to the fourth power of its absolute temperature

$$B = \sigma T^4 \tag{2.4}$$

where $\sigma = 5.7 \times 10^{-8}$ Wm^{-2} K^{-4} sr^{-1},
B is the integral of the Planck function .

This law is used in the climate study to describe the overall energy which Earth radiates into space (see chapter 1).

Kirchhoff's law (Grey Bodies)

As no real body is a perfect emitter, the emission for real materials (grey bodies) can be expressed as a fraction of the emission of a perfect blackbody which has the same temperature:

$$B_{\nu g}\,(grey\ body) = \varepsilon_\nu (B_\nu\,(black\ body)) \tag{2.5}$$

where ε_ν is the emissivity at frequency ν

Real materials are usually referred to as grey bodies as they emit less energy than a blackbody does with the same temperature. The equivalent radiometric temperature for a grey body in equation (2.3) is called brightness temperature T_B (Ulaby et al. 1986). Writing the same equation for real matter as in (2.3), gives the grey body radiation energy as:

$$B_{\nu g} = \frac{2\nu^2 k T_B}{c^2} \tag{2.6}$$

For a blackbody the brightness temperature is equal to the physical temperature, while for a grey body the brightness temperature is always less than the physical temperature.

From equations (2.3) , (2.5) , and (2.6) the emissivity, ε_ν :

$$\varepsilon_\nu = \frac{B_{\nu g}}{B_\nu} = \frac{T_B}{T} \tag{2.7}$$

Equation (2.7) is a radiometric expression for microwave emissivity. The next question is what are the surface geophysical properties affecting microwave emissivity and how these properties contribute to emissivity.

2.2.2 Physical Properties Affecting Microwave Emission

Many terrestrial materials have distinctive properties which affect the microwave emissivity in various ways. These may be described in terms of dielectric properties and roughness. Emission from a smooth and homogeneous terrain medium (uniform dielectric profile) is governed by the dielectric properties and the Fresnel reflection laws at all frequencies, while for nonhomogeneous smooth terrain medium is governed by dielectric properties and the effective reflectivity at low frequencies (see later).

Dielectric properties

Dielectrics are substances that contain few or no free charges and are poor conductors of electric current. A good dielectric is one which the electromagnetic absorption losses are minimum. Vacuum is considered as a perfect dielectric and other dielectrics are measured relative to this.

Dielectric constants for materials such as soils, depend not only on the frequency of the emitted radiation but also on different physical parameters: soil moisture, bulk density, soil texture, soil temperature, salinity, and frequency (section 2.3). Sea water's dielectric constant depends on water temperature, salinity, and the frequency of the emitted electromagnetic radiation (section 2.4). The relative complex dielectric constant is defined as (Ulaby et al, 1981) :

$$\varpi = \varpi' - j\varpi'' \tag{2.8}$$

where

$j = \sqrt{-1}$

ϖ is the complex dielectric constant.

ϖ' is the real part defining velocity and wavelength,

ϖ'' the imaginary part defining the energy losses in the medium.

Emissivity from smooth surfaces

Fresnel reflection (specular reflection) applies for smooth semi-infinite homogeneous media, coherent monochromatic electromagnetic radiation and a medium in which multiple reflections do not occur. The Fresnel reflection has the following forms for vertical and horizontal polarizations:

$$\Gamma(\theta,h) = \left[\frac{\cos\theta - (\varpi - \sin^2\theta)^{1/2}}{\cos\theta + (\varpi - \sin^2\theta)^{1/2}} \right]^2 \tag{2.9}$$

$$\Gamma(\theta,v) = \left[\frac{\varpi\cos\theta - (\varpi - \sin^2\theta)^{1/2}}{\varpi\cos\theta + (\varpi - \sin^2\theta)^{1/2}} \right]^2 \tag{2.10}$$

where $\Gamma(\theta,h)$ is the horizontal Fresnel reflectivity, $\Gamma(\theta,v)$ is the vertical Fresnel reflectivity, and θ is the angle of incidence, and ϖ is as defined before.

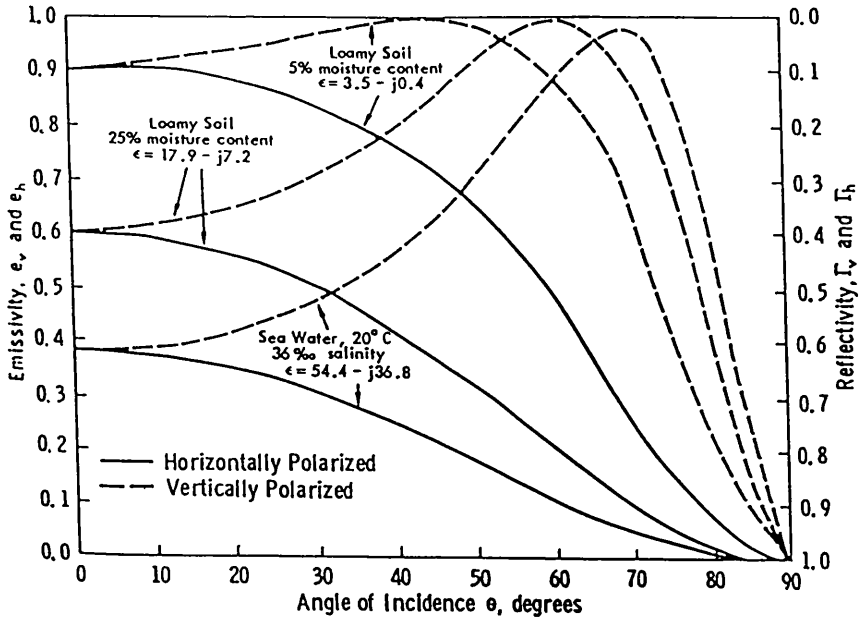

Figure 2.3 Calculated reflectivities and emissivities as a function of incidence angle at 10 GHz (Ulaby et al. 1981)

The behaviour of both reflectivities and emissivities for both horizontal and vertical as function of incidence angle at 10 GHz is shown in figure 2.3. This figure shows that for nadir angle (i.e. $\theta = 0$) horizontal emissivity equal to vertical emissivity for sea water and loamy soil with different soil moisture content. At higher incidence angles the vertical emissivity is always higher that horizontal emissivity.

The emissivity of the surface can be determined from reflectivity by using both the conservation of energy and Kirchhoff's law. From conservation of energy and for opaque surfaces (i.e. transmittance = 0):

$$\Gamma_\nu + a_\nu = 1 \tag{2.11}$$

where Γ_ν is the reflectivity and a_ν is the absorptivity of the surface at frequency ν.

Kirchhoff's law states that in thermal equilibrium the emissivity, ε_ν, equals the absorptivity *(a)*. Therefore, it is possible to write equation (2.11) as:

$$\varepsilon_\nu = 1 - \Gamma_\nu \tag{2.12}$$

Homogeneous medium with uniform temperature profile

The simplest configuration is represented by a semi-infinite homogeneous (i.e. uniform dielectric profile) isothermal (i.e. uniform temperature profile) medium at nadir angle. In this case, the physical temperature in equation (2.7) is the soil surface thermometric temperature, T_S, and for a smooth surface boundary the emissivity is the specular emissivity of a soil surface, ε_V , which is derived from Fresnel reflection. The radiometric brightness temperature T_B at nadir:

$$T_B = \varepsilon_V T_S = [1 - \Gamma_V] T_S \tag{2.13}$$

where $\Gamma_V = \Gamma(0,h) = \Gamma(0,v)$, is the Fresnel reflection.
Equation (2.13) is valid for all frequencies as far as the medium is smooth and semi-infinite and has a uniform temperature and dielectric profile in which no reflections occur except at the surface boundary.

Nonhomogeneous medium with uniform temperature profile

Smooth terrain medium with nonuniform dielectric profile (nonhomogeneous medium) but with uniform temperature profile has the same brightness temperature as in equation (2.13) except the effective reflectivity, Γ_{eff}, of the medium will replace the Fresnel reflectivity, Γ_V. The radiometric brightness temperature T_B at nadir (Ulaby et al. 1981):

$$T_B = \varepsilon_{eff} T_S = [1 - \Gamma_{eff}] T_S \tag{2.14}$$

The effective reflectivity Γ_{eff} is the steady-state solution incorporating all the multiple reflections within the medium. There are two approaches to compute Γ_{eff}, these are the coherent approach, which account for both amplitudes and phases of the fields reflected within the medium in the absence of volume scattering, and the incoherent approach, which relies on amplitudes only. The justification for incoherent approach relies on the assumption that the medium consists of a large number of scatterers with dimensions comparable to the wavelength in the medium.

The coherent and incoherent reflectivities are function of the loss factor, L, of the terrain medium. If the loss is very large, the effective reflectivity, Γ_{eff}, reduces to Fresnel reflectivity, Γ_V

For nadir angle, the loss factor is written as:

$$L = e^{\kappa_a d} \tag{2.15}$$

where κ_a is the absorption coefficient and d is the layer thickness.

$$\kappa_a = \frac{4\pi}{\lambda_o}\left\{\frac{\mu_r \varpi'}{2}\left[\left(1 + \left(\frac{\varpi''}{\varpi'}\right)^2\right)^{1/2} - 1\right]\right\}^{1/2} \qquad (2.16)$$

where λ_o is the free-space wavelength, μ_r is the relative permeability
We can see from equation (2.16) that for high frequencies, the absorption coefficient is high. Therefore, the loss factor is very large as the dependence on absorption from equation (2.15) is exponential and the effective reflectivity, Γ_{eff}, reduces to Fresnel reflectivity, Γ_v

Assumptions and constraints

Two assumption are made in this study:

1. Surfaces mentioned in this study can be considered approximately homogeneous and therefore we can use Fresnel reflectivities . Note that the new technique to correct the emissivity from atmospheric effect (presented in chapter 4) is valid for homogeneous and nonhomogeneous mediums.

2. Infrared radiometers retrieve the surface temperature (see chapters 3&4) and not the effective temperature. Therefore, the approximation of constant temperature profile is necessary when most of the microwave emission from soil comes from 1 to 50 cm (depending on the microwave frequency) and in which the temperature profile might not be constant over this depth especially over deserts. The uniformity of the temperature profiles is a good approximation from 6 p.m. to 6 a.m. for cool months (England, 1990). Over the ocean, microwave emission depth decreases from 1 cm at 1 GHz to 1 mm at 16 GHz (Ulaby et al. 1986). The approximation of constant temperature profile over the ocean surface is fairly well in this study as we will be using 37 GHz (Ulaby et al. 1986) (see chapter 5).

Under assumptions 1 and 2, the use of equation (2.13) in this research is satisfied fairly well.

Finally this thesis is simplified by instrumental constraints, in which we will be using near normal incidence angle. In this case, the vertical emissivity is equal to the horizontal emissivity and the term ε will be used for emissivity, without referring to vertical or horizontal emissivities.

2.3 Emission model for smooth bare soil

For a smooth bare soil the dielectric properties govern the microwave emission. The dielectric constant of soil is a function of moisture content, bulk density, soil textural composition, soil temperature, salinity, and frequency. The dielectric constant is strongly dependant on soil moisture and to a lesser extent on soil textural composition (Ulaby et al. 1982). Different studies have investigated the microwave dielectric behaviour of soils (e.g. Schmugge, 1980; Wang and Schmugge, 1980; Shutko and Reutov, 1982 ; Dobson et al. 1985; Hallikainen et al. 1985).

Electromagnetically, soil medium is four component dielectric mixture of air, bulk soil, bound water, and free water (Hallikainen et al. 1985). Bound water refers to the water molecules contained in the first few molecular layers surrounding the soil particles, while free water refers to water molecules that are located several molecular layers away from soil particles and are able to move within the soil medium with relative ease. The interaction with electromagnetic waves is different for bound water and free water. Bound water has a low dielectric constant because it is held strongly on to the surface of soil particles and therefore its dipoles are immobilized, while free water has a high dielectric constant since its molecules dipoles are free to rotate at microwave frequencies.

Hallikainen et al. (1985) presented experimental measurements of dielectric constant for five soil types at frequencies between 1.4 GHz and 18 GHz. These results showed that soil texture has an effect on dielectric behaviour over the entire frequency range and is most pronounced at frequencies below 5 GHz.

Based on the observed behaviour of soil-water mixtures made by Hallikainen et al. (1985). Dobson et al. (1985) presented two dielectric mixing models : 1. a semi-empirical model which is a convenient means for predicting a soil dielectric constant that requires only soil texture and volumetric moisture as inputs, and 2. a theoretical four-component mixing model that explicitly accounts for the presence of bound water.

Dobson et al. (1985) pointed out that the semi-empirical yields an excellent fit to measured data above 4 GHz, but at 1.4 GHz the model does not fully account for the dielectric properties of bound water at low moisture contents. The Dobson model has been used in different studies (e.g. Coppo et al . 1991, Strawbridge 1992, and Rao et al. 1993).

Dependence of microwave emission on soil properties for smooth soil

The dielectric constant of soil mixture is a function of frequency as well as the following surface parameters (Dobson et al. 1985):

a. volumetric soil moisture content
b. soil texture (sand, silt, clay fraction) and salinity.
c. bulk density
d. temperature

Now the question is: what is the dependence of microwave emissivity on each of these parameter? A simulation code written by Dr. Jeff Ridley at MSSL was used in the simulations of Dobson's model to show the dependence of microwave emissivity on each of the above parameter.

a. soil moisture content

The large difference between the dielectric properties of water and dry soil, in particular at low frequencies, makes the microwave emission very sensitive to soil moisture. Figure 2.4 shows the dependence on soil moisture for 1.4GHz, 18GHz, and 37GHz frequencies. The emissivity at 1.4 GHz is more sensitive to soil moisture than those at higher frequencies (i.e. 18 GHz and 37 GHz). The 18 GHz and 37 GHz are TOPEX channels which will be used in soil moisture retrieval from Simpson Desert in chapter 6. Note the simulations in this work are performed for volumetric soil moisture with values from 0.0 to 0.20 cm^3 cm^{-3} as this is the expected range of soil moisture in desert regions.

b. soil texture (sand, silt, clay fraction) and salinity

Soil texture affects the dependence of the emissivity upon soil moisture. The soil texture is described by the fraction of sand, silt, and clay. The reason for the dependence of microwave emission on texture is that water molecules which are close to the particle surface are tightly bound and does not contribute significantly to the dielectric properties (Schmugge 1980). Therefore, the dielectric constant of the clay soil (having larger surface area, therefore more bound water molecules) is lower than that of sandy soil (having lower surface area and therefore lower bound water molecules). Another reason for the dependence on texture is salinity (Hallikainen et al. 1985). The deficiency of salinity in sandy soils (salinity increases with clay fraction of soil) affects the ionic conductivity for frequencies below 10 GHz. However, the exact

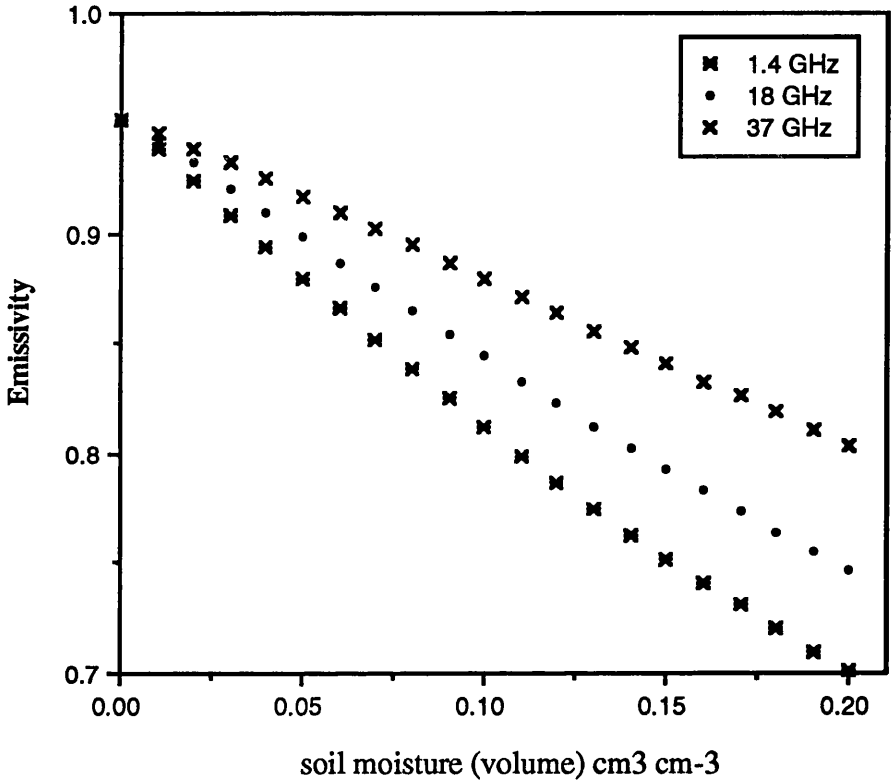

Figure 2.4 Simulation of emissivity dependence upon soil moisture using Dobson dielectric model. T=24°C, bulk density=1.2 g/cc, sand fraction=0.9.

form of the dependence of dielectric constant on soil salinity is not well understood (Ulaby et al. 1986).

c. bulk density

Another important parameter which affects microwave emission is the bulk density. The bulk density of a surface layer is a measure of the packing density of soil solids. It depends upon the composition of soil (texture and organic inclusions), the structure of soil fabrics, and the soil moisture. The dependence of bulk density on soil moisture for sandy soils is relatively slight (Dobson, et al, 1985), whereas soils with high clay fraction has a tendency to expand upon wetting, which reduces their density as moisture increases.

Simulations of Dobson model show the variation in emissivity with soil moisture is sensitive to bulk density change. Figure 2.5(a) and 2.5(b) shows simulations using the Dobson model for 18GHz and 37GHz frequencies respectively. These graphs show that at both frequencies, emissivity is sensitive to bulk densities values. For both frequencies (18 GHz and 37 GHz) the effect of bulk density is similar.

d. temperature

The temperature dependence of microwave emissivity was examined, using the Dobson model, by varying the temperature from 0 to 50°C. At a low frequency (1.4 GHz) there is a little effect and the emissivity decreases with decreasing temperature, figure 2.6(a), For a high frequency (18 GHz) the emissivity increases with decreasing temperature. However in both cases the emissivity dependence on temperature is very weak in comparison with the emissivity dependence on soil moisture. The difference in the behaviour with temperature between the 1.4 and 18 GHz is explained by the resonance frequency of dielectric model of water (Ulaby et al. 1986). The resonance frequency (or relaxation frequency) change with temperature. For example at 20° C the resonance frequency is ~ 17 GHz while at 0°C it is 9 GHz. Therefore for frequencies less than the resonance frequency such as 1.4 GHz the emissivity decreases with decreasing temperature, while for frequencies higher than the resonance frequency such as 18 GHz the emissivity increases with decreasing temperature (see Ulaby et al. 1986).

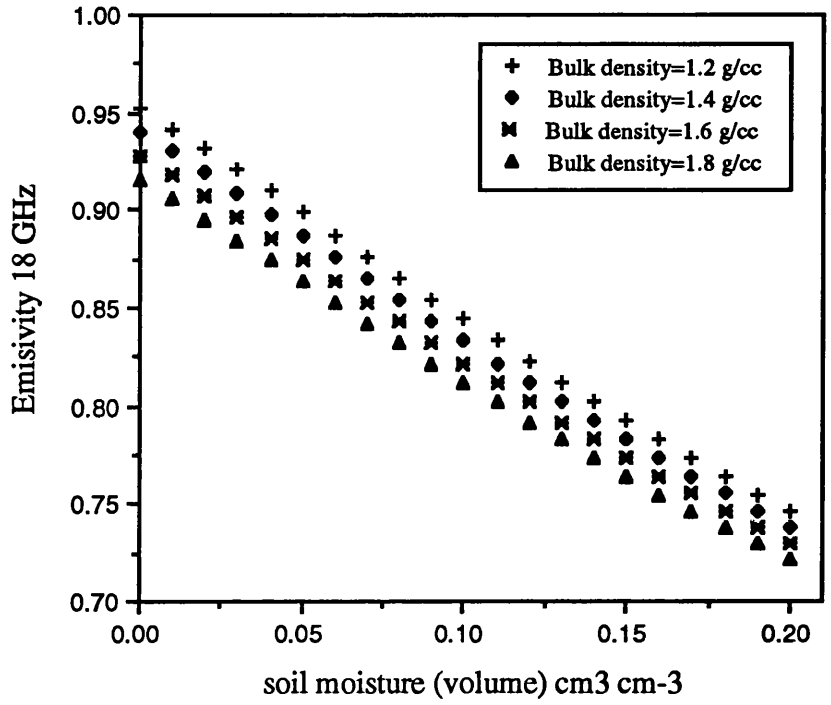

Figure 2.5a Simulation of Dobson's model for different bulk densities for 18 GHz. T=24°C, sand fraction=0.9.

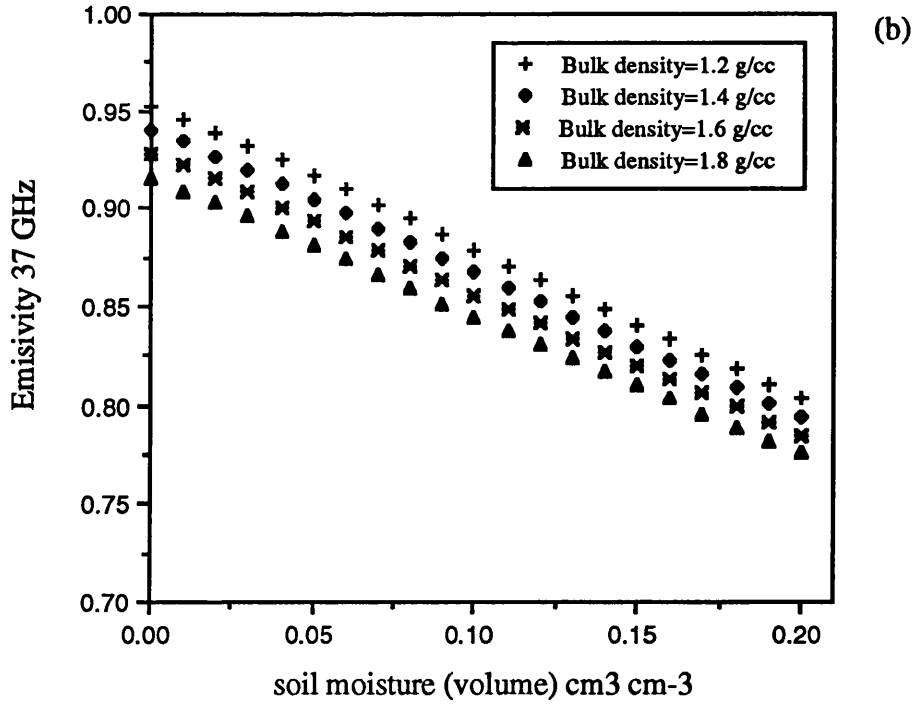

Figure 2.5b Simulation of Dobson's model for different bulk densities for 37 GHz. T=24°C, sand fraction=0.9.

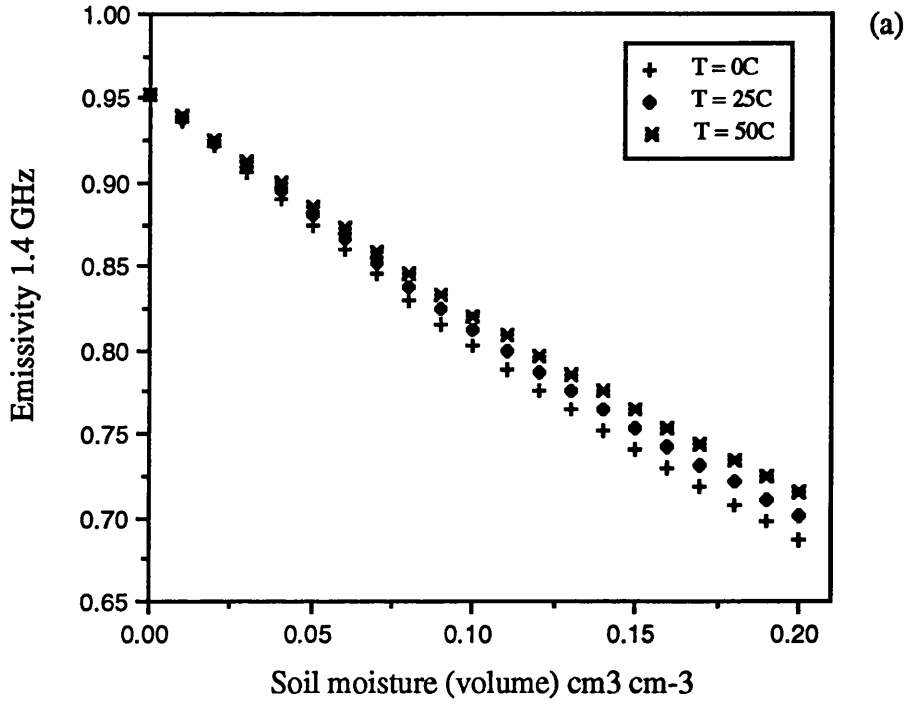

Figure 2.6a This figure shows that effect of changing temperature from 0 to 50° C for 1.4GHz. (Simulation of Dobson' model). Bulk density=1.2 g/cc, sand fraction=0.9.

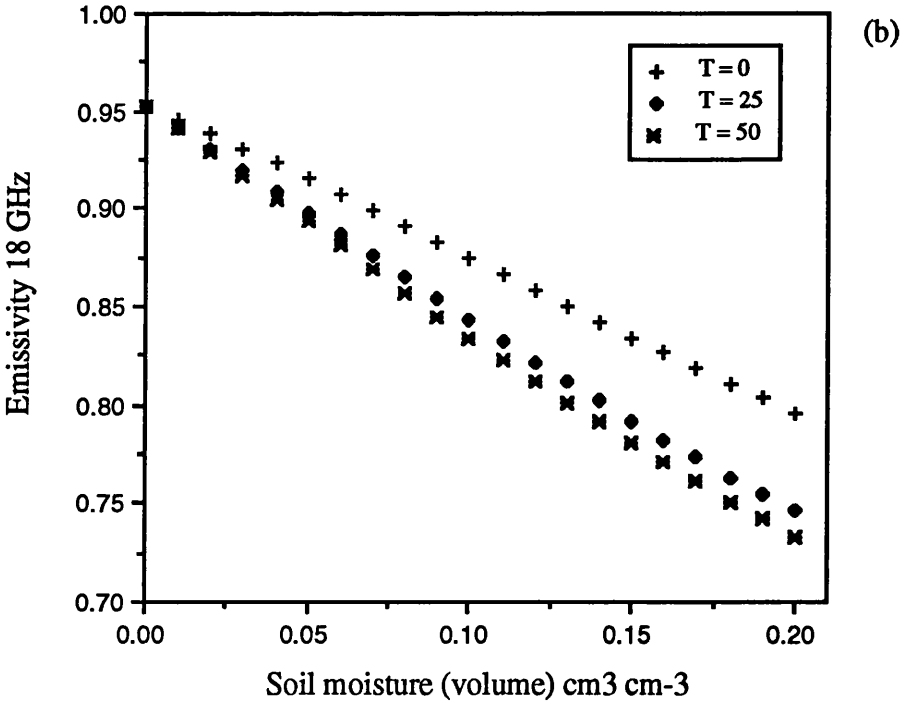

Figure 2.6b This figure shows that effect of changing temperature from 0 to 50° C for 18GHz. (Simulation of Dobson' model). Bulk density=1.2 g/cc, sand fraction=0.9.

2.3.1 Roughness effect

The effect of surface roughness on microwave emission has been investigated in both experimental and theoretical studies. It has been shown in these studies that roughness raises the apparent emissivity of a surface over the emissivity of a smooth surface, this has been attributed to the increase of soil surface area.

One early field experiment was done in 1974 at Texas A&M University (Newton and Rouse, 1980). They showed that there is an increase in emissivity with increasing surface roughness and therefore a decrease in sensitivity to soil moisture. Although only measurements at 1.4 and 10.7 GHz were reported, Newton and Rouse, (1980) and Newton et al. (1982) showed that there was a wavelength dependence of surface roughness effect. The higher the frequency, the stronger the roughness effect. Other experiments have been done by other groups (e.g. Wang 1983, Wang et al. 1983, Schmugge et al. 1985, Wegmuller et al. 1989, Paloscia et al. 1993) which demonstrated the roughness effect on microwave emission.

Theoretically, Kirchhoff method is the most widely used theory for surfaces with gentle undulations. The basic assumption of Kirchhoff scattering method is that plane boundary reflection occurs at every point on the surface, that is, in a local region the boundary may be looked in as an inclined plane (Ulaby et a;. 1981). The two fundamental parameters usually used to describe surface roughness statistically are: the standard deviation of surface height, σ, and surface correlation length, l. The standard deviation represents the r.m.s of surface heights. The correlation length of a surface provides a reference for estimating statistical independence of two points on the surface. If the two points are separated by a horizontal distance greater than l, then their heights may be considered to be statistically independent of one another For a perfectly smooth surface the correlation length $l = \infty$. The mathematical description for the standard deviation of surface height and the correlation length are given by (Ulaby et al. 1982).

In some scattering models, the surface is described in terms of its r.m.s. slope *(s)*. For a Gaussian correlation function:

$$s = \sqrt{2}\frac{\sigma}{l} \qquad (2.17)$$

Theoretical models which can be applied to all frequencies are not available and every theoretical model has limits on the range of surface type for which it may be applied. The emissivity can be predicted from reflectivity by using two analytic approaches: the Kirchhoff approximation at high frequencies, and small perturbation theory at low frequencies (Coppo et al. 1991).

In the Kirchhoff approximation, the horizontal correlation length and radius of curvature must be larger than electromagnetic wavelength λ. There are two different approaches for Kirchhoff's approximations: the geometric optics approach (stationary phase approximation) and the physical optics approach (scalar approximation). The full theoretical development of these models is found in Ulaby et al. (1982). In summary, the scattering for the geometric optics approach can occur only along directions for which there are specular points on the surface, excluding local effects of diffraction. The coherent component is very small and the scattering may be considered to be purely incoherent. The solution is frequency independent and depends only on the ratio between σ and l. This approach can be applied for surfaces with large standard deviation of surface heights (i.e. for $\sigma > \lambda$). The physical optics approach is applied when σ is small compared to λ and the correlation length is large. For natural surfaces this condition appears too restrictive except for deserts. These two approaches for Kirchhoff's model require that the condition $2\pi l/\lambda > 6$ must be satisfied. For slightly rough surfaces with $2\pi l/\lambda < 6$, the small perturbation theory is applied. The surface here is considered smooth, with small variations.

Other models based upon Kirchhoff method, including both coherent and incoherent scattering are described by Tsang and Newton (1982), Mo et al. (1987) and Mo and Schmugge (1987). In Mo et al. (1987), the bistatic scattering coefficients are integrated over the scattered angles to obtain the surface reflectivity which also contains a rough surface shadowing function for representing the probability of a point on a rough surface not being shadowed by other parts of the surface. Another model was developed by Mo and Schmugge (1987). In this model it was shown that the reflectivities for a rough surface can be represented by an analytic formula in the form of a smooth surface reflectivity Γ_V attenuated by a rough thickness G:

$$\Gamma = \Gamma_V \, e^{-G} \tag{2.18}$$

where G is given by

$$G = (\alpha - \delta m_V) \, s \, \beta \tag{2.19}$$

where α, δ, and β are adjustable parameters and m_V is the volumetric soil moisture.

Different models which are much simpler than the previous theoretical models are the semi-empirical models. One early model is provided by Choudhury et al. (1979) in which they used only the coherent term of the scattered field and found that the reflectivity is :

$$\Gamma = \Gamma_V e^{[-h\,(cos\theta)2]} \tag{2.20}$$

where
Γ_V is the smooth surface reflectivity
$h = 4(k\sigma)^2$ and $k = 2\pi/\lambda$.

Choudhury et al. (1979) used an empirical value for h to fit the model to their data, although this value did not have a proportional relation with surface height variations. This discrepancy occurred because the model did not consider the incoherent part of the scattered field which depends on the horizontal scale of the surface height variations. Strawbridge (1992) showed that the Mo and Schmugge (1987) model gave better agreement with satellite observations than that of Choudhury et al. (1979).

Figure 2.7 shows a simulation of Mo and Schmugge (1987) model which will be used in this works (chapter 6). This simulation is for TOPEX frequencies: 18 GHz and 37 GHz. The two graphs show the decrease in the sensitivity of microwave emissivity with soil moisture for the two frequencies. This decrease in sensitivity is more for the 37 GHz.

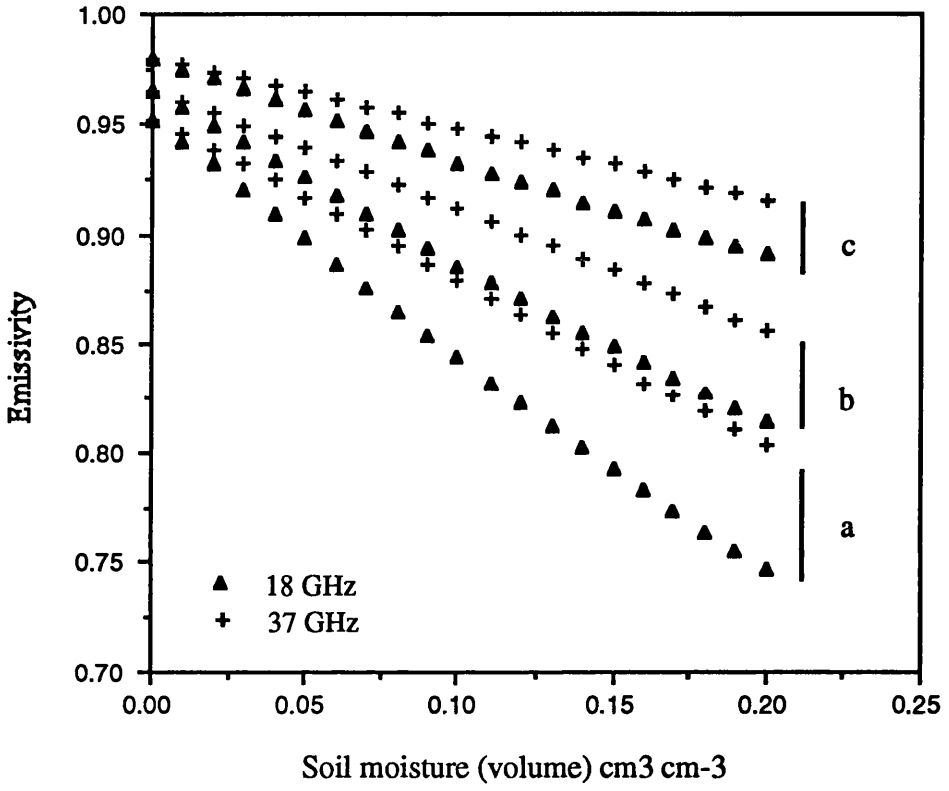

Figure 2.7 Emissivity dependence upon soil moisture for 18 GHz and 37 GHz for three types of surfaces: (a)smooth with slope= 0, (b) medium rough with slope = 0.3, (c) very rough with slope = 0.5 (Simulation of Mo and Schmugge model for roughness using Dobson's dielectric model)

2.3.2 Rock fraction effect

The inclusion of rocks in a soil surface reduces the sensitivity of emissivity to soil moisture for high frequencies (Jackson et al. 1992). In the previous models (section 2.3), the dielectric properties of any rock fraction were not considered. Recent work by Jackson et al. (1992) investigated the effects of rocks on the relation between soil moisture and microwave emission through a combination of laboratory measurements and field observations of emissivity for 21-cm and 6-cm wavelengths.

The observations indicated that for the higher microwave frequencies, it would not be possible to estimate soil moisture when the studied level of rocks was present. For the lower frequencies, the effects of rock fraction are not significant in estimating the soil moisture. Jackson et al. (1992), pointed out that the reduction in sensitivity to soil moisture by higher frequencies might be influenced by an increased sensitivity to surface roughness. Jackson et al. (1992) examined the effect of rock fraction on the emissivity-soil moisture relationship, using a soil dielectric mixing model and rock-soil mixing model, (see figure 2.8). They found that laboratory measurements of soil and rock dielectric constants produced the results expected from the use of the dielectric mixing models. In this thesis, areas with no rock fraction are chosen for use in the validation of the atmospheric correction and soil moisture retrieval. This is because rock fraction reduces the sensitivity of microwave emission to soil moisture, and because rock fraction is difficult to model.

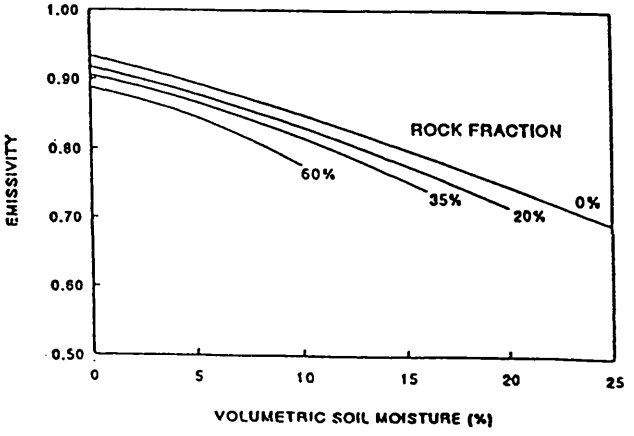

Figure 2.8 Soil - rock mixing model (exponential model) which shows the effect of rock fraction of the relationship between emissivity and soil moisture at L-band (i.e. $\lambda = 21$ cm) and 10^{o} look angle. (Jackson et al. 1992)

2.3.3 Vegetation effect

The microwave emission of bare soil is governed by dielectric properties and the surface roughness of soil. When a vegetation layer is present over the soil surface, it introduces attenuation and scattering of radiation emitted by soil, and it contributes thermal emission of its own (Ulaby et al. 1983). This will reduce the sensitivity of microwave emission to soil moistures shown in figure 2.9.

Several studies have shown that vegetation attenuates the soil emission. The attenuation depends upon the microwave wavelength and decreases with increasing wavelength (Wang et al. 1982). The purpose of most of the radiometric observations of vegetation canopies made, has been to determine the feasibility of using microwave radiometry to estimate the soil moisture content of the underlying soil medium (Ulaby et al. 1986). Different experiments have shown that vegetation reduces the sensitivity of microwave to soil moisture (e.g. Newton and Rouse 1980, Wang et al. 1982, Ulaby et al. 1983, Ferrazzoli et al. 1992, Palocia et al. 1993),

Models for the effect of vegetation on emission and the dielectric constant are found in Ulaby et al. (1982) and Ulaby et al. (1986). A full discussion of radiative transfer models are not within the scope of this thesis. More comprehensive study on the effect of vegetation on microwave emission is found in Strawbridge (1992). In this thesis, desert surfaces with few vegetation are used for the application technique in chapter 6 due to the complexity of emission from vegetated surfaces.

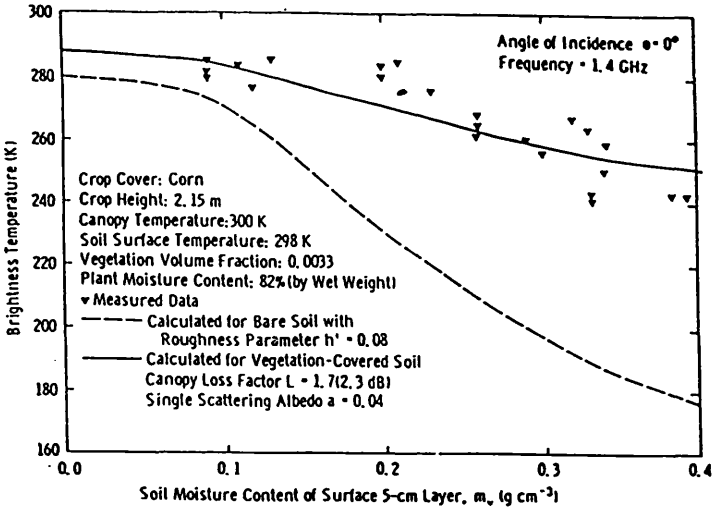

Figure 2.9 Nadir brightness temperature with soil moisture for both bare and corn fields at 1.4 GHz (Ulaby et al. 1983).

2.4 Emission model for ocean Surface

The microwave emission for a smooth ocean is governed by the dielectric properties of saline water. The dielectric constant for saline water is a function of frequency, water temperature, and salinity. If the dielectric constant is known, it is possible to calculate the emission of smooth sea surfaces at microwave wavelength using the Fresnel equations (section 2.2) and emissivity = $1 - \Gamma_v$. For smooth ocean, the microwave emissivity is very sensitive to sea surface temperature, see figure 2.10.

The dielectric model which is used is this thesis (chapter 5) is expressed by Chang and Wilheit (1979). This model was used by Wilheit (1979), Wilheit and Chang (1980), and Wilheit et al (1984).

The next section considers the effect of wind roughening of the sea surface upon the microwave emission.

2.4.1 Wind-induced surface roughness effect

When wind blows across the sea surface it generates roughness in the form of waves. Observations have shown that there is a relationship between microwave emissivity and wind speed (e.g. Webster et al. 1976, and Blume et al. 1977). Eymard et al. (1994) pointed out that although both theoretical and empirical models have been developed to relate the dependence of microwave emissivity to wind speed, our knowledge of this dependence is mostly empirical.

Wilheit (1979) provided an empirical model to infer the dependence of sea surface microwave emissivity on surface roughness using the Cox and Munk (1955) sea surface slope distribution. Cox and Munk (1955) have described the distribution of sea surface slopes as a function of wind speed and they found that the surface slopes were normally distributed about the mean with a variance given by:

$$\sigma_{20}^2 = 0.003 + 0.0048 u_{20} \qquad (2.21)$$

where u_{20} is the wind speed in metres/second at 20-m height. The coefficient multiplied by u_{20} is slightly different from that in the Cox and Munk (1955) as the winds were measured at 12.5 m height.

Wilheit (1979) assumed that there is a linear change of variance with frequency, ν:

$$\sigma^2(v) = (0.3 + .02v(GHz))\sigma_{20}^2 \quad \text{for } v < 35\ GHz$$
$$\sigma^2(v) = \sigma_{20}^2 \quad \text{for } v \geq 35\ GHz \qquad (2.22)$$

By averaging the Fresnel relations over the distribution of surface slopes, it is possible to calculate the emissivity and the problem reduces to geometric optics.

Although Wilheit (1979) geometric optics model using the Cox and Munk (1955) sea surface slope distribution agrees well with observations (see references cited in Wilheit, 1979) in at view angle of 50°, one of its limitation is the lack of physical optics effects. Therefore, if one calculates the nadir emissivity of surface according to the Wilheit model, there is substantially no change in emissivity through the entire 0-7 m/s wind speed range (see figure 2.11). Blume et al (1977) observations at 2.65 GHz, showed an increase with increasing wind speed of approximately 0.2 K/m/s even at very low wind speeds (i.e. 0-7 m/s).

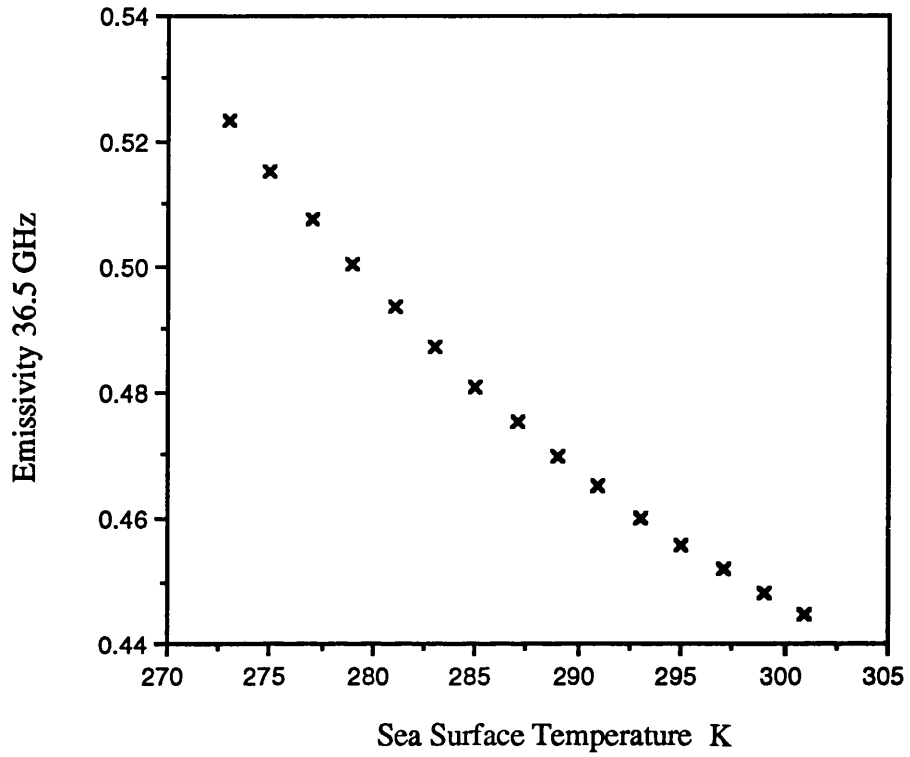

Figure 2.10 Emissivity at 36.5 GHz versus sea surface temperature over smooth ocean, salinity = 35°/°°

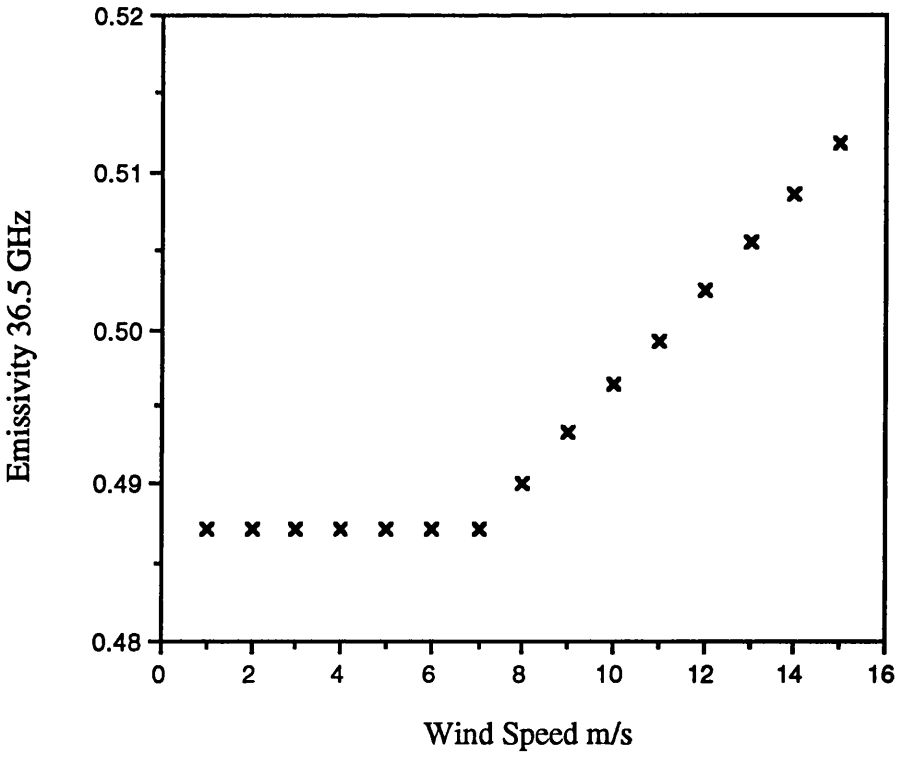

Figure 2.11 Emissivity at 36.5 GHz versus wind speed at sea surface temperature =283 K, salinity=35°/°°

2.5 Microwave interaction with the atmosphere

Microwave emissivities as seen by the satellite for all types of Earth surfaces is affected by the atmosphere. The magnitude of the effect depends on the microwave frequency (see chapter 3), various atmospheric parameters (water vapour, cloud, rain), and the surface emissivity (see chapter 4) .

In the 1-15 GHz region of the electromagnetic spectrum, the atmosphere is transparent even in the presence of clouds and moderate rain. At higher frequencies, the microwave radiation emitted from the Earth's surface experience interactions with the atmosphere before reaching the microwave remote sensor. The work in this research considers the effect of the atmosphere on the microwave radiation for clear sky conditions only.

Different molecules are found in the atmosphere, including nitrogen, oxygen, water vapour , ozone,nitrous oxide, nitrogen dioxide. However water vapour and oxygen are the only constituents that exhibit significant absorption bands in the microwave region. Water vapour absorption resonance is at 22.2 and 183.3 GHz, while oxygen has absorption lines in the 50-60 GHz region and at 118GHz. Up to 90 km above sea level, the atmospheric composition is constant except for water vapour (Ulaby et al. 1982).

The variation of water vapour density in the atmosphere depends mostly on temperature. For example, for a very cold dry climate it might fall as low as 10^{-2} gm^{-3} while for hot and humid climate it may reach 30 gm^{-3}. On microwave remote sensing the region of most interest is the lowest part of the atmosphere, as it contains the bulk of the total atmospheric mass and hence the lowermost 30 km of the atmosphere is considered.

2.5.1 Gaseous Absorption and Emission

In gases, when electromagnetic radiation interacts with an isolated molecule, transition between two quantum states occurs and this results in a sharp absorption or emission spectral lines. If transition is from a lower energy state to a higher energy state, absorption of radiation takes place. On the other hand, if the transition is from a higher energy state to a lower state of energy, radiation is released which corresponds to the difference in energy between the two states. The ability of a volume of gas to emit or to absorb the radiation, depends on the number of molecules occupying the states of higher or lower energy respectively (Schanda, 1986). In normal thermodynamic

conditions, the upper energy states are always occupied by a smaller number of molecules than the lower states.

Molecules in gases have a large number of energy levels available, due to the large number of different modes (rotational, vibrational, and electronic). Rotational energy is associated with rotational motions of the atoms of the molecule about the molecules centre of mass. The vibrational energy is associated with vibrational motions of the atoms about their equilibrium positions and the electronic involves the transition of electrons from one energy level to another energy level.

In the microwave region, the oxygen and water vapour spectral lines arise from transition between rotational energy levels only. The oxygen molecule has a permanent magnetic moment. Magnetic interaction with the incident microwave radiation produces splitting of each rotational state into a triplet of energy states resulting in what is so called fine structure of the rotational levels. These transitions are in the 50 to 60 GHz region except for the ground state where the energy transition gives an isolated line at 118.8 GHz. Water vapour, which has an electric dipole, interacts with the microwave field and produces rotational lines at 22.2 GHz and 183.3 GHz.

In an isolated, undisturbed, and stationary molecular system, interaction can occur only at frequencies ν_{lm} which will result in a sharp spectral line. The frequencies ν_{lm} is given by Bohr's formula (Ulaby et al. 1981):

$$\nu_{lm} = (E_m - E_l)/h \tag{2.23}$$

where h is Planck's constant, and E_m and E_l are the internal energies of the higher and lower molecular states respectively.

But, in the real case in the atmosphere, gas molecules are in motion, colliding with one another. Therefore, the absorption or emission spectral lines are not sharp lines any more, but are broadened due to different mechanisms (e.g. pressure and Doppler), figure (2.12). In the microwave region, the most important mechanism which causes broadening is pressure (collision). The general expression for the absorption coefficient between states l and m may be written as (Ulaby et al. 1981):

$$\kappa_a = \frac{4\pi\nu}{c} S_{lm} F(\nu,\nu_{lm}) \tag{2.24}$$

where κ_a is the power absorption coefficient (Npm^{-1}), ν is the frequency in Hz, ν_{lm} is the molecular resonance frequency, c is the velocity of light, S_{lm} is the line strength of

the lm line in Hz and it depends on the number density, the temperature of the gas, and the molecular parameters associated with that transition, and F is the line-shape function in Hz^{-1} and describes the shape of the absorption spectrum with respect to the resonance frequency ν_{lm}. There are several shape functions, based on different models. The simplest is known as Lorenzian function.

A mathematical description of the models used for the calculation of absorption coefficients for both water vapour and oxygen in this thesis is found in Ulaby et al. (1986). However the absorption coefficients of oxygen were modified for those provided by Rosenkranz (1988).

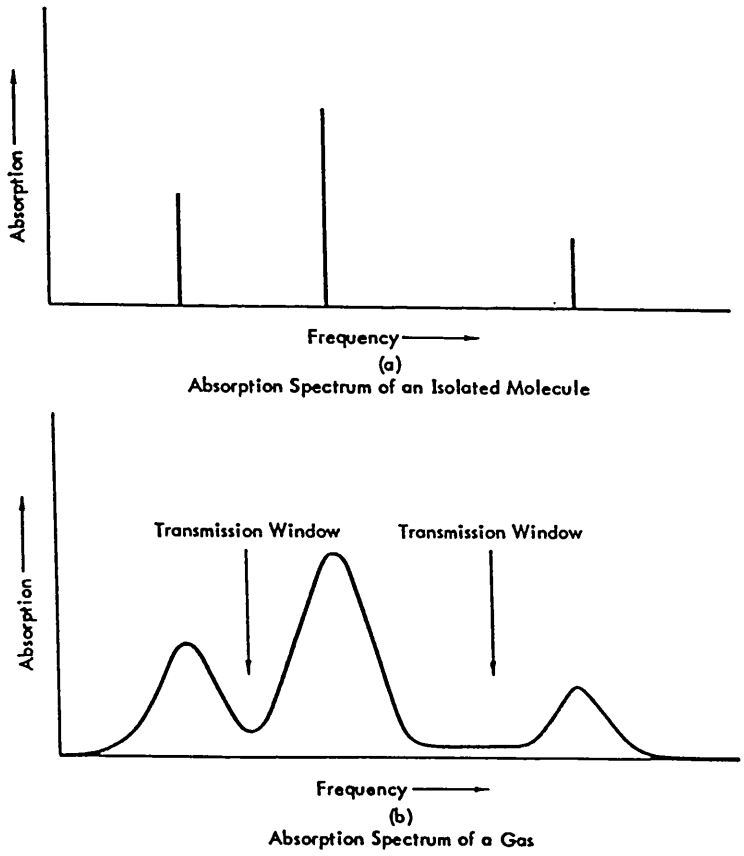

(a)

(b)

Figure 2.12 (a) Sharp absorption spectrum for a single isolated molecule, and (b) broadened line for a gas containing many molecules (Ulaby et al. 1981).

2.5.2 Radiative transfer model (clear sky)

Radiative transfer is the exchange of energy between the Earth's surface and the different layers of the atmosphere. The Earth emits radiation in the microwave region depending on its emissivity, and this radiation is attenuated by the atmosphere. The atmosphere also emits microwave radiation. In the microwave region, absorption and emission by the atmosphere is mainly due to water vapour and oxygen (section 2.5.1). The microwave radiation emitted by the atmosphere can be divided into two components as shown in figure 2.13: upwelling radiation and downwelling emission. The downwelling emission is reflected at Earth's surface and attenuated by the atmosphere. This energy exchange is called radiative transfer. The following is a mathematical description of this process.

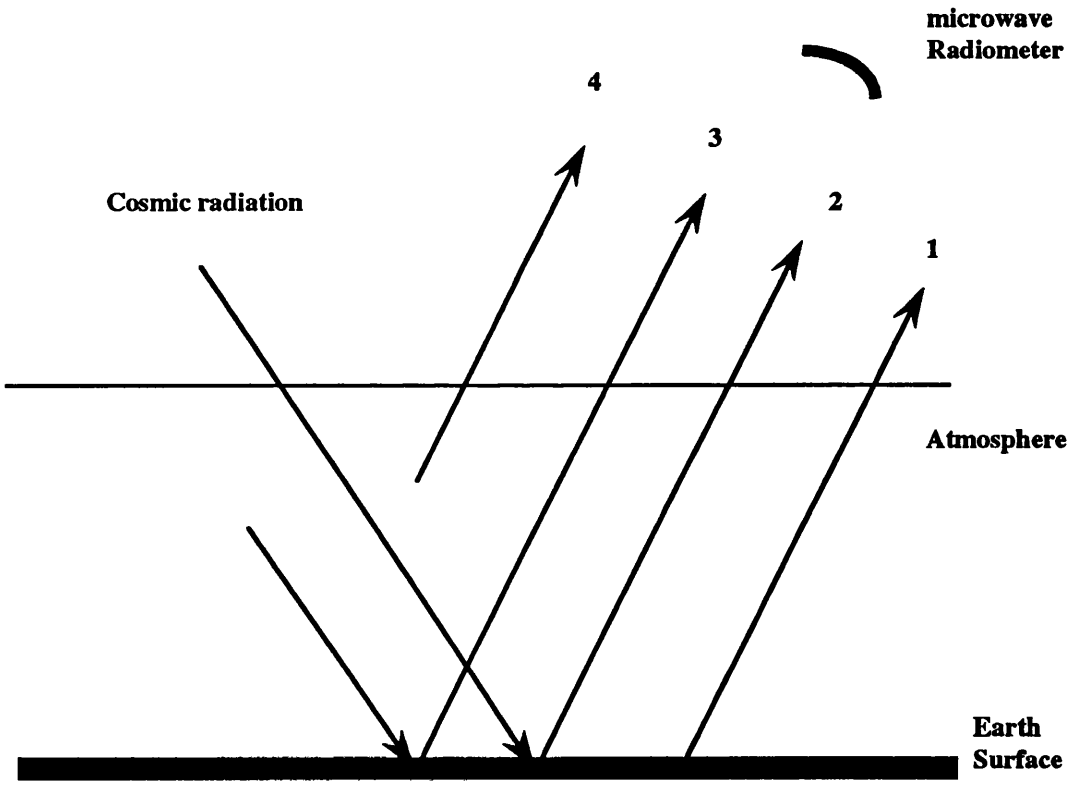

Figure 2.13 Contributions to satellite brightness temperature measurement from Earth's surface and the atmosphere.

1 is the ground brightness temperature attenuated by the atmosphere.
2 is the cosmic background radiation attenuated by the atmosphere, then reflected by the surface and then attenuated again by the atmosphere.
3 is the downwelling atmospheric emission, reflected by the surface and then attenuated by the atmosphere.
4 is the upwelling atmospheric emission by the atmosphere.

The Radiative transfer equation in the microwave region

The radiative transfer equation is a differential equation which describes the intensity of radiation leaving a small element dz. The total radiation received at the satellite is the integral of this equation. The classical work for radiative transfer theory and an extensive treatment of the equation of transfer is given by Chandrasekhar (1960). Here only the summary of radiative transfer theory as described by Ulaby et al. (1981) is given.

For a scatter-free medium, the loss in brightness by absorption due to the propagation over the thickness dr and cross section dA for a small cylindrical volume, as shown in figure 2.14, is given by:

$$dB(absorption) = \kappa_a B\, dr \tag{2.25}$$

where κa is the absorption coefficient

At the same time the amount of radiation emitted by the same cylindrical volume:

$$dB(emission) = \kappa a\, J\, dr \tag{2.26}$$

where J for a scatter-free medium is called the source function for absorption or emission (in thermodynamic equilibrium, thermal emission has to be equal to absorption).

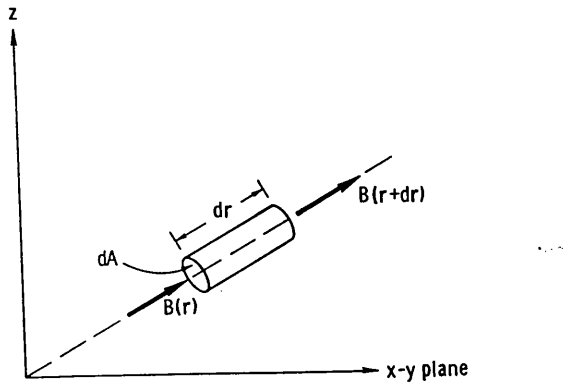

Figure 2.14 Radiation transfer across an infinitesimal cylinder (Ulaby et al. 1981)

The difference between the microwave radiation emitted and absorbed by the cylinder is given by:

$$dB = B(r+dr) - B(r) \tag{2.27}$$

or

$$dB = \kappa_a J\, dr - \kappa_a\ B\, dr = \kappa_a\ dr\,(J - B) \tag{2.28}$$

where $B(r)$ and $B(r+dr)$ are the radiation entering and leaving the cylinder respectively.

Equation (2.28) is a differential equation (called equation of transfer) which may be written as:

$$\frac{dB}{d\tau} + B = J \tag{2.29}$$

where an increment of optical depth $d\tau$ is equal to $\kappa_a\, dr$.

Ground emission and upwelling atmospheric emission

The integral of equation (2.29) gives the solution for the brightness $B(r)$ at any point r., Ulaby et al. (1981):

$$B(r) = B(0)e^{-\tau(0,\,r)} + \int_0^r K_a(r')J(r')e^{-\tau(r',r)}dr' \tag{2.30}$$

where, $B(0)$ is the brightness at the boundary, reduced in magnitude by $e^{-\tau(0,\,r)}$ due to extinction by the material between 0 and r. The second term represent the sum of contributions from infinitesimal thickness, each dr' in length. The contribution from a layer at point r' is given by $\kappa_a(r')J(r')dr'$, reduced by $e^{-\tau(r',r)}$ due to extinction by the material between the layer at point r' and r.

As Rayleigh-Jeans law is used in the microwave region, (2.30) can be written in terms of apparent temperature T_{AP}:

$$T_{AP}(r) = T_{AP}(0)e^{-\tau(0,\,r)} + \int_0^r K_a(r')T(r')e^{-\tau(r',r)}dr' \tag{2.31}$$

where,

$$T\uparrow = \int_0^r K_a(r')T(r')e^{-(\tau up(r'))}dr \qquad (2.32)$$

$T\uparrow$ is the upwelling atmospheric emission, $\tau\uparrow$ is the upward atmospheric opacity:

$$\tau\uparrow = \int_0^r K_a dr \qquad (2.33)$$

Downwelling atmospheric emission

The atmosphere emits microwave radiation directed down to the Earth's surface. Then the radiation is reflected by the surface back to the microwave radiometer. This radiation is called the downwelling radiation:

$$T\downarrow = \int_r^0 K_a(r')T(r')e^{-(\tau dn(r'))}dr \qquad (2.34)$$

The apparent temperature as seen by the satellite microwave radiometer

The general solution of the radiative transfer equation at the top of the atmosphere gives the apparent brightness temperature at microwave frequency ν:

$$T_B^* = T_{GB}e^{-(\tau\uparrow)} + T\uparrow + (1-\varepsilon)(T\downarrow + T_{sky}\, e^{-(\tau\downarrow)})e^{-(\tau\uparrow)} \qquad (2.35)$$

where T_B^* is the apparent brightness tempertaure, T_{sky} is the cosmic background radiation, T_{GB} (ground brightness temperature) = $\varepsilon_V T_S$, and $\tau\downarrow$ (downward atmospheric opacity) is the same as equation (2.34) except the limit of integral is from top of the atmosphere (r) to the surface (0). The values of $\tau\uparrow$ and $\tau\downarrow$ depend mostly on water vapour and oxygen constituents (for clear sky conditions). However we will assume in this study that $\tau\uparrow \approx \tau\downarrow$, as their values may be slightly different depending upon atmospheric temperature and constituent profiles (Kerr and Njoku 1990).

The first term in equation (2.35) represents the ground emission reduced by the factor $e^{-(\tau\uparrow)}$ which is called the fractional transmission (t_V,). The second term is the upwelling atmospheric emission. The third term is the cosmic atmospheric emission T_{sky} attenuated by the atmosphere plus the downwelling atmospheric emission, reflected by $r = 1 - \varepsilon$ and then attenuated by the atmosphere.

Equation 2.35 shows that variations in the true surface emissivity will affect the contributions from the reflected microwave atmospheric emission and the ground emission to the apparent brightness temperature. The emissivities in the microwave region varies over very wide range (figure 2.15). The emissivity ranges of this figure are based on a theoretical models and experimental observations reported in the literature for frequencies in the 1-100 GHz range (Ulaby et al. 1982). The ranges shown in this figure are due to variations of emissivity with frequency, convolved with variations due to conditions (i.e. variations of surface parameters). The atmospheric effect in the microwave region increases significantly at different terrestrial surfaces, as the downwelling atmospheric emission reflected by the surface increases with decreasing emissivity (chapter 4).

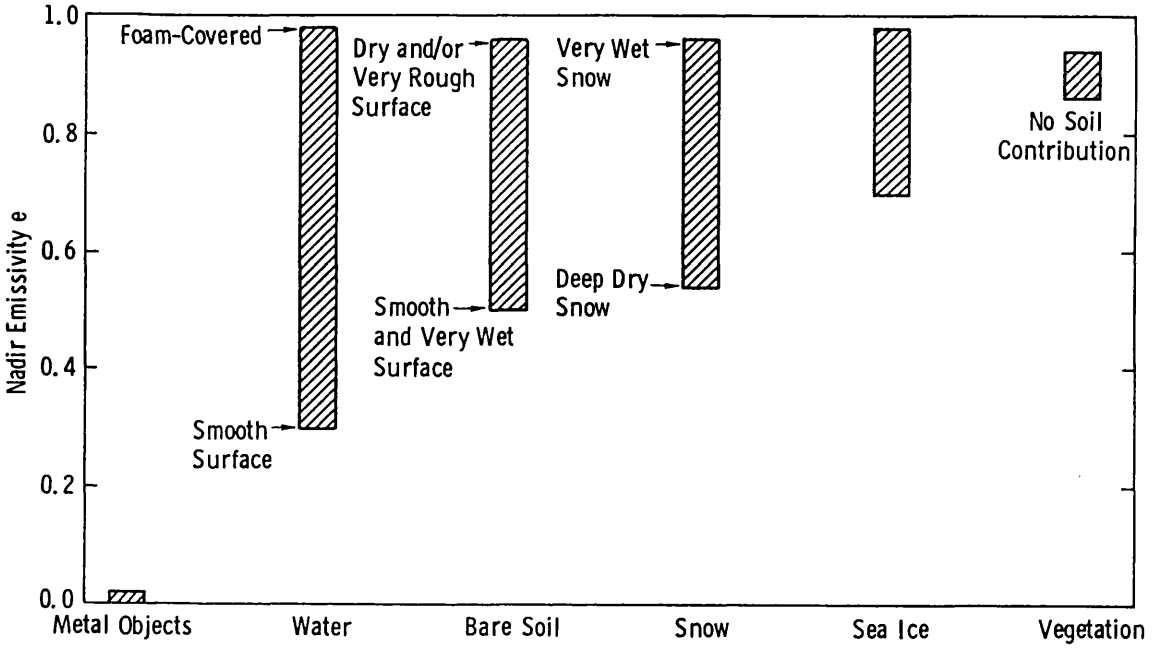

Figure 2.15 Range of values that the microwave nadir emissivity may cover for a different terrestrial surfaces (Ulaby et al. 1982).

2.6 Summary

In this chapter the following aspects of microwave emission have been demonstrated:

- Rayleigh-Jean's approximation of Planck's law for Blackbodies, and Kirchhoff's law for grey bodies give the well known relation between microwave radiometric brightness temperature and physical emissivity: $T_B = \varepsilon_V Ts$. Emissivity is calculated from reflectivity by the following relation: $\varepsilon_V = 1 - \Gamma_V$. This relation is derived from conservation of energy and Kirchhoff's law of thermal equilibrium.

- Surfaces used in this study can be considered approximately homogeneous and therefore we can use Fresnel reflectivities . Infrared radiometers retrieve the surface temperature (see chapters 3&4) and not the effective temperature. Therefore, the approximation of constant temperature profile is necessary when most of the microwave emission from soil comes from 1 to 50 cm. The uniformity of the temperature profiles is a good approximation from 6 p.m. to 6 a.m. for cool months (England, 1990). Over the ocean, microwave emission depth decreases from 1 cm at 1 GHz to 1 mm at 16 GHz (Ulaby et al. 1986). The approximation of constant temperature profile over the ocean surface is fairly well, as we will be using 37 GHz over the ocean in this study (Ulaby et al. 1986) (see chapter 5).

- Surface emission models for both soil and ocean depend on various geophysical parameters. The sensitivity of microwave emission on these parameters has been demonstrated. The models which are used in both validation and application of the new technique in this thesis have been reviewed. These models are:

    a. Dobson et al. (1985) for dielectric constant of soil.
    b. Mo and Schmugge (1987) for the effect of soil roughness on emissivity.
    c. Wilheit (1979) for the ocean surface.

- The effect of the atmosphere on the satellite measurement of microwave emission has been demonstrated through the radiative transfer process for clear sky conditions. The atmospheric radiative transfer model used in the simulation of the new technique (chapter 4) is that of Ulaby et al. (1986) but modified with the absorption coefficients of oxygen provided by Rosenkranz (1988). Finally, the atmospheric effect and its dependence on surface emissivity was briefly addressed. Chapter 4 will address this problem in more detail and a new technique to correct for the satellite microwave emissivity is presented.

Chapter 3

Satellite Radiometer Systems Used in this Study

3.1 Introduction

In this study, the atmospheric correction technique used in the retrieval of true surface microwave emissivity from the apparent microwave emissivity as seen by satellite (described in chapter 4) uses two types of passive satellite radiometers: microwave and infrared. Microwave radiometer measurements of brightness temperature, T_B^*, together with the surface physical temperatures, T_S, corrected from the brightness temperature of the infrared radiometer are used to determine the apparent microwave emissivity. The microwave apparent emissivity, εv^*, as seen by the satellite is given by:

$$\varepsilon_v^* = \frac{T_B^*}{T_S} \tag{3.1}$$

The accuracy in correcting the apparent microwave emissivity in equation (3.1) for atmospheric effects is expected to be limited by the radiometric noise from the microwave and infrared. The assessment of how much this effect will be, is demonstrated in chapter 4. Note that the microwave and infrared instruments have different spatial resolutions, and thus must be taken into account, especially if the surface is non uniform in its temperature or emissivity.

In this chapter, the microwave and infrared radiometers used in this work are described in terms of their characteristics, performances, radiometric resolution, calibration, and accuracy.

3.2 Microwave radiometers

A microwave radiometer measures the intensity of microwave radiation from the target. It is a system that receives and processes emitted radiation from a target at a physical temperature greater than zero Kelvin. The microwave portion of the spectrum extends from frequencies near 1 GHz to frequencies of ~ 300 GHz. In wavelengths this is approximately from 30 centimetres to 0.1 centimetres. This region is bounded at the low frequency end by the UHF radio band (Ultra-high-frequency), where noise in the form of television broadcasting and other man-made sources make remote sensing difficult, and at the high frequency end by the far infrared or submillimeter frequencies at which alternative techniques for detection become practical (NASA, 1987).

At low microwave frequencies, the water vapour in the atmosphere has very little effect upon satellite brightness temperature measurements, even in cloudy conditions, as shown in figure 3.1. At higher microwave frequencies there is a stronger atmospheric effect, although at frequencies away from resonance absorption lines of common atmospheric gases the effect is small compared with the infrared. For clear sky conditions, the radiation received by a microwave antenna is due to upwelling emission from the surface and the atmosphere, combined with downwelling atmospheric emission and sky radiation reflected by the surface.

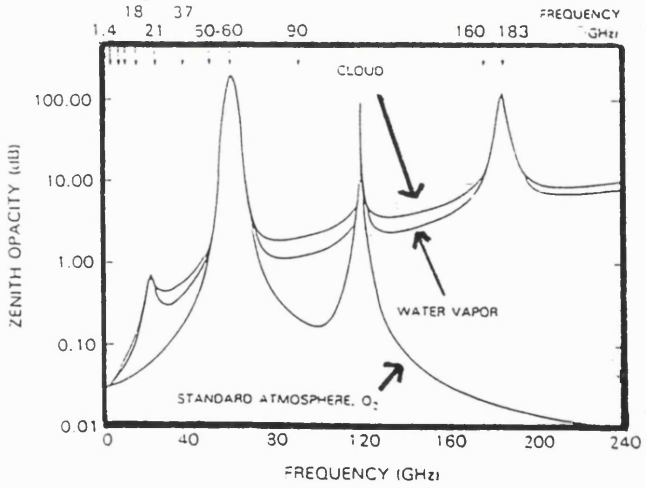

Figure 3.1 The dependence of microwave absorption in the atmosphere on different microwave frequencies. The lower curve shows the atmospheric opacity due to oxygen. The middle curve is due to water vapour with total water vapour content of 20 kg/m2 (the water vapour is added to the oxygen). The upper curve is due to 0.2 kg/m2 stratus cloud added to oxygen and water vapour. (NASA, 1987)

Microwave sensors are of two types: thermal microwave imaging sensors and microwave sounders. Thermal imaging sensors scan the surface and measure the emission in atmospheric transmission windows. They are used for land, ocean, or ice applications. Microwave sounders provide information about vertical profiles of temperatures and species concentration by sensing the emitted radiation at different heights in the atmosphere. In addition to using near resonance frequencies, sounders also operate at window frequencies, where they may be useful for land, ocean, or ice applications. However, they have a very limited global coverage, as they are nadir-looking only.

Microwave Radiometer Terminology

The following is a brief summary of terminology relevant to this study:

1. Antenna patterns

If the received power is constant, then as the angles (θ, ϕ) vary, where θ and ϕ are spherical angles as shown in figure 3.2(a), the received power $P_r(\theta, \phi)$ will also vary. A polar or rectangular graph of this function is known as antenna power pattern, and normally will be composed of a main lobe, sidelobes and backlobes (Colwell, 1983), as shown in figure 3.2(b). The width of the main lobe at half-power point is known as the half-power beamwidth (HPBW). The HPBW depends on the wavelength of the target radiation, λ, and on the diameter of the antenna, D. For a parabolic antenna:

$$HPBW = a\frac{\lambda}{D} \tag{3.2}$$

where a is a constant approximately equal to 1.2.

The $HPBW$ of the antenna and the height of the satellite, h, determine the spatial resolution, see figure 3.4:

$$Spatial\ resolution = HPBW \times h \tag{3.3}$$

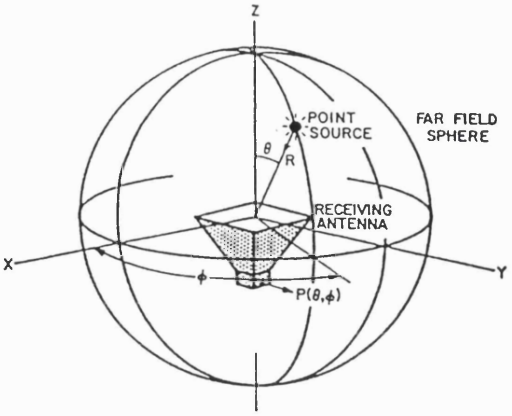

Figure 3.2 The geometry for describing the received antenna pattern (Colwell, 1983).

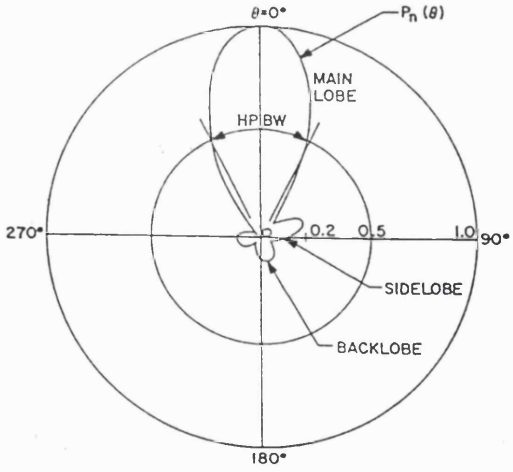

Figure 3.3 Antenna pattern in polar form. (Colwell, 1983)

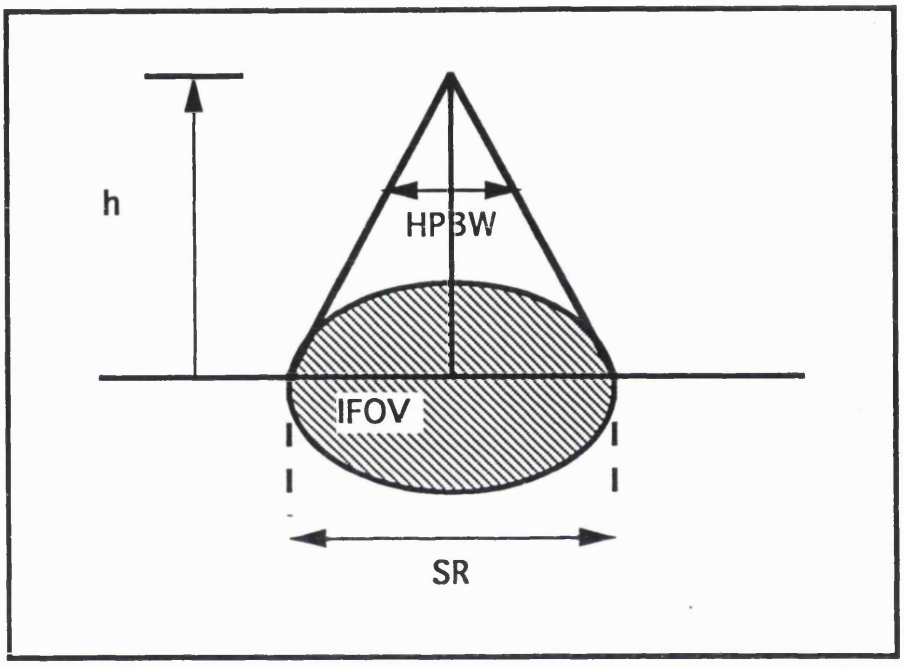

Figure 3.4 The spatial resolution and the Instantaneous Field of View (IFOV) for a nadir-pointing antenna (with circular symmetric pattern). The height of the satellite is h, the half-power beamwidth is (HPBW), and SR is the spatial resolution.

So, for a higher resolution, larger antenna is needed. For example an antenna of 100m in diameter would be needed for a wavelength between 10 cm and 20 cm in order to obtain a resolution of 1 km from low Earth orbit (~ 400-800 km).

2. Antenna Gain

The gain of an antenna is determined by both the shape of the radiation pattern and the antenna loss, and is a measure of antenna performance. The gain $G(\theta, \phi)$ of an antenna in the direction (θ, ϕ) is defined as the ratio of the power density radiated by the subject antenna to the power density radiated by a lossless isotropic antenna (Ulaby at al. 1981):

$$G = \frac{4\pi A_{eff}}{\lambda^2} \tag{3.4}$$

where A_{eff} is the effective area, which is 40% - 80% of the physical aperture of the antenna and is calibrated generally prior to launch.

3. Antenna temperature

The antenna temperature T_A is related to the power received by a radiometer antenna P_A, the bandwidth B, and the receiver gain G by equation (3.5) as follows (Pedersen 1990) :

$$T_A = \frac{P_A}{kBG} \tag{3.5}$$

where k is Boltzmann's constant.

Equation (3.5) is for an ideal radiometer which has no noise, but in fact the electronic components in real radiometers will add noise to the desired signal. This noise is referred to as the equivalent noise source T_N. Therefore the power received by a radiometer is:

$$P_A = k\,B\,(T_A + T_N)\,G \tag{3.6}$$

In order to reduce the effect of variations in T_N, a Dicke switch is used (Ulaby et al. 1981). A Dicke switch changes periodically at a high rate between the incoming signal and a known reference source T_{ref}. Before integration, the signal from the power detector is multiplied by +1 if the switch is in the T_A position and by -1 if in T_{ref} position, resulting in subtraction of the signal in the integrator (Pedersen 1990). Therefore the power received by a radiometer is corrected for measurement noise, and it will be

$$P_A = k B (T_A + T_N) G - k B (T_{ref} + T_N) G = k B (T_A - T_{ref}) G \qquad (3.7)$$

The relation between the antenna temperature and scene brightness temperature:

If the scene observed by the antenna is characterised by uniform brightness temperature T_B, then $T_A = T_B$. But T_A represents all radiation incident upon the antenna and integrated over all possible directions and weighted according to the antenna directional pattern represented by the gain pattern $G(\theta,\phi)$. If $d\Omega$ represents the element solid angle then T_A is (see figure 3.5) :

$$T_A = \frac{1}{4\pi} \iint_{4\pi} TB(\theta,\phi) G(\theta,\phi) d\Omega \qquad (3.8)$$

Consequently, microwave radiometric measurements are susceptible to contributions by brightly emitting objects of surface segments which lie in the sidelobes.

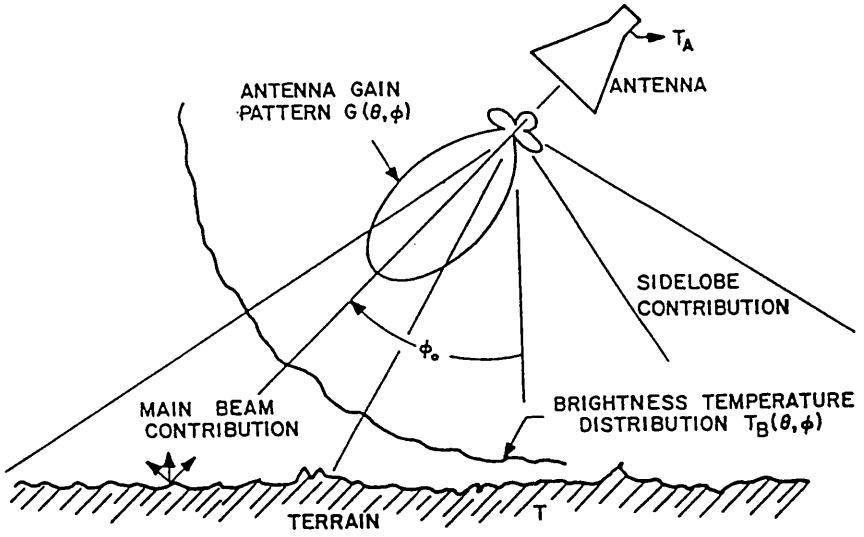

Figure 3.5 Geometry showing the gain weighted sum of the individual brightness temperatures from each direction (Colwell, 1983).

Radiometric calibration

A radiometer is said to be calibrated when an accurate and precise relationship has been established between the receiver output voltage and the antenna integrated absolute brightness temperature. There are two steps in the radiometric calibration (Ulaby et al. 1981). The first step is to relate the receiver output (voltage, count) to the noise temperature at the radiometer input. This is achieved by measuring the output as a function of noise temperature T_{cal} of a calibration source connected to the radiometer input. The resultant relationship between the output indicator and T_{cal} provides the scale factor for calibration to get the antenna radiometric temperature. This is called the receiver calibration step. The second step involves relating the antenna radiometric temperature to the radiative properties of the scene. The antenna radiometric temperature consists of three contributions: (1) energy received through the mainlobe, which is related to the energy radiated from the scene; (2) sidelobe contributions (this is energy received from directions outside the antenna mainbeam); and (3) thermal energy emitted by the antenna. Therefore it is necessary to the know the radiative properties of the antenna with high accuracy in order to separate factor (1), which we are interested in from the others.

Radiometric error sources

The radiometric contribution to the brightness temperature errors are mainly of two types (Bernard et al 1993):

A. The radiometric resolution (radiometric sensitivity) is defined as the smallest change in the antenna radiometric temperature that can be detected by the radiometric output (Ulaby et al. 1981). This is a small error source, reduced by time integration. It defines the minimum detectable temperature variations. In a Dicke radiometer, the minimum detectable temperature variation is given by:

$$\Delta T = 2\,(T_{ref} + T_{RC})/(Bt)^{1/2} \qquad (3.9)$$

where T_{ref} as defined before, T_{RC} is the receiver input noise, B is the receiver bandwidth, and t is the integration time. Therefore we can see that the radiometric resolution will improve with increasing bandwidth and integration time.

B. The absolute accuracy of antenna radiometric temperature is dictated by the accuracy with which the absolute values of the calibration noise temperature are known. Absolute calibration errors can be either from on ground or in flight calibration errors:

3.2.1 ERS1 Microwave Sounder (ATSR/M)

The microwave sounder (MWS) was designed and built by the Centre de Recherches en Physique de l'Environnement (CRPE). It is physically attached to the infrared radiometer called Along Track Scanning Radiometer (ATSR), (see figure 3.6), aboard the European Space Agency's satellite ERS-1 that was launched in July 1991. ERS-1 is in a retrograde, sun-synchronous orbit at an altitude of 777 km, and orbital inclination of 98.6°. Repeat cycles of 3, 35, and 176 days are achieved throughout the mission by making slight adjustments to the spacecraft's altitude.

The main purpose of the MWS is to measure the tropospheric path delay to determine the range correction of the altimeter radar, through the measurement of the integrated water vapour content, and the attenuation of the altimeter signal by liquid water. It provides a measurement of atmospheric liquid water and water vapour over the ocean and in principle may provide soil moisture and surface emissivity measurements over land (Bernard et al. 1993).

The MWS measures the brightness temperature in two channels, 23.8 and 36.5 GHz, each with a 200 MHz bandwidth. Each channel operates in a Dicke mode, comparing the antenna temperature to an internal reference temperature at a switching frequency of 1 KHz. The radiometric resolution of MWS is 0.4 K for the basic time sampling interval (0.15s), and is reduced with temporal integration.

The raw output signal, synchronized with the ATSR scan rate, is integrated and sampled every (0.15s). This signal, together with the reference load temperature and other internal temperatures are transmitted to the ground (Bernard et al. 1993). Internal calibration is done by connecting the antenna input either to the sky horn receiving the cold sky background temperature, or to a second internal reference load.

The main antenna is an offset reflector antenna of diameter 0.6 m, with one feed horn for each frequency. Each channel is pointing at an angle close to the nadir, the 36.5 GHz channel slightly in the forward direction, the 23.8 GHz slightly in the backward direction, as illustrated in figure 3.7. Each channel is linearly polarized in the orbit plane (vertical polarization). The sky horn is a 7.5 cm in diameter. It is pointed into space and is used in the MWS calibration.

The absolute calibration error is less than 3 K. This error is mostly dependent on side lobe contributions (Bernard et al. 1993).

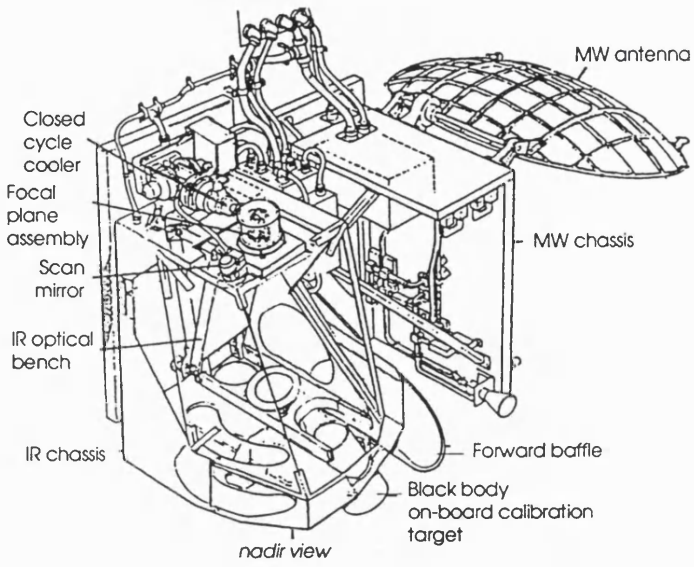

Figure 3.6 The Along Track Scanning Radiometer. This diagram shows the microwave and infrared radiometers mounted on a common baseplate. (Vass and Handoll 1991)

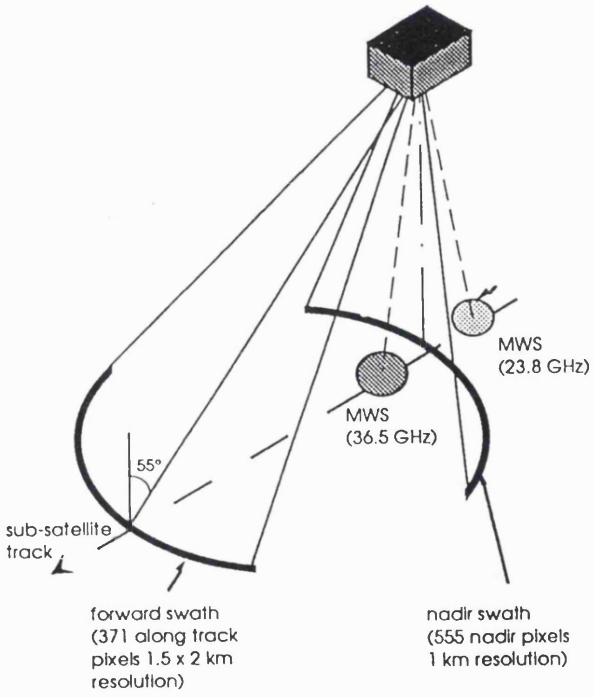

Figure 3.7 Geometry of the two ATSR/M channel field of view and ATSR : Scans projected on to the Earth's surface. The 36.5 GHz channel is pointed forward, and the 23.8 GHz channel backward (Vass and Handoll 1991)

3.2.2 TOPEX Microwave Sounder

TOPEX/Poseidon satellite launched in August 1992 carries a microwave radiometer called TMR (TOPEX Microwave Radiometer). TMR is a NASA instrument which is used to correct the error in the altimeter measurement of height due to water vapour. The radiometer measures the brightness temperature at nadir at three frequencies (18 GHz, 21 GHz, and 37 GHz).

The antenna is an offset parabolic antenna of 74 cm diameter. The brightness temperature from the Earth's surface is averaged over a period of one second. The radiometer uses refurbished electronics from Nimbus-7 scanning multi-channel microwave radiometer (SMMR), but differs from this instrument in its operation (Janseen et al. 1995).

The TMR footprints are 43.4 km at 18 GHz, 36.4 km at 21 GHz, and 22.9 km at 37 GHz (Janseen et al. 1995). The net brightness temperature uncertainties range from 0.79 to 0.88 K for the three TMR frequencies, and include the radiometer calibration uncertainties range from 0.54 to 0.57 K.

3.3 Infrared radiometers

Satellite infrared radiometers are passive instruments that measure the intensity of upwelling infrared radiation. They usually operate in an imaging mode by scanning the image point across the surface using a rotator mirror. The images from these infrared radiometers provide information at much a higher spatial resolution than those from microwave radiometers. This is because the spatial resolution depends on the ratio of wavelength of radiation to the aperture of the sensing instrument and the wavelength of infrared is much shorter than that in the microwave (Cracknell and Hayes, 1991).

The disadvantage of infrared radiometry is that infrared radiation does not penetrate clouds, and in cloudy conditions it is the temperature and radiation of the upper surface of the clouds which is seen by the infrared radiometer.

Infrared radiometers measure the radiance of the electromagnetic radiation within the 3-15μm spectral region. They consist of a telescope, an optical interference filter, beamsplitter, and a detector at focal plane for each spectral band. Detector cooling (down to 100-70 K) is necessary to achieve maximum radiance resolution (Barrett and Curtis 1992).

3.3.1 ERS1 - ATSR

ATSR characteristics and operation

The Along-Track Scanning Radiometer (ATSR) was designed and constructed by a consortium, consisting of Rutherford Appelton Laboratory, Oxford University, Mullard Space Science Laboratory, UK Meteorological Office and CSIRO in Australia.

The ATSR is a four channel infrared radiometer operating at 1.6, 3.7, 11, and 12 μm. The 1.6μm channel was added to the original three radiometer channels to improve sea surface temperature retrievals by detecting cloud during day-time. Note, only three channels can be operated simultaneously, a choice having to be made between the 1.6 and 3.7μm. The 3.7μm channel failed in May 1992. These channels are spatially co-registered. ATSR observes the Earth's surface along two curved swaths, nadir and forward looking, which are produced by a scanning mirror with an axis of rotation inclined 23.45° from the vertical. Both swaths are 500 km in width, while the two views are separated by approximately 900 km in along-track distance. ATSR was

designed to provide sea surface temperature better that 0.5 K with geometric instantaneous field of view (IFOV) of 1 km square on the Earth's surface.

The ATSR optics consist of a plane, rotating scan mirror and an off-axis parabolic mirror which are gold plated for high reflectivity. The plane inclined mirror is continuously rotating to scan a cone. The scan cone is tilted forward to give the two views of the Earth at nadir, and forward along the subsatellite track at approximately 47° to the nadir (Mason 1991) of viewing vectors into the primary paraboloid and then focused into a field stop to ensure good spatial co-registration between the IFOV for each channel, (see figure 3.8). The beam diverges into the Focal Plane Assembly (FPA), where it is spectrally divided into four channels by beam splitters and blocking filters and then re-imaged on to the detectors, (see figure 3.9). The FPA is cooled to 80°K to enable detectors to function and to enable radiometric accuracy by reducing the amount of radiation that would otherwise be emitted from filters themselves .

The detectors for the 1.6 and 3.7 μm channels are 200 μm square photovoltaic InSb devices, while the 11 and 12 μm channels are photoconductive HgCdTe detectors. The response of the HgCdTe is non-linear. So, at high photon fluxes this effect causes a reduction in the measured detector signal. Empirical correction factors for these channels were calculated at Oxford University (Mason 1991). The resulting radiometric accuracy for these two channels was predicted to be better than 0.05 K for scene temperatures in the range 265 K to 310 K.

A pre-launched testing was considered as an essential part of the instrument design concepts and to determine if ATSR would meet its scientific requirements. This pre-launched calibration was performed by a team at Oxford University. A detailed description of this test is found in Mason (1991).

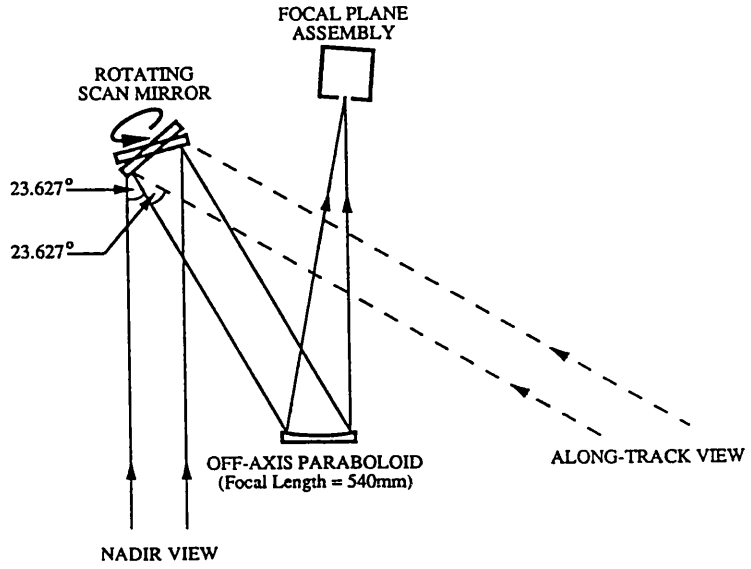

Figure 3.8 ATSR optics layout. (Mason 1991)

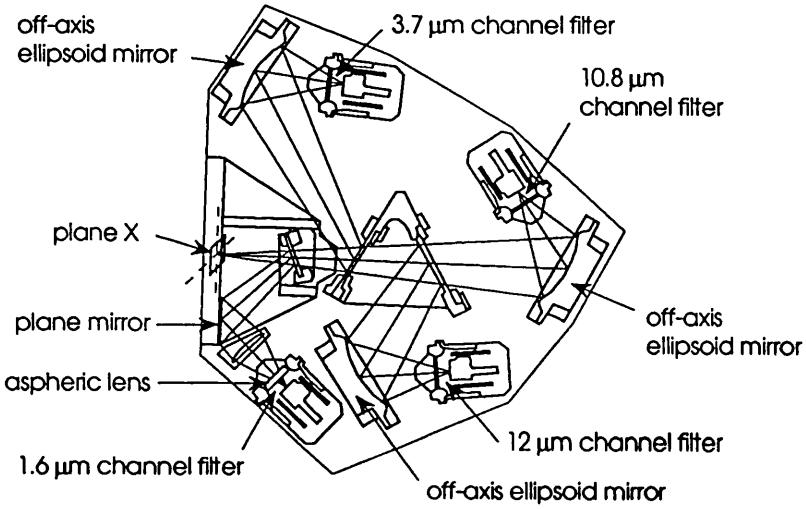

Figure 3.9 ATSR Focal Plane Assembly. (Vass and Handoll 1991)

On-board calibration

Radiometric calibration as defined by Lauritson et al. (1979) involves exposing a radiometer to sources of radiation that have been calibrated against primary or secondary standards and determining the relationship between the output of the radiometer and the intensity of the incident radiation.

ATSR needs to be calibrated continuously in flight as the detectors and electronics may suffer from unavoidable drifts in gain and offset. Two on-board calibration targets (black bodies) were designed and built by the Mullard Space Science Laboratory of University College London. Each blackbody is a cylindrical cavity, closed at one end and treated with a highly absorbing surface finish inside to achieve high emissivity. Their temperature is measured by miniature platinum resistance thermometers (PRT's). The absolute temperature readout accuracy has been calibrated to 0.01° C at the National Physical Laboratory (NPL), and over the satellite lifetime it is expected be < 0.03° C.

One of these black bodies is heated and the other floats at the fore-optics temperature. The black bodies have an emissivity exceeding 0.998 (Mason et al. 1990), and are designed to span the expected sea surface temperature range, thus providing a continuous 2-point calibration of the radiation. The absolute accuracy of this calibration is 0.1 K over a range of ~ 270 K to ~305 K (Mason et al. 1990).

3.3.2 Advanced Very High Resolution Radiometer (AVHRR)

This radiometer is operated by the National Oceanic and Atmospheric Administration of the (NOAA) of the USA. It is a scanning radiometer with four channels for the type AVHRR/1 and five channels in the visible, near infrared and thermal infrared for type AVHRR/2, carried on the near polar orbiting NOAA series of satellites. These satellites are sun-synchronous with orbits inclined at 99° to the equator and altitude around 850 km (Barrett and Curtis 1992). The satellites are sun-synchronous viewing the same point on the surface at the same local time twice a day. The AVHRR swath width is 3000 km and resolution is 1.1 km.

There are two calibrations for AVHRR : the in-orbit and the pre-launched calibrations. In-orbit calibration is necessary as sensitivity (output in digital counts per unit incident radiance) is expected to vary with orbit. Also, the instrument components age with time (Lauritson et al. 1979). The in-orbit calibration of the infrared channels in AVHRR is obtained from measurements of radiation emitted by an internal calibration target (ICT) and space. This gives two points on a calibration curve and would determine the calibration assuming that the responses of AVHRR channels were linear. However, the responses in channels 4 and 5 are not linear because these channels use photoconductive HgCdTe detectors. Neglecting the nonlinearity in the two channels may cause errors of several degrees in the scene temperatures Weinreb et al. (1990). Therefore, a nonlinearity correction before launch is calculated to provide a tabulated correction against scene temperature for users. The absolute radiometric accuracy of AVHRR data that have been corrected for nonlinearity is approximately 0.55° C, of which 0.35°C is traceable to the calibration of the laboratory blackbody.

Pre-launch calibration is needed to obtain two main calibration coefficients. The first one is to get the coefficients for calibrating the temperature sensors (PRT) in the internal blackbody of AVHRR. The second is to get coefficients to account for the nonlinearity of the AVHRR detector response. More details for the pre-launched calibration to get the coefficients of PRTs and nonlinearity response of AVHRR are found in (Weinreb et al. 1990).

3.4 Summary

In this chapter the following aspects of microwave and infrared radiometers have been considered :

- **Characteristics**

- Microwave sounders look only at nadir and therefore they have a very limited global coverage. The microwave sounders used in this study are: ATSR/M operating at 35.5 GHz and 22.8 GHz, and TMR operating at 18 GHz, 21 GHz, and 37 GHz.

- Infrared radiometers usually operate in an imaging mode by scanning the image point across the surface using a rotating mirror. The infrared radiometers used in this study are: ATSR operating at four channels of which two are in the thermal infrared (~11μm, and ~12 μm) and AVHRR on NOAA-11 and NOAA-12 operating at five channels, again two of which are in the thermal infrared (~11μm, and ~12 μm).

- The spatial resolution of microwave radiometers is poor compared with infrared radiometers. The ATSR and AVHRR spatial resolution is 1 km, while it is ~20 km for the ATSR/M frequencies. For TOPEX microwave radiometer it ranges from ~45 km at 18 GHz to ~24 km at 37 GHz.

- The ATSR/M radiometric resolution is 0.4 K. The absolute accuracy of the ATSR/M thought to be better than 3 K

- The net brightness temperature uncertainties range from 0.79 to 0.88 K for the three TMR frequencies, and include the radiometer calibration uncertainties range from 0.54 to 0.57 K.

- The ATSR radiometric accuracy is better than 0.05 K for scene temperatures in the range 265 K - 310 K, while the AVHRR radiometric accuracy is ~ 0.5 K.

- **Advantages and disadvantages**

- Although the low microwave frequencies (e.g. 1.4 GHz, 6 GHz) are subject to small atmospheric effects, even in cloudy conditions, their spatial resolution is

poor compared with higher microwave frequencies (e.g. 18 GHz) which are affected more by atmosphere.

- Microwave radiometers suffers from large error due to poor absolute calibration. Absolute calibration errors are caused mostly by unknown side lobe contributions.

- Infrared radiometers can not image the surface in cloudy conditions.

- **Implications for the technique described in this thesis**

- The new technique proposed in this thesis is applied only for non-cloudy conditions.

- It is necessary to average the infrared data over the microwave footprint as the spatial resolution for the microwave footprint is much larger than that for the infrared.

- Radiometric noise, especially from the microwave radiometers are significant. Therefore, it is necessary to consider the effect of measurement noise on the atmospheric correction technique proposed in the next chapter.

Chapter 4

A New Technique for Atmospheric Correction of Microwave Emissivity

4.1 Introduction

The microwave surface emissivity is an important parameter because it is determined by physical surface characteristics which are of importance to climate studies. In principle, satellite remote sensing offers the global data sets which are required for climate studies (chapter 1). However the required accuracy of microwave surface emissivity is different for different physical parameters. For example, the fractional soil moisture accuracy needed for soil moisture retrieval for the validation of climate models is 0.02 for the 100 km resolution grid (Rowntree, personal communication). This is translated to an accuracy of ~ 0.02 in microwave emissivity. Since atmospheric variability affects the satellite observed microwave radiance, the accuracy in retrieving the true surface emissivity will be degraded (e.g. Wang et al. 1992; Choudhury, 1993). Therefore, atmospheric correction should be an important consideration.

In this chapter, a novel technique to correct and retrieve microwave surface emissivity from atmospheric effects using simultaneous measurements from passive and infrared radiometers is proposed. Radiative transfer simulations using a microwave atmospheric model and a set of different atmospheres are used. This technique offers a significant improvement in terms of emissivity accuracy compared with the current methods (see chapter 1). It provides an independent method for correcting the satellite microwave data for atmospheric effects without the need to use additional information about any atmospheric parameters (e.g. simultaneous meteorological data).

4.2 Theoretical Approach

The microwave radiation received by the satellite comes from four sources, as shown in figure 2.14 in chapter 2:

1. The terrestrial surface microwave emission (which we are attempting to measure) attenuated by the atmosphere.
2. The cosmic background radiation attenuated by the atmosphere, then reflected by the surface and again attenuated by the atmosphere.
3. The downwelling atmospheric emission, reflected by the surface and then attenuated by the atmosphere.
4. The upwelling atmospheric emission of the atmosphere.

The apparent microwave brightness temperature measured by the satellite radiometer, TB^*, at a microwave frequency ν, is the sum of the four components described above.

Writing equation (2.35) again as follows :

$$TB^* = \varepsilon_V T_S t_V + T\downarrow'(1-\varepsilon_V) t_V + T\uparrow \tag{4.1}$$

where $T\downarrow' = (t_V T_{sky} + T\downarrow)$ and t_V, ε_V, $T\downarrow$, $T\uparrow$, T_{sky}, and T_S are as defined in chapter 2.

For a given atmosphere, as the surface microwave emissivity decreases, the contribution from the downwelling reflected atmospheric emission (source 3) increases due to the corresponding increase in surface reflectivity. At the same time, the contribution from (source 1) decreases due to the decrease of surface emissivity. This will be referred to as the surface microwave emissivity effect.

For a given emissivity, but for different atmospheres (different in water vapour and temperature profiles), the attenuation due to water vapour increases as the water vapour content increases, therefore the contribution from source 1 will decrease. At the same time the reflected downwelling atmospheric emission (source 3) and the upwelling atmospheric emission increase as total water vapour increases (source 4). This will be referred to as the water vapour effect. Approaches to correct these surface microwave emissivity and water vapour effects are demonstrated.

First order correction

Dividing equation (4.1) by the true surface temperature T_S, it is possible to derive the apparent microwave emissivity, ε_V^*, as seen by the satellite radiometer:

$$\varepsilon_V^* = \varepsilon_V (t_V - \frac{T\downarrow' t_V}{T_S}) + \frac{T\downarrow' t_V}{T_S} + \frac{T\uparrow}{T_S} \tag{4.2}$$

$$\text{where, } \varepsilon_V^* = \frac{T_B^*}{T_S} \tag{4.2a}$$

Equation (4.2) describes a linear relation between the apparent microwave emissivity and different true surface microwave emissivities, for a given atmosphere. The slope and intercept of this equation depend on total water vapour at a given microwave frequency (which will be demonstrated in the simulation in section 4.4).

We now assume a set of N different atmospheres each with a value of t_V, $T\downarrow$, and $T\uparrow$ that may be calculated in each case (section 4.3) using the microwave atmospheric model described in chapter 2.

The value of Ts adopted is the same as that for the near surface air temperature Ta from each atmosphere. This is a reasonable approximation for both day and night over the ocean (Minnett, 1986) and deserts at night time (Choudhury, 1993). Note that even for day time, when the difference between the surface and air temperatures can go up to 15 degrees over deserts (Choudhury, 1993), the effect of this difference upon the apparent emissivity in equation (4.2) is very small (~ 0.001 to 0.002).

By taking the mean of the N values of t_V, $T\downarrow$, $T\uparrow$, and T_S, it is possible to write equation (4.2) as :

$$\varepsilon_V^* = (a-b)\,\varepsilon_V + (b+c) \tag{4.3}$$

where

$$a = \overline{t_V}, \tag{4.3a}$$

$$b = \frac{\overline{T'\downarrow}\,\overline{t_V}}{\overline{T_S}}, \tag{4.3b}$$

$$c = \frac{\overline{T\uparrow}}{\overline{T_s}} \tag{4.3c}$$

Equation (4.3) gives the apparent microwave emissivity in terms of the true surface microwave emissivity but for the mean atmospheres. Next, this equation will be used in the first order correction. A first order correction to the apparent emissivity may be estimated through the application of the mean atmospheric properties as follows:

Subtracting the true surface emissivity ε_V from both sides of equation (4.3), we will have:

$$\varepsilon^* - \varepsilon_V = (a - b)\,\varepsilon_V + (b + c) - \varepsilon_V \tag{4.4}$$

$$\Delta\varepsilon_1 = (a-b-1)\,\varepsilon_V + (b+c)$$

where $\Delta\varepsilon_1$ is the first order correction which is equal to $\varepsilon^* - \varepsilon_V$

From equation (4.3) the true surface emissivity, ε_V, can be written as:

$$\varepsilon_V = \frac{\varepsilon^* - (b+c)}{(a-b)} \tag{4.5}$$

Substituting for ε_V in the right hand side of equation (4.4), we derive a first order correction $\Delta\varepsilon 1$

$$\Delta\varepsilon_1 = (a-b-1)\left(\frac{\varepsilon^* - (b+c)}{(a-b)}\right) + (b+c)$$

$$= \frac{(a-b-1)\varepsilon^*}{(a-b)} - \frac{(a-b-1)(b+c)}{(a-b)} + (b+c)$$

$$= \left(1 - \frac{1}{(a-b)}\right)\varepsilon^* + (b+c)\left(1 - \frac{(a-b-1)}{(a-b)}\right)$$

$$= \left(1 - \frac{1}{(a-b)}\right)\varepsilon^* + \frac{(b+c)}{(a-b)} \tag{4.6}$$

The coefficients in equation (4.6) are independent of the true surface emissivity and they are dependent mostly on the amount of water vapour in the atmosphere.

The microwave emissivity after first order correction, ε_1, is :

$$\varepsilon_1 = \varepsilon^* - \Delta\varepsilon_1$$

$$= \varepsilon^* - \left(\left(1 - \frac{1}{(a-b)}\right) \varepsilon^* + \frac{(b+c)}{(a-b)} \right) \qquad (4.7)$$

The first order correction, as we will see later on, corrects for the effect of surface emissivity.

Second order correction

It is possible to derive a second order correction to the estimate of surface emissivity that accounts for the effect of water vapour in a specific atmosphere. This correction assumes that any residual following the first order correction is due principally to the mean atmospheric parameters - chiefly due to variations in atmospheric water vapour.

A residual error in microwave emissivity after the first order correction, $\Delta\varepsilon_2$:

$$\Delta\varepsilon_2 = \varepsilon_1 - \varepsilon_V \qquad (4.8)$$

The second correction makes use of two microwave radiometer frequencies, one of which is more sensitive to atmospheric water vapour than the other. The coefficients of the second correction, which accounts for atmospheric water vapour, are calculated from the least squares fit of residuals in emissivity after first order correction, $\Delta\,\varepsilon_2$, against the difference in microwave brightness temperature at two frequencies for N different atmospheres.

The microwave emissivity after second order correction, ε_2, is:

$$\varepsilon_2 = \varepsilon_1 - (m\,(TB_{V1} - TB_{V2} + n) \qquad (4.9)$$

where m is the slope, and n is the intercept of the least square fit of residuals

Any intrinsic errors in this procedure will result from third order atmospheric effects, $\Delta\varepsilon_3$

$$\Delta\varepsilon_3 = \varepsilon_2 - \varepsilon_V \qquad (4.10)$$

$\Delta\varepsilon_3$ is the residual after the second correction.

The second order correction, as we will see later on, corrects for the effect of water vapour.

4.3 Methodology

4.3.1 Generating the Correction coefficients

The coefficients of the first and second order corrections are generated from simulations using a microwave atmospheric model for a set of N different atmospheres provided by radiosonde* measurements. The simulation at each atmosphere is run for a range of all possible value of terrestrial microwave emissivities. The simulations are based on a microwave atmospheric model described by Ulaby et al. (1981) (see chapter 2) but modified for the absorption coefficient of oxygen as given by Rosenkranz (1988).

The simulations predict upwelling and downwelling emission and opacities (see section 2.5.2) for each atmosphere in an N radiosonde set and at each surface emissivity. From the predicted atmospheric parameters, the apparent brightness temperatures and emissivities as seen by the microwave radiometer are calculated for different atmospheres. To determine how apparent emissivity, ε^*, varies as a function of the true surface emissivity (ε_V), we vary ε_V through all likely values for terrestrial surfaces in incremental steps.

The following are the inputs of the simulation of the microwave atmospheric model:

1. The microwave frequency of interest.

2. A radiosonde set with N different atmospheres.

3. A range of all possible terrestrial emissivities for ocean and land from 0.4 to 1.0 with increments of 0.01, see figure 2.16.

4. Surface temperature for each atmosphere (see section 4.2).

The simulations are carried out for each atmosphere in a radiosonde set for a given

---

* Radiosondes are free flying balloons released up into air generally at 0000 and 1200 local time daily. They climb at about 5 m/s until they burst between 20 and 30 km above sea level (McIlveen, 1992). The instrumentation consists of a small barometer, a thermometer, and a hygrometer for measuring pressure, temperature and humidity at various height levels respectively. The measurements are transmitted by radio to ground station, and the sonde's position is monitored by a radar.

microwave frequency and each given surface microwave emissivity. Each atmospheric profile is read into the model and is interpolated to fill 128 equal pressure intervals in the atmosphere (note: each atmosphere consists of measurements of pressure, temperature, and humidity at various height levels). First the model calculates the optical depth and the upwelling emission at each pressure interval starting from the bottom of the atmosphere to the current height. Inside this loop, the integration is performed to obtain the total upwelling atmospheric emission and opacity. Secondly, the same loop is run again, but this time from the top of the atmosphere to the bottom to obtain the total downwelling atmospheric emission and opacity. After running the model for all atmospheres (i.e. N times), the simulation is run again for the next given microwave surface emissivity, $\varepsilon_v + 0.01$. This simulation goes on as described above until the microwave surface emissivity is 1.0 (note: natural surfaces do not have microwave emissivity = 1.0, this value is taken only to demonstrate the simulations).

The outputs from these simulations of the microwave atmospheric model are:

1. The upwelling and downwelling emission and opacities.

2. The apparent brightness temperature and emissivity as seen by the satellite. The apparent brightness temperature is calculated from equation (4.1) and the apparent microwave emissivity as seen by the satellite is calculated from equation (4.2). Then the coefficients of the first and second corrections are derived from the outputs as will demonstrated in section 4.4. A schematic diagram showing the inputs and the outputs of the simulation of microwave atmospheric model is shown in figure 4.1.

4.3.2 A New Algorithm for Atmospheric Correction

A schematic diagram of the new-multi sensor technique is shown in figure 4.2 which demonstrates how to derive surface microwave emissivity from apparent microwave emissivity by applying the first and second order corrections. This figure shows the approach in obtaining the surface microwave emissivity by the following steps:

1. The apparent emissivity, ε^*, is calculated as in equation (4.2a) from the microwave satellite measurements (brightness temperature) and the corrected physical surface temperature from the infrared radiometer, see chapters 5&6. The surface temperature computed from the infrared is averaged or weighted over the microwave radiometer footprint, since the resolution in the microwave case is much coarser than the resolution in the infrared (chapter 3).

2. The apparent emissivity is corrected from the effect of the atmosphere by applying the first and second order correction coefficients obtained before as described in section 4.3.1.

After correcting the emissivity from the emissivity and water vapour effects, it is possible to retrieve a geophysical parameter from a surface emission model assuming that certain other parameters are known. One potential application of this technique is to retrieve soil moisture as one of the critical geophysical parameter for climate studies (chapter 6).

Simulation of Microwave Atmospheric model

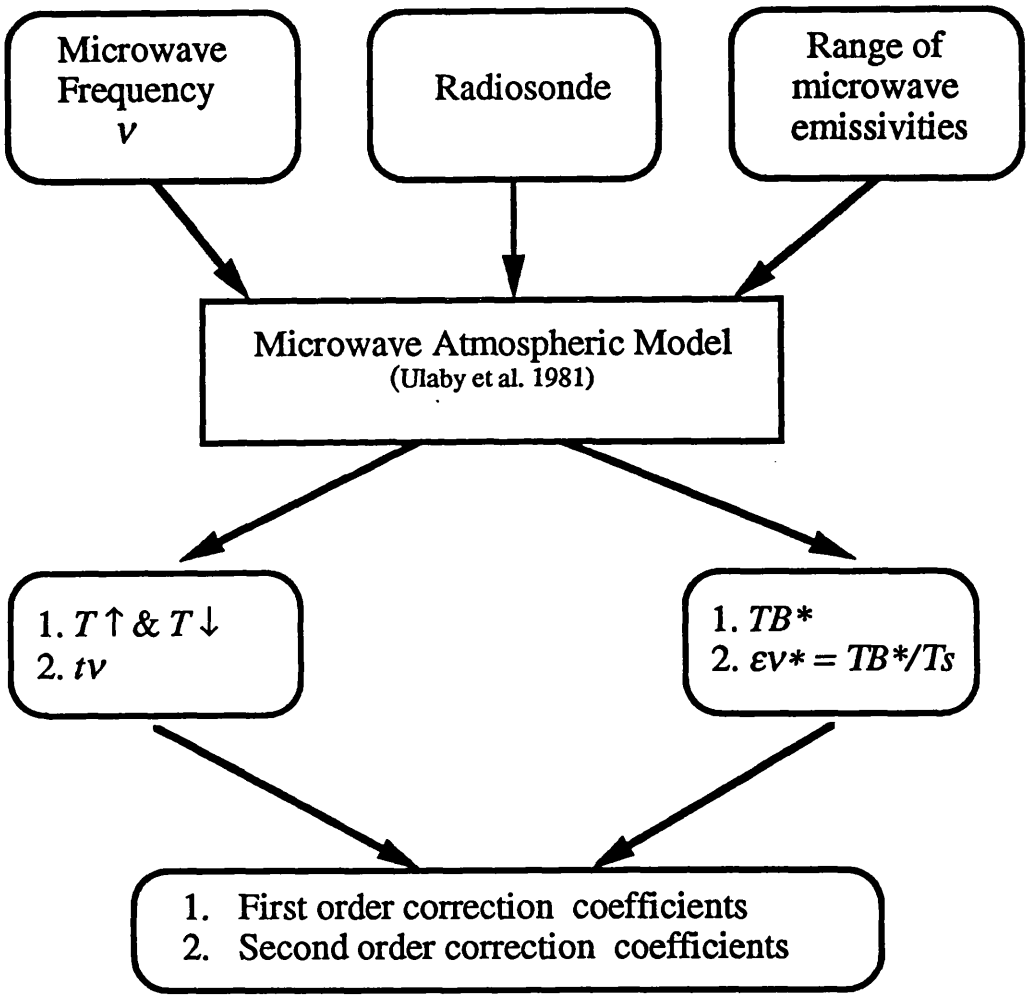

Figure 4.1 Schematic diagram showing the inputs and the outputs of the simulation of atmospheric model. TB^* and ε^* are the apparent microwave brightness temperature and emissivity respectively as seen by the radiometer from space.

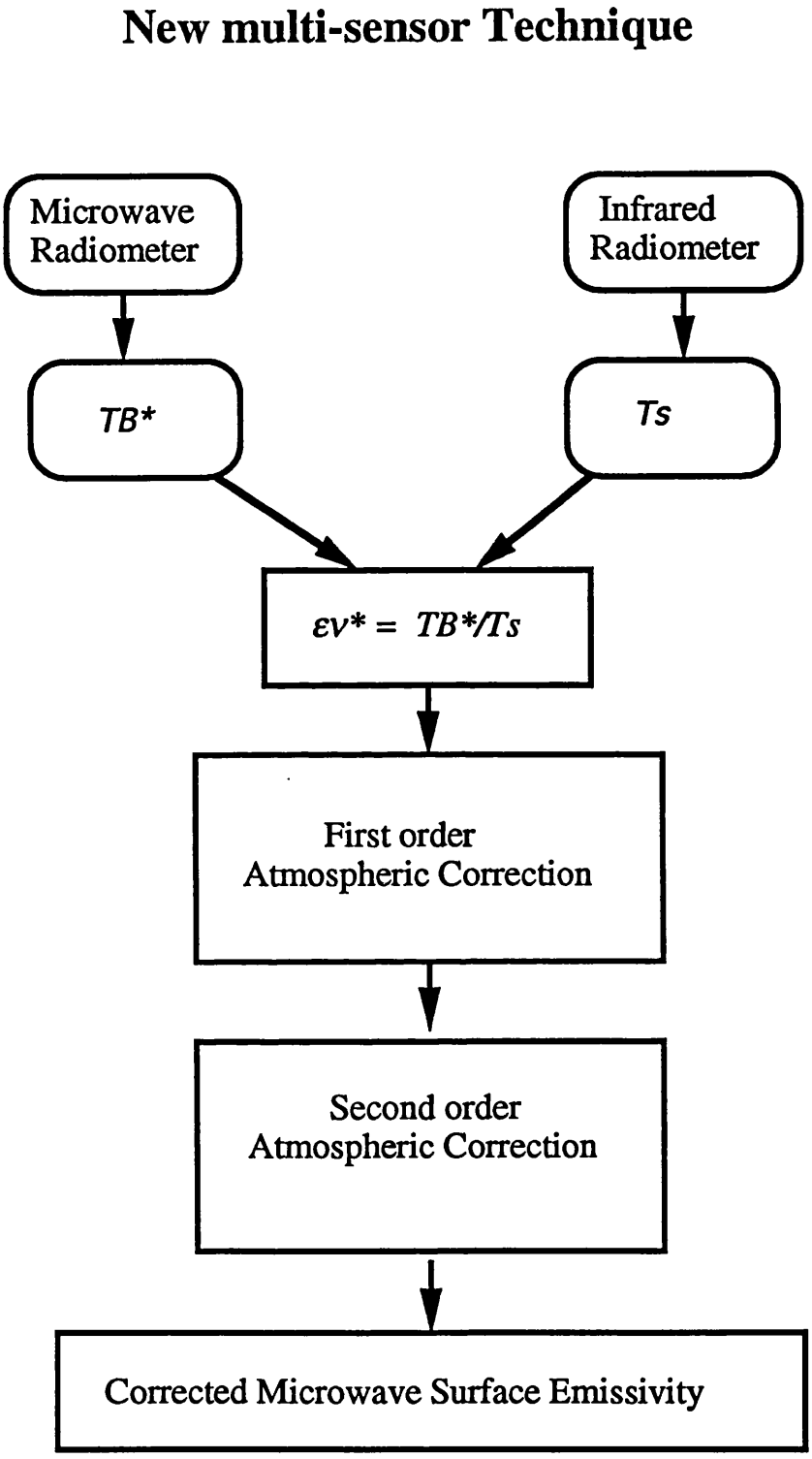

Figure 4.2 Showing the basic scheme of the multi-sensor technique to correct the apparent emissivity as seen by the microwave radiometer from space and retrieve the surface microwave emissivity.

4.4 Simulations of the Atmospheric Correction

The surface emissivity can be estimated from the apparent emissivity, provided that the atmospheric properties are known. However, in general, these will not be known for any specific satellite measurement. This section will demonstrate how generic atmospheric parameters may be used for a specific surface under observation. These parameters are generated from a selected radiosonde sets which are representative of the area of study. The coefficients of the first and second order corrections are generated in this section for the following radiosonde sets and frequencies:

1. *North Atlantic radiosondes* (60 atmospheres) for ATSR/M frequencies 36.5 GHz and 23.8 GHz. North Atlantic radiosondes cover different seasons within the North Atlantic area and were originally provided by NOAA. The results from these simulations will be used in a validation study in the next chapter. The simulations of the microwave brightness temperatures for the second correction are performed for four possibilities of the differences between the true surface emissivities at frequencies 36.5 GHz and 23.8 GHz. These four different cases (based on the model of Wilheit (1979), see chapter 2) are: 0.04, 0.05, 0.06, and 0.07. According to the Wilheit model the microwave emissivity does not depend on wind speed for wind speeds less than 7 m/s and it is mostly dependent on sea surface temperature (see chapter 2). Therefore, it is possible to predict the difference between two microwave surface emissivity by knowing the surface temperature from IR data, (see section 4.5) for wind speeds less than 7 m/s according to Wilheit model.

2. *Global radiosondes* (56 atmospheres) which have atmospheres with higher vapour contents (see later) will be used in the next simulations for ATSR/M frequencies 36.5 GHz and 23.8 GHz. The global radiosondes were originally supplied by NOAA and cover seasonally and geographically diverse conditions. The results of these simulations are then compared with these from the North Atlantic which have atmospheres with lower water vapour contents (see later). The simulations of the microwave brightness temperatures for the second correction are performed for four possible values of the differences between the true surface emissivity at frequencies 36.5 GHz and 23.8 GHz. These four cases are the same as mentioned in the North Atlantic case.

3. *Alice Springs radiosondes* (40 atmospheres at 8 a.m. local time and covering different seasons) from Alice Springs in central Australia for TOPEX microwave radiometer frequencies: 18 GHz, 21 GHz, and 37 GHz. These radiosondes are provided by the Alice Springs meteorological station. The coefficients of corrections

obtained from simulations using the Alice Springs radiosondes will be used in the application of the new technique for soil moisture measurement in the Simpson Desert in chapter 6. Based on the surface simulations of microwave surface emissivities for bare soil in chapter 2 (i.e. Dobson et al. (1985) and Mo and Schmugge (1987) models), the atmospheric simulations of the microwave brightness temperatures for the second correction are run for two possible values of the differences between the surface emissivities at 18 GHz and 21 GHz. The same two values of emissivity differences are used for 37 GHz and 21 GHz frequencies. These two possible values are 0.02 and 0.0. Unlike the ocean case, the difference in microwave surface emissivities between two frequencies for the soil surface is difficult to predict. However, the assessment of the effect due to the uncertainty in knowing the difference between the two emissivities at the two frequencies is found in section 4.5.

4. *The Saudi Arabian radiosondes* (47 atmospheres at 3 a.m., and 45 atmospheres at 3 p.m. local time covering different seasons from 4 different towns in Saudi Arabia: Riyadh, Dhahran, Jeddah, and Tabouk) were used in simulations to obtain the coefficients of corrections for ATSR/M frequencies 36.5 GHz and 23.8 GHz. The results were then compared with the Alice Springs coefficients at the same frequencies. These radiosondes were provided by the MEPA (Meteorological Environmental Protection Agency) in Saudi Arabia.

Inspection of these various radiosonde data sets should provide information such as:

- How different are the atmospheric parameters of ocean (North Atlantic and Global) and desert (Alice Springs and Saudi), and how do these differences affect the coefficients of corrections ?

- How different are the Alice Springs and Saudi Desert atmospheric parameters, and how do such differences (if any) affect the coefficients of corrections ?

- How do desert atmospheric mean parameters change between day and night, and do any changes affect corrections significantly? A difference between day and night atmospheric parameters over the desert is expected, therefore it is important to investigate if there is any significant difference between radiosonde measurements made at different stages of the diurnal cycle. It will be shown later that measurements made at night are to be preferred for various reasons, and it is important to establish the nature of any bias that may result from such sampling strategy.

4.4.1 Results Using North Atlantic Radiosondes

Simulations of the microwave atmospheric model for 60 different North Atlantic atmospheres were carried out for a surface emissivity range from 0.4 to 1.0 with 0.01 increment at 36.5 GHz and 23.8 GHz frequencies. The results and their interpretations are presented below :

First order correction

Figure 4.3 is a plot of apparent emissivity versus true surface emissivity at 36.5 GHz for 60 different atmospheres. As expected from equation (4.3), each atmosphere gives a straight line for different surface emissivities in the 0.4 to 1.0 range. The slope and the intercept of each line depend on water vapour. This figure shows the two factors which affect the apparent microwave emissivity: (a) the microwave surface emissivity effect is evident from the increase of the difference between the 1:1 line and the points as emissivity decreases. (b) the water vapour content which is shown from the spread of the points at each surface emissivity (see later). The spread in these points decreases as the true surface emissivity increases (see later).

Plotting $\Delta\varepsilon_1$ versus the apparent emissivity at 36.5 GHz , figure 4.4 shows more clearly the behaviour seen in figure 4.3. The higher water vapour atmospheres generate steeper gradients and higher intercepts (see section 4.5). The emissivity effect which is seen from the difference between the points and the horizontal line decreases until it becomes zero at an emissivity of ~ 0.96 and then it becomes negative for higher emissivities (see later). By knowing the coefficients of the fitted line it is possible to predict $\Delta\varepsilon_1$ and bring the averaged fitted line of the points to the horizontal line (first order correction).

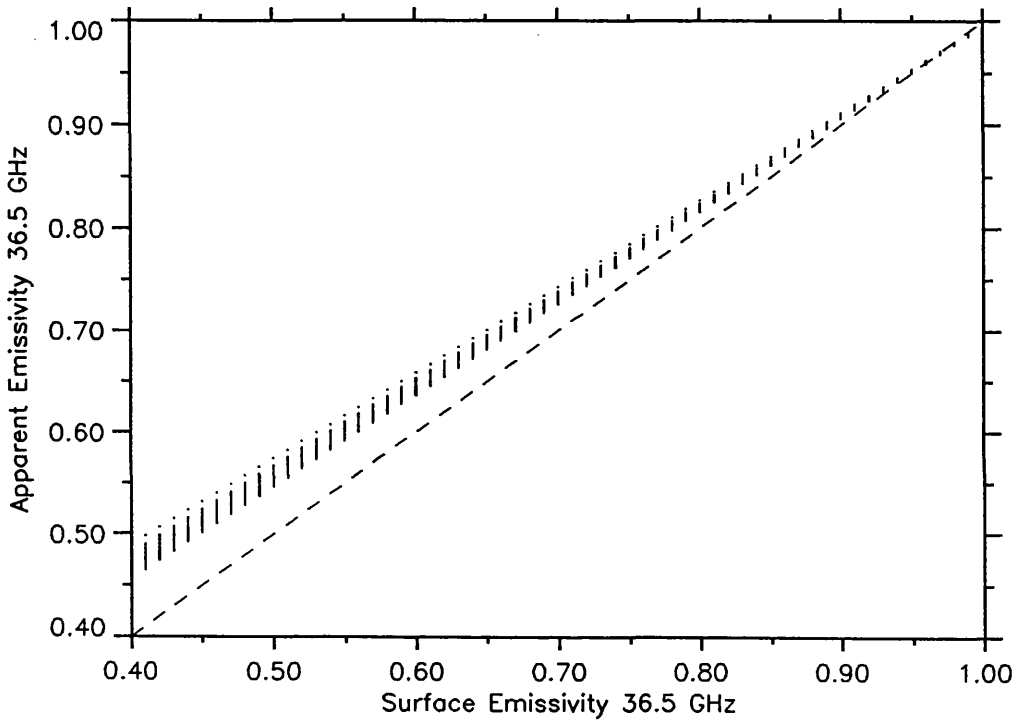

Figure 4.3 Apparent microwave emissivity dependence on true surface microwave emissivity at 36.5 GHz (ATSR/M channel) for different North Atlantic atmospheres. The points at each microwave surface emissivity represent 60 atmospheres. The bias of these points and their spread increases as emissivity decreases.

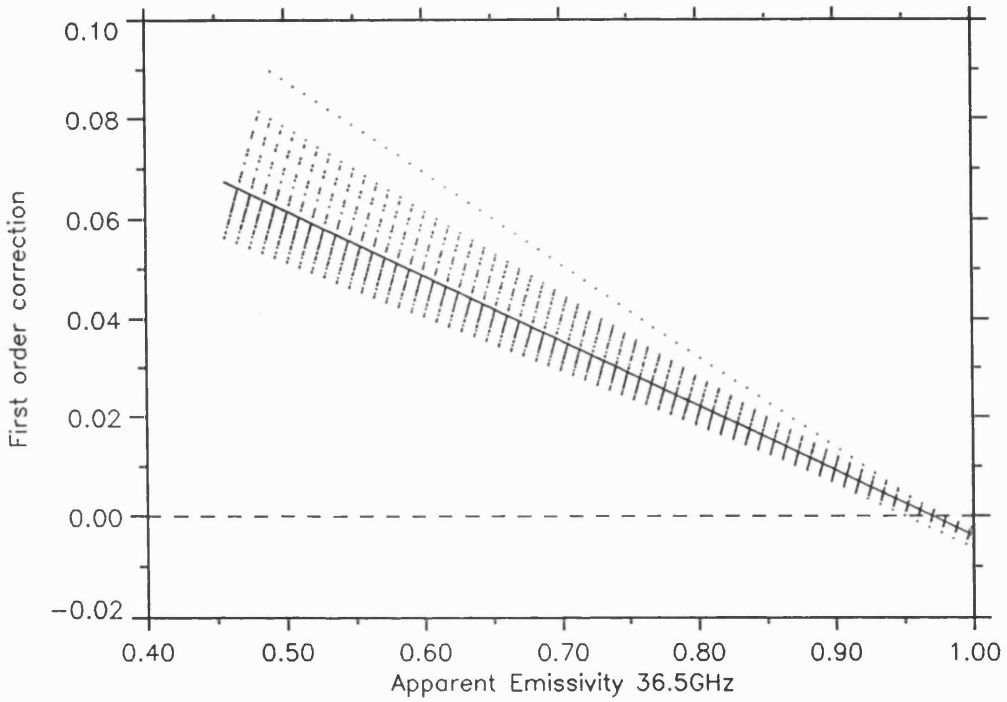

Figure 4.4 First order correction plotted against apparent emissivity at 36.5 GHz (ATSR/M channel) for North Atlantic radiosondes. This diagram represents the difference between the points in figure (4.3) and the 1:1 line (surface emissivity) as the y-axis. The bias of these points and their spread increases as emissivity decreases. The line passing through these points represents the least square fitted line. Note that the x-axis line is the apparent emissivity, while in figure 4.3 it is the true surface emissivity

Interpretation:

To explain the behaviour of the first order correction, $\Delta\varepsilon_1$, in figure 4.4, an example is given in table 4.1 for three different surface emissivities but for the same atmosphere. Table 4.1 shows that the increase in $\Delta\varepsilon_1$ with decreasing emissivity (i.e. reflectivity increase) is due to:

1. The increase in the reflected component of downwelling atmospheric emission.
2. The upwelling atmospheric emission. Although, the upwelling is unaffected by emissivity it adds a significant amount up to 0.06 to the apparent emissivity in the example given (table 4.1).
3. The decrease in the fraction of attenuated surface emissivity as the emissivity decreases. This is clear from the decrease in the difference between the true surface emissivity (ε_{37}) and the attenuated surface emissivity (ε'_{37}).

At an emissivity of ~ 0.96, where $\Delta\varepsilon_1$ is ~ 0.0, the reflected downwelling and upwelling atmospheric emission compensate for the effect of the attenuation of the ground emission by the atmosphere. At very high emissivities $\Delta\varepsilon_1$ is negative as the downwelling reflected emission tends to zero and, as the surface-emitted radiance increases with emissivity, the quantity absorbed by the atmosphere increases in proportion..

The second observation from figures 4.3 and 4.4 is that the increase in the spread of the points as surface emissivity decreases. This is due to the increased effect of the reflected downwelling atmospheric emission for different atmospheres.

Coefficients of first order correction

The coefficients generated from the average atmosphere using equation (4.6) (see table 4.2) are almost identical to the coefficients of the least squares fit for the points in figure 4.4. The r.m.s residual after the first order correction for different ranges of emissivities are listed in table 4.3. The mean of the residuals at each emissivity range is zero. As discussed previously, these residuals may be further reduced by correcting for the effect of water vapour.

Throughout the simulations using the various radiosonde sets, the coefficients generated by least squares regression are used to determine the first order correction.

Table 4.1 This table shows the effect of upwelling, $\varepsilon_{37}\uparrow$, downwelling emissivities reflected by the surface and then attenuated by the atmosphere, $\varepsilon'_{37}\downarrow$, and the attenuated surface emissivity, ε'_{37}, on the first order correction $\Delta\varepsilon_1$. The atmosphere used in this example has the following parameters and surface temperature: $t_V = 0.9$, $T\uparrow = 17$ K, $T\downarrow = 17$ K, $Ts = 275$ K.

where, ε_{37} is the true surface emissivity, $\varepsilon'_{37} = \varepsilon_{37} t_V$, $\varepsilon'_{37}\downarrow = \frac{T\downarrow' t_V}{T_S}(1 - \varepsilon_V)$, and $\varepsilon_{37}\uparrow = \frac{T\uparrow}{T_S}$

ε_{37}	ε'_{37}	$\varepsilon_{37}\uparrow$	$\varepsilon'_{37}\downarrow$	ε_{37}^*	$\Delta\varepsilon_1$
0.4	0.36	0.06	0.033	0.453	0.053
0.7	0.63	0.06	0.017	0.707	0.007
0.99	0.89	0.06	0.0006	0.95	- 0.04

North Atlantic first order correction coefficients

Table 4.2 Coefficients of 1st order correction for ATSR/M channel 36.5 GHz and for 0.4 to 1.0 emissivity range. This table shows a comparison between the slope and the intercept from least square fit of figure (4.4) and from the averaged atmospheric parameters represented by the coefficients in equation (4.6).

Coefficients of fit	Intercept	slope
Least square	0.127	-0.131
Equation (4.6)	0.128	-0.132

Table 4.3 North Atlantic r.m.s residuals after first correction for different ranges of emissivities

Emissivity range	r.m.s.
0.4-0.5	0.007
0.5-0.6	0.006
0.6-0.7	0.005
0.7-0.8	0.003
0.8-0.9	0.002
0.9-1.0	0.001

Second order correction

The residual $\Delta\varepsilon_2$ at 36.5 GHz from the first correction is due to the water vapour effect, as shown in figure 4.5. Since the 23.8 GHz channel lies near to the water vapour absorption resonance frequency (22.2 GHz), it is much more sensitive to atmospheric water vapour. Thus the higher the water vapour content in a given atmosphere the greater the emission at 23.8 GHz, as there is more of the downwelling reflected and upwelling atmospheric emission. A plot of the value of total water vapour column for the North Atlantic radiosonde atmospheres against the difference between the apparent microwave brightness temperature at 36.5 GHz and 23.8 GHz (figure 4.6), shows this strong sensitivity of the 23.8 GHz channel to water vapour with respect to 36.5 GHz channel. The true microwave surface emissivity at 36.5 GHz in this figure is 0.4 and at 23.8 GHz is 0.36, assuming the difference between the two frequencies to be 0.04 .

Figures 4.5 and 4.6 demonstrate that it is possible to obtain a second order correction by plotting the remaining residual, $\Delta\varepsilon_2$, against the difference in apparent microwave brightness temperature at 36.5 GHz and 23.8 GHz (figure 4.7). The points with the largest negative values of $TB_{36.5}$-$TB_{23.8}$ corresponding with atmospheres with highest water vapour contents, have the highest residuals. The scatter in this figure is due to the effect of high air temperatures in some of these radiosondes which increases the atmospheric emission (i.e. downwelling and upwelling atmospheric emission), although this effect is small compared to the water vapour effect. Also, to a lesser extent higher atmospheric temperature increases the strength of oxygen line absorption at 37 GHz due to line broadening and hence atmospheric emission increases.

Figure 4.8 shows the same plot but for the whole range of emissivities from 0.4 to 1.0. Note that the coefficients of the least square fit of figure 4.8 are the same as figure 4.7. However, the least square fits are generated at small ranges of surface emissivities: 0.4 to 0.5, 0.5 to 0.6, 0.6 to 0.7, 0.7 to 0.8, 0.8 to 0.9, and 0.9 to 1.0 (see tables 4.4a to 4.4d). This is because the residuals remaining after the first order correction (and therefore the coefficients of the second order correction) will depend on the water vapour content at different surface emissivities (see figure 4.9). Although this dependence is small for the North Atlantic case can be seen clear from tables 4.4(a) to 4.4(d) and figures 4.8 and 4.7, it will be important for the higher water vapour atmospheres, as we will see later. The choice of the range of emissivity to be 0.1 is quite reasonable as the first estimate of surface emissivity is known within that range after the first order correction.

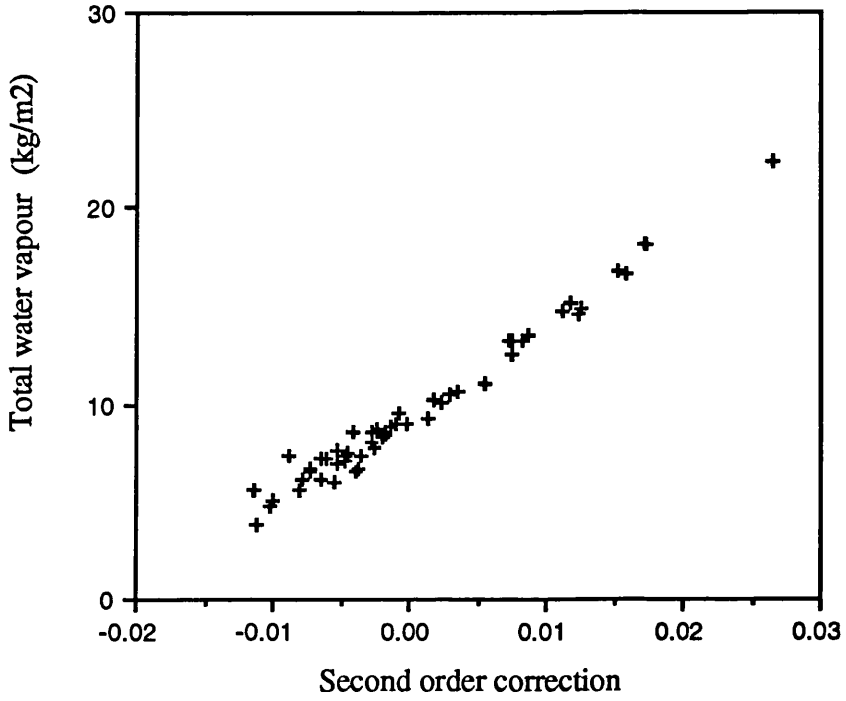

Figure 4.5 Plot of total water vapour for 60 atmospheres of North Atlantic radiosonde measurements against the second order correction at 36.5 GHz for surface microwave emissivity = 0.4.

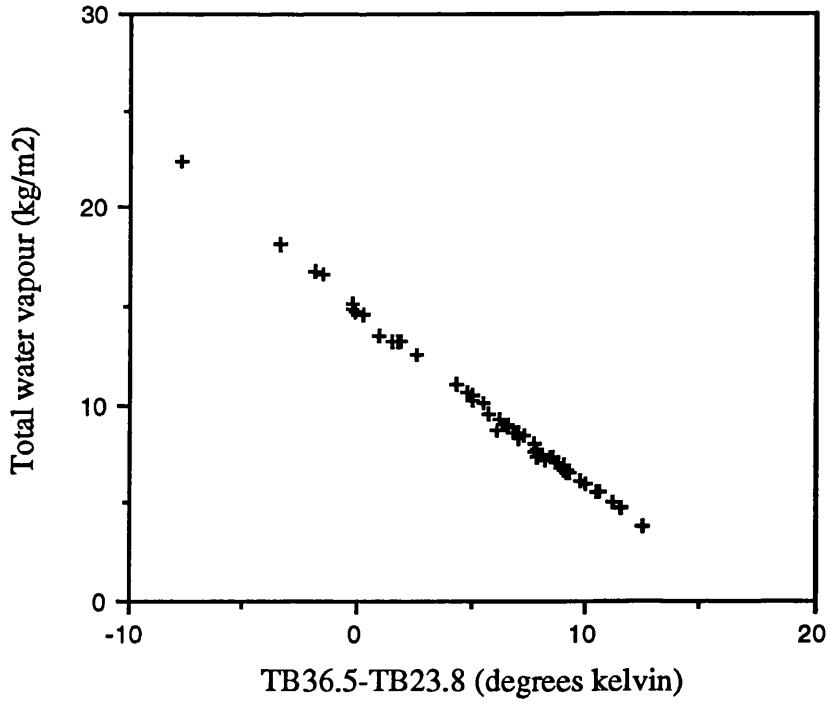

Figure 4.6 Plot of total water vapour against the difference in microwave brightness temperature between 36.5 GHz and 23.8 GHz.

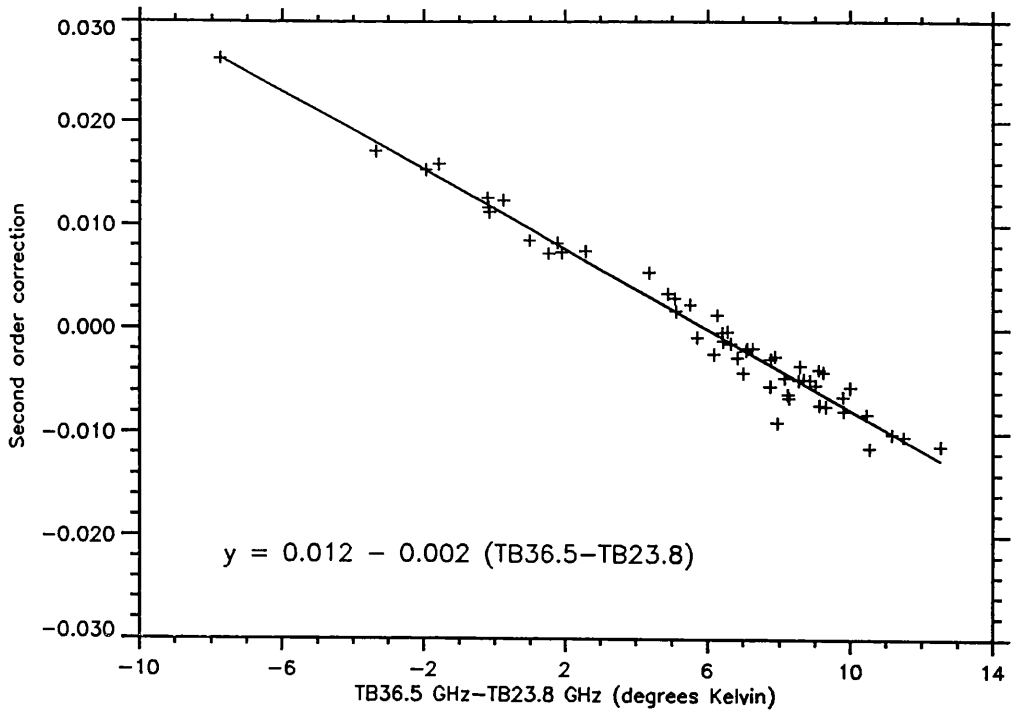

Figure 4.7 The dependence of the second order correction on the difference between 36.5 GHz and 23.8 GHz microwave brightness temperatures for 60 different North Atlanticat atmospheres. The surface emissivity in this figure is 0.4, and the emissivity difference for the two channels is 0.04.

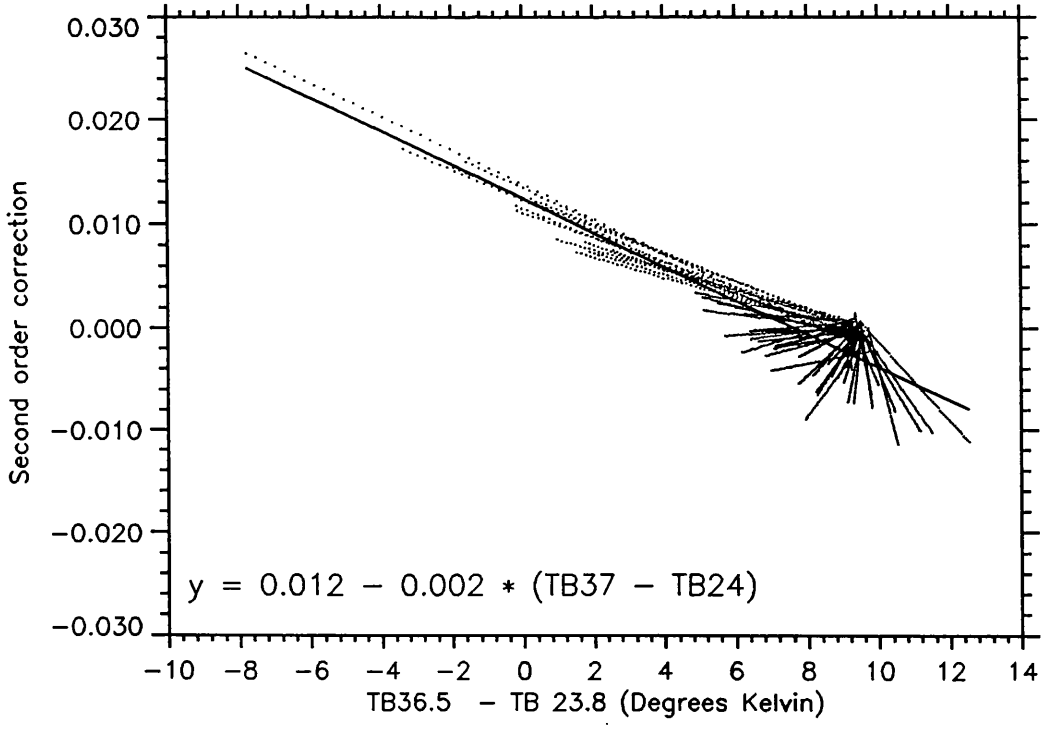

Figure 4.8 As for figure 4.6 but for 61 different surface emissivities from 0.4 to 1.0. The coefficients of a straight line fits over smaller ranges of emissivities are shown in tables 4.4a to 4.4d.

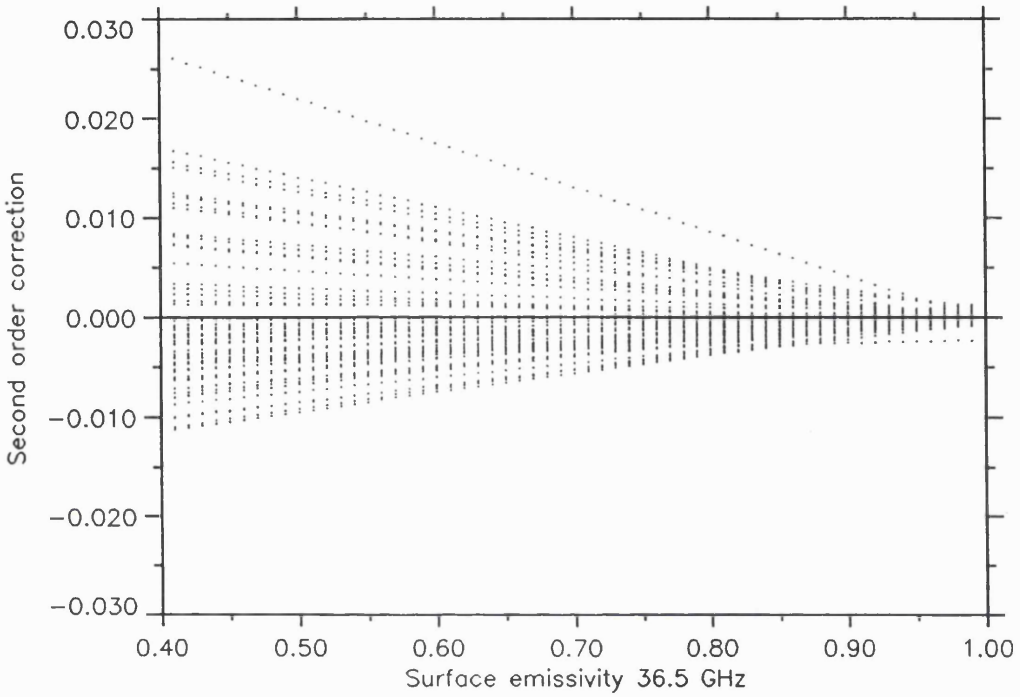

Figure 4.9 The variation of the second order correction with different atmospheres at different surface emissivity at 36.5 GHz. The graph shows 60 atmospheres (North Atlantic) at each surface emissivity.

Tables 4.4(a) to 4.4(d) show that the slopes for all the four possibilities of the differences between the true surface emissivities at 36.5 GHz and 23.8 GHz are the same, although the intercepts increase with increasing emissivity, and increasing difference between the two channels (see section 4.5). The r.m.s residuals after the first and second corrections are shown in figures 4.10(a) and 4.10(b). Note that the 0.001 residuals after the second order correction show a factor 2 up to 7 improvement with respect to residuals after the first order correction. Also, note that the there is no need to perform a second correction if the emissivity is in the 0.9 to 1.0 range, as the r.m.s residual after the second correction is the same as the one after the first correction.

Finally, comparing figure 4.3 with figures 4.11 and 4.12, the first order correction adjusts for the microwave emissivity effect by bringing the points to the 1:1 line (figure 4.11). The second order correction reduces the spread at each surface emissivity for all the atmospheres and adjusts for the water vapour effect (figure 4.12).

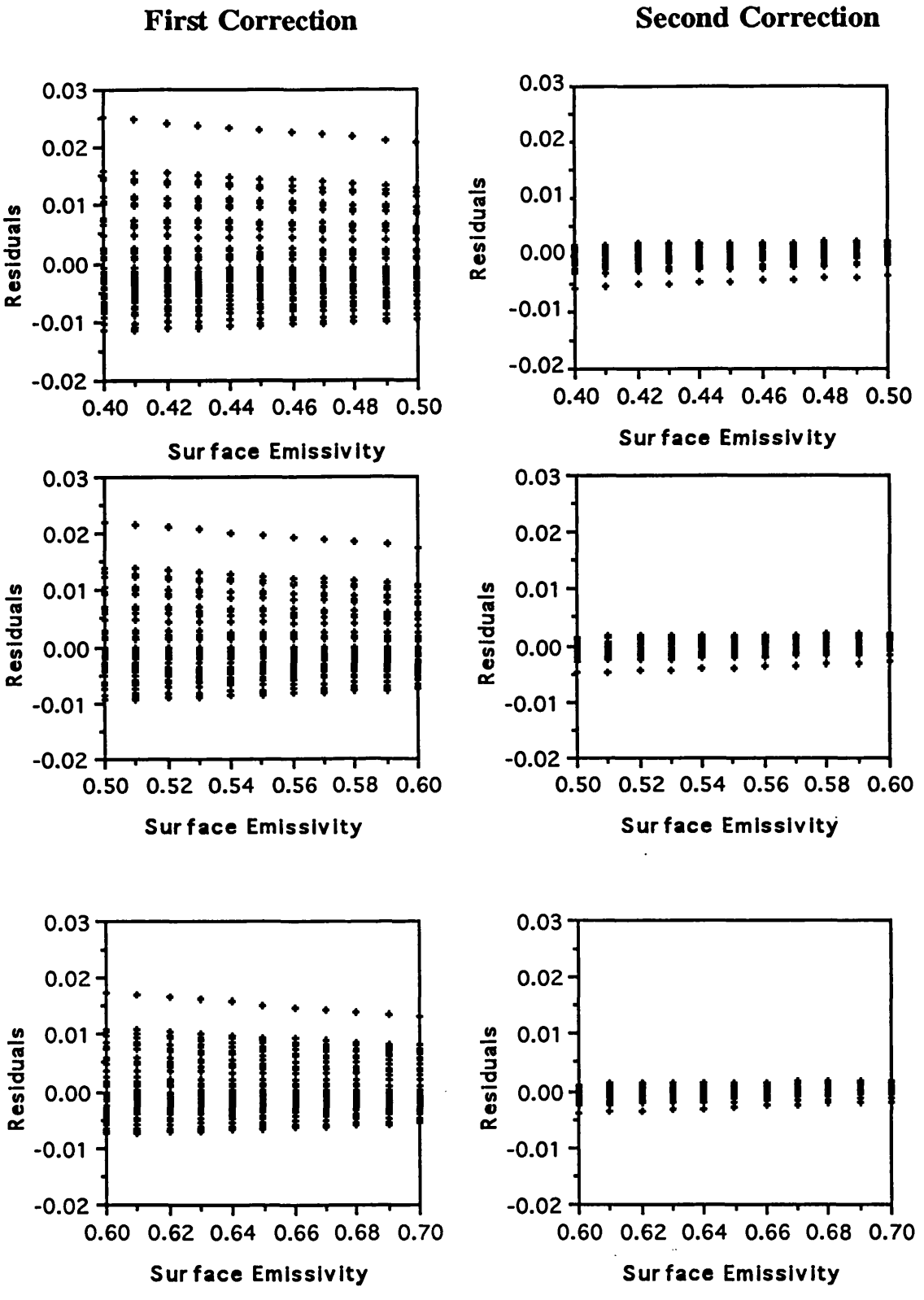

Figure 4.10a The residuals after first and second order corrections for 0.4 -0.5, 0.5-0.6, and 0.6-0.7 emissivity ranges. Note that the r.m.s after the second correction is the same for all emissivity ranges and for all the 4 possible differences between ε36.5 GHz and ε23.8 GHz.

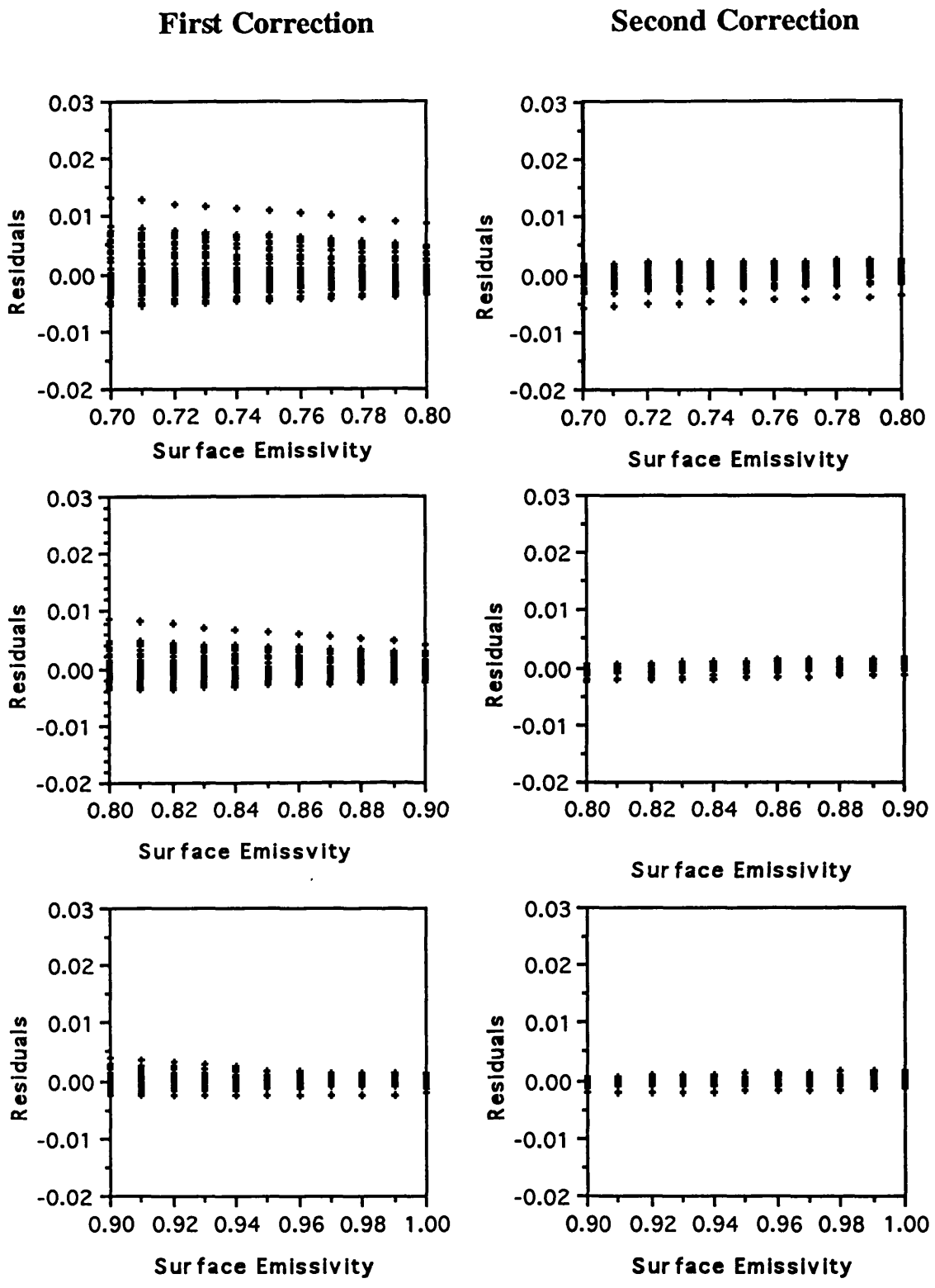

Figure 4.10b The residuals after first and second order corrections for 0.7-0.8, 0.8-0.9, and 0.9-1.0 emissivity ranges.

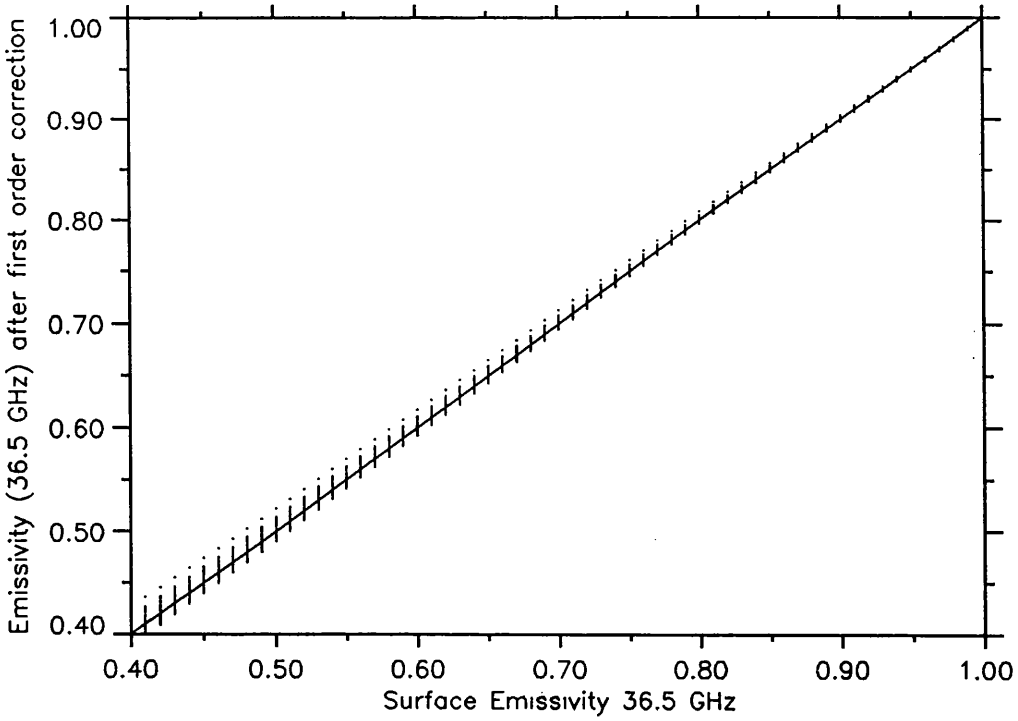

Figure 4.11 The first corrected microwave emissivity at 36.5 GHz against the true microwave surface emissivity.

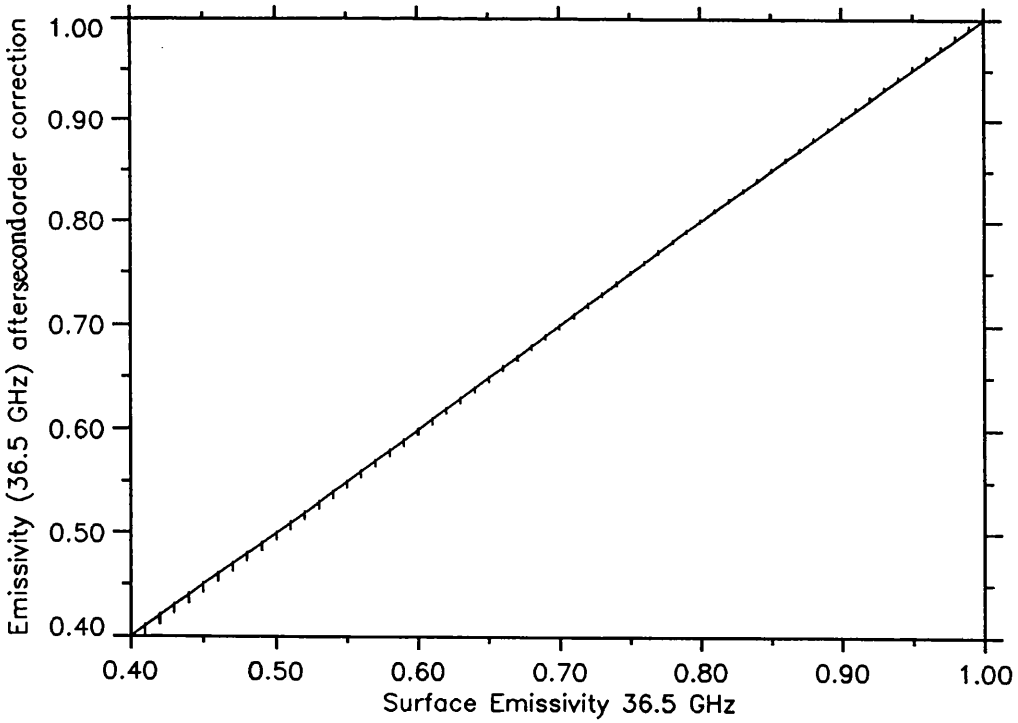

Figure 4.12 The second corrected microwave emissivity at 36.5 GHz against the true microwave surface emissivity. Comparing the above two figures with figure 4.3, the first correction compensate for the emissivity effect and the second correction compensate for the water vapour effect.

North Atlantic second order correction coefficients & r.m.s. residuals

Table 4.4a For ATSR/M channels, assuming 0.04 difference in emissivity between 36.5 GHz and 23.8 GHz.

Case	Emissivity range	Intercept	Slope	r.m.s.
1	0.4 - 0.5	0.012	-0.002	0.001
2	0.5 - 0.6	0.013	-0.002	0.001
3	0.6 - 0.7	0.014	-0.002	0.001
4	0.7 - 0.8	0.014	-0.002	0.001
5	0.8 - 0.9	0.014	-0.002	0.001
6	0.9 - 1.0	0.011	-0.001	0.001

North Atlantic second order correction coefficients & r.m.s. residuals

Table 4.4b For ATSR/M channels, assuming 0.05 difference in emissivity between 36.5 GHz and 23.8 GHz.

Case	Emissivity range	Intercept	Slope	r.m.s.
1	0.4 - 0.5	0.016	-0.002	0.001
2	0.5 - 0.6	0.017	-0.002	0.001
3	0.6 - 0.7	0.018	-0.002	0.001
4	0.7 - 0.8	0.018	-0.002	0.001
5	0.8 - 0.9	0.017	-0.002	0.001
6	0.9 - 1.0	0.013	-0.001	0.001

North Atlantic second order correction coefficients & r.m.s. residuals

Table 4.4c For ATSR/M channels, assuming 0.06 difference in emissivity between 36.5 GHz and 23.8 GHz.

Case	Emissivity range	Intercept	Slope	r.m.s.
1	0.4 - 0.5	0.020	-0.002	0.001
2	0.5 - 0.6	0.021	-0.002	0.001
3	0.6 - 0.7	0.021	-0.002	0.001
4	0.7 - 0.8	0.021	-0.002	0.001
5	0.8 - 0.9	0.019	-0.002	0.001
6	0.9 - 1.0	0.014	-0.001	0.001

North Atlantic second order correction coefficients & r.m.s. residuals

Table 4.4d For ATSR/M channels, assuming 0.07 difference in emissivity between 36.5 GHz and 23.8 GHz.

Case	Emissivity range	Intercept	Slope	r.m.s.
1	0.4 - 0.5	0.024	-0.002	0.001
2	0.5 - 0.6	0.025	-0.002	0.001
3	0.6 - 0.7	0.021	-0.002	0.001
4	0.7 - 0.8	0.024	-0.002	0.001
5	0.8 - 0.9	0.022	-0.001	0.001
6	0.9 - 1.0	0.015	-0.001	0.001

4.4.2 Results Using the Global Radiosondes

Simulation of microwave radiative transfer were performed using the global atmospheres described in section 4.4 for surface emissivities ranging from 0.4 to 1.0. The interpretation and analysis are similar to that already described in the North Atlantic case.

First order correction

A first order correction, plotted against apparent emissivity at 36.5 GHz for global radiosondes is shown in figure 4.13. The apparent emissivity at 36.5 GHz as seen by the radiometer overestimates the surface emissivity by 0.14 at emissivity of 0.4 for the atmosphere with the highest water vapour content. This behaviour is similar to that seen for the North Atlantic case, except that the first order correction is higher for all surface emissivities due to the increase in water vapour which will increase the amount of the upwelling atmospheric emission, and downwelling reflected atmospheric emission.

The coefficients of the first order correction are shown in table 4.5. The difference in the coefficients from a least squares fit of the points in figure 4.13 and from equation (4.6) has a very small effect on the predicted residuals after the first order correction (less than 0.001).

From table 4.5 the intercept is higher than the North Atlantic case, and the slope is steeper. In section 4.5, it will be shown that this is due to the greater total water vapour content in the global set.

Global first order correction coefficients

Table 4.5 Coefficients of 1st order correction for ATSR/M channel 36.5 GHz and for 0.4 to 1.0 emissivity range. This table also shows a comparison between the slope and the intercept from the least square fit of figure 4.13 and from the averaged atmospheric parameters represented by the coefficients in equation (4.6).

Coefficients of fit	Intercept	slope
Least squares	0.222	-0.226
Equation (4.6)	0.228	-0.234

The r.m.s residuals after the first correction are shown in table 4.6. These range from 0.022 to 0.002 for different microwave surface emissivity ranges. The residuals in the global case are higher than the North Atlantic residuals. This is expected, as the residuals after the first order correction depend on water vapour content in the atmosphere which is larger and more variable in the Global radiosonde set (see later section 4.5).

Table 4.6 Global r.m.s residual s after first order correction for different ranges of emissivities

Emissivity range	r.m.s.
0.4-0.5	0.022
0.5-0.6	0.017
0.6-0.7	0.013
0.7-0.8	0.009
0.8-0.9	0.005
0.9-1.0	0.002

Second order correction

The plots of the second order atmospheric correction against the difference in microwave brightness temperatures between 35.6 GHz and 23.8 GHz are shown in figure 4.14 for small ranges of emissivities and the coefficients of the least square fit are listed in tables 4.7a to 4.7d.

The intercepts increase with increasing differences in surface emissivity between the two channels, as in the case of the North Atlantic (see section 4.5). However, the intercept differences between different emissivity ranges is higher than that for the North Atlantic due to the effect of water vapour as expected. The slopes are the same for all cases (i.e. 0.04, 0.05, 0.06, 0.07) and at different emissivity ranges. The r.m.s. residual gets smaller for higher emissivities. For the worst case (at 0.4-0.5 emissivity range) the r.m.s residual is 0.005 which is 4.4 times smaller than the residual after the first correction. As in the case of the North Atlantic atmospheres, there is no need to perform a second correction for the emissivity range from 0.9 to 1.0, as the r.m.s. residual after the second correction is the same as that after the first correction.

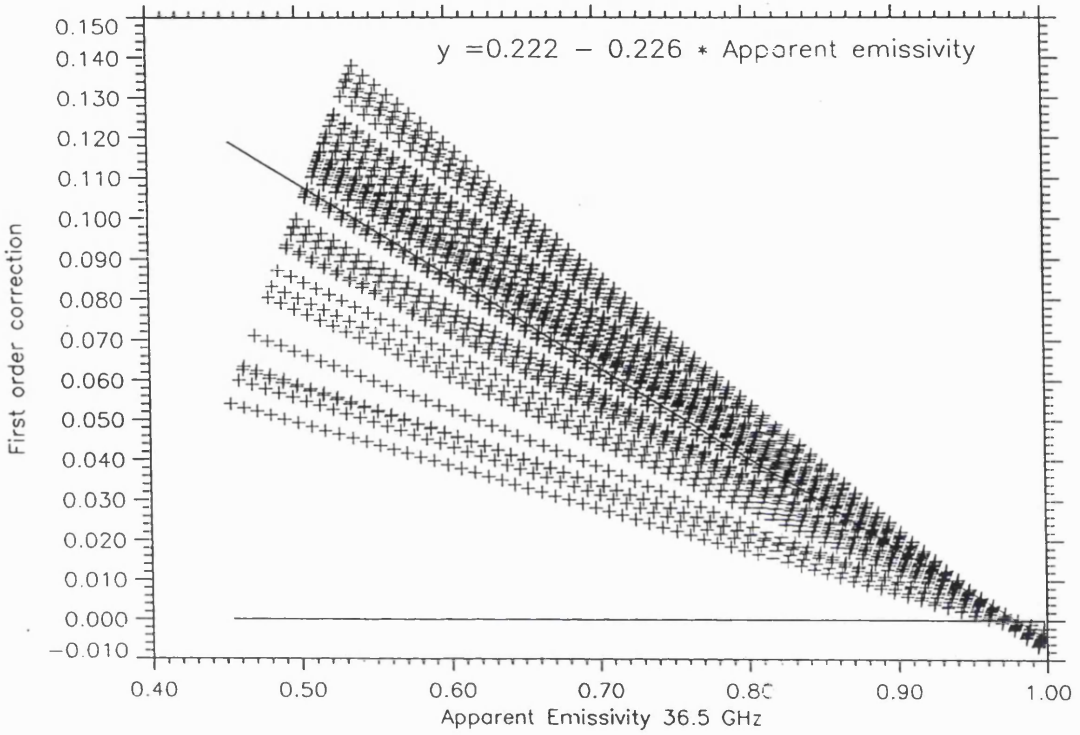

Figure 4.13 A first order correction plot against ε(apparent) at 36.5 GHz for the global radiosondes. There is more bias and spread of the points compared with figure 4.4 for North Atlantic as there is a greater range of water vapour in global atmospheres (see later).

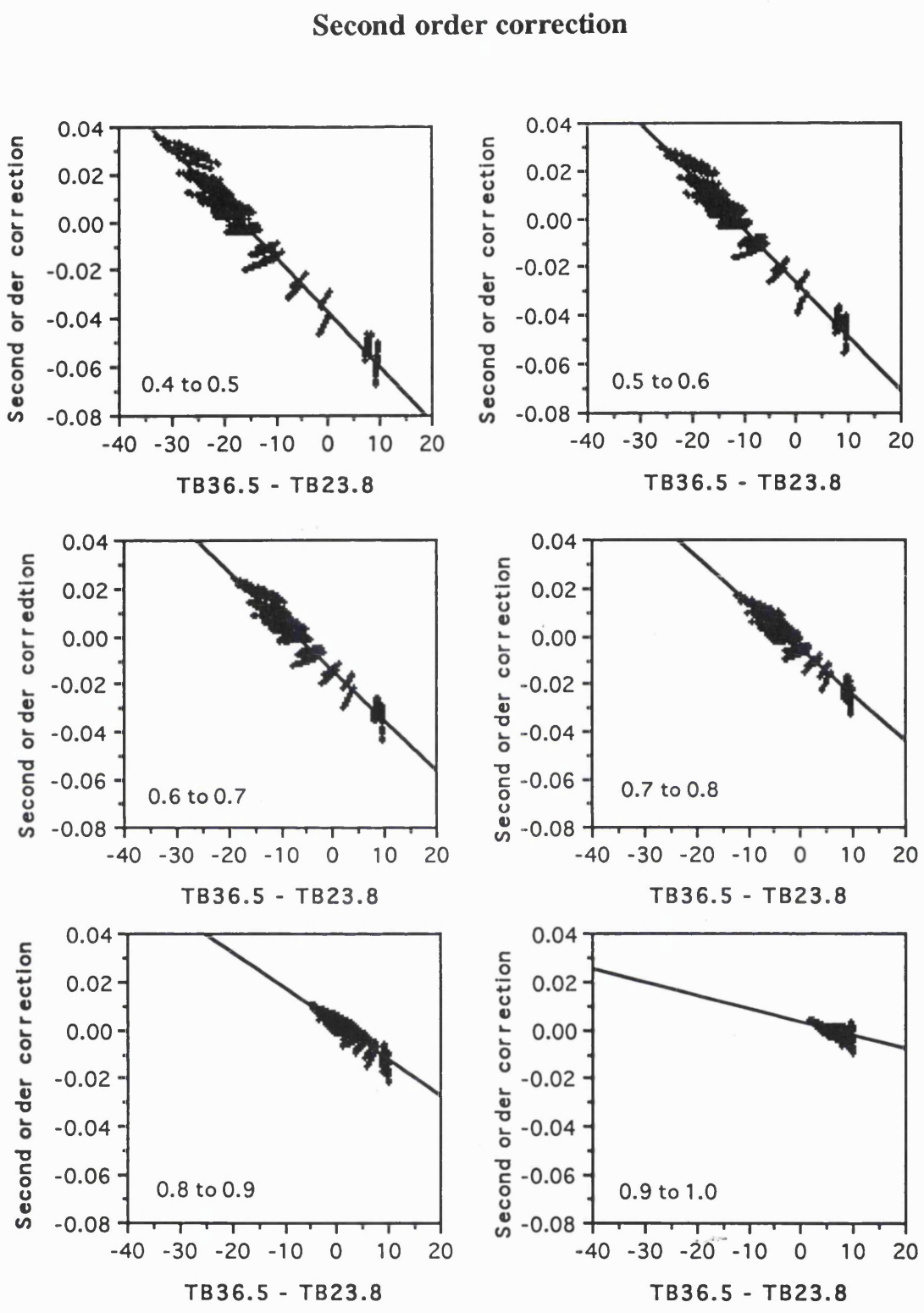

Figure 4.14 Second order atmospheric correction for different ranges of emissivities. See tables 4.7a to 4.7d for the slopes and intercepts.

Global second order correction coefficients & r.m.s. residuals

Table 4.7a For ATSR/M channels, assuming 0.04 difference in emissivity between 36.5 GHz and 23.8 GHz.

Case	Emissivity range	Intercept	Slope	r.m.s.
1	0.4 - 0.5	-0.038	-0.002	0.005
2	0.5 - 0.6	-0.026	-0.002	0.005
3	0.6 - 0.7	-0.015	-0.002	0.004
4	0.7 - 0.8	-0.005	-0.002	0.003
5	0.8 - 0.9	0.003	-0.002	0.003
6	0.9 - 1.0	0.003	-0.001	0.002

Global second order correction coefficients & r.m.s. residuals

Table (4.7b) For ATSR/M channels, assuming 0.05 difference in emissivity between 36.5 GHz and 23.8 GHz.

Case	Emissivity range	Intercept	Slope	r.m.s.
1	0.4 - 0.5	-0.032	-0.002	0.005
2	0.5 - 0.6	-0.022	-0.002	0.004
3	0.6 - 0.7	-0.011	-0.002	0.004
4	0.7 - 0.8	-0.002	-0.002	0.003
5	0.8 - 0.9	0.005	-0.002	0.003
6	0.9 - 1.0	0.004	-0.001	0.001

Global second order correction coefficients & r.m.s. residuals

Table 4.7c For ATSR/M channels, assuming 0.06 difference in emissivity between 36.5 GHz and 23.8 GHz.

Case	Emissivity range	Intercept	Slope	r.m.s.
1	0.4 - 0.5	-0.028	-0.002	0.005
2	0.5 - 0.6	-0.017	-0.002	0.004
3	0.6 - 0.7	-0.007	-0.002	0.004
4	0.7 - 0.8	0.002	-0.002	0.003
5	0.8 - 0.9	0.008	-0.001	0.002
6	0.9 - 1.0	0.005	-0.001	0.001

Global second order correction coefficients & r.m.s. residuals

Table 4.7d For ATSR/M channels, assuming 0.07 difference in emissivity between 36.5 GHz and 23.8 GHz.

Case	Emissivity range	Intercept	Slope	r.m.s.
1	0.4 - 0.5	-0.023	-0.002	0.005
2	0.5 - 0.6	-0.013	-0.002	0.004
3	0.6 - 0.7	-0.003	-0.002	0.004
4	0.7 - 0.8	0.005	-0.002	0.003
5	0.8 - 0.9	0.010	-0.002	0.002
6	0.9 - 1.0	0.006	-0.001	0.001

4.4.3 Results Using Alice Springs Radiosondes

Simulations of the microwave radiative transfer were performed using the Alice Springs atmospheres described in section 4.4. The microwave surface emissivity range taken here is from 0.5 to 1.0 for the TOPEX frequencies of 37 GHz, 21 GHz, and 18 GHz. This range of surface emissivity spans the range of emissivity in the microwave region for soil (see figure 2.16 in chapter 2).

First order correction

First order correction plotted against the apparent emissivity at 18 and 37 GHz for Alice Springs radiosondes are shown in figures 4.15(a) and (b) respectively. These figures show the different effect of the atmosphere on the microwave emissivities at different frequencies. The apparent emissivity at 18 GHz overestimates the surface emissivity by ~ 0.07 at 0.5 emissivity for the atmosphere with the highest water vapour content, while the emissivity at 37 GHz overestimate the surface emissivity by 0.09 for the same emissivity and atmosphere. This is expected as 37 GHz is more affected by the atmosphere (principally oxygen) than that at 18 GHz (see figure 3.1). Therefore, for the same atmosphere and surface emissivity, there will greater amount of the upwelling atmospheric emission and the downwelling atmospheric emission reflected by the surface at 37 GHz than at 18 GHz. As a consequence, the slope and intercept for 37 GHz are greater than those at 18 GHz (table 4.8).

The coefficients of first order corrections from the least squares fit and equation (4.6) are very similar (table 4.8) for 18 GHz and 37 GHz Therefore, the choice of the coefficients from a least square fit or from equation (4.6) has a very small effect on the predicted residuals after the first order correction (less than 0.001). The residuals after the first order correction for the 18 GHz and 37 GHz are shown in tables 4.9 and 4.10 respectively.

Alice Springs first order correction coefficients and r.m.s. residuals

Table 4.8 Coefficients of 1st order correction for TOPEX channels at 18 GHz and 37 GHz for 0.5 to 1.0 emissivity range.

Coefficients of fit	Intercept	slope
Least square (18 GHz)	0.100	-0.101
Equation (4.6) (18 GHz)	0.103	-0.105
Least square (37 GHz)	0.158	-0.161
Equation (4.6) (37 GHz)	0.161	-0.165

Table 4.9 Alice Springs r.m.s residuals after first correction at 18 GHz for different ranges of emissivities

Emissivity range	r.m.s.
0.5-0.6	0.013
0.6-0.7	0.010
0.7-0.8	0.007
0.8-0.9	0.004
0.9-1.0	0.001

Table (4.10) Alice Springs r.m.s residuals after first correction at 37 GHz for different ranges of emissivities

Emissivity range	r.m.s.
0.5-0.6	0.013
0.6-0.7	0.010
0.7-0.8	0.007
0.8-0.9	0.004
0.9-1.0	0.002

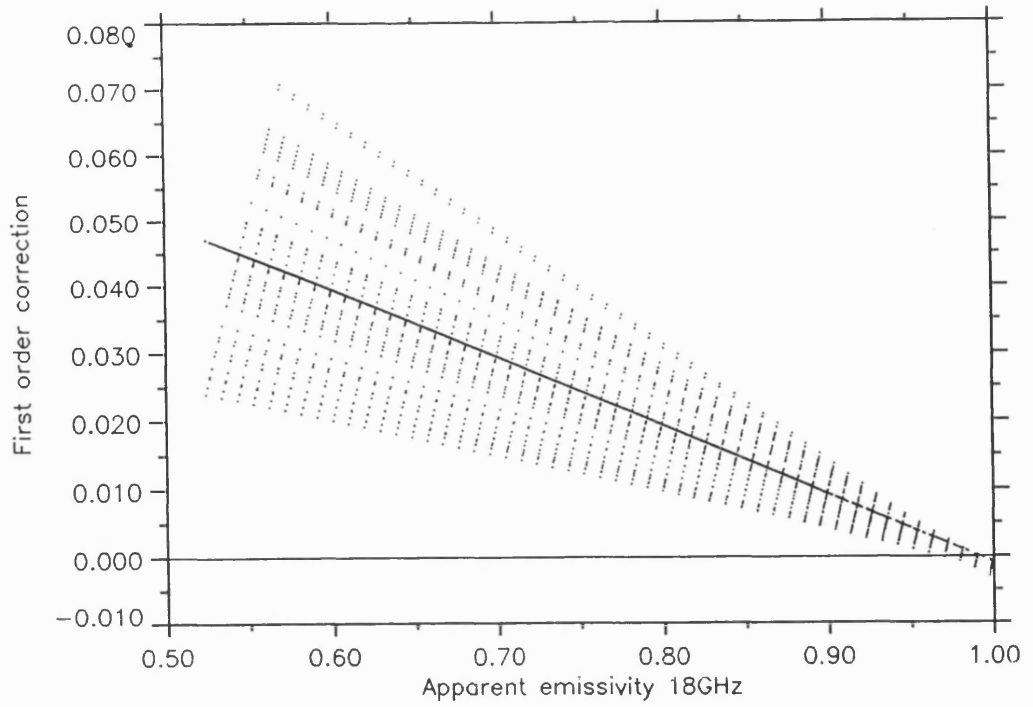

Figure 4.15a A first order correction plot against apparent emissivity at 18 GHz (TOPEX channel) for Alice Springs radiosondes.

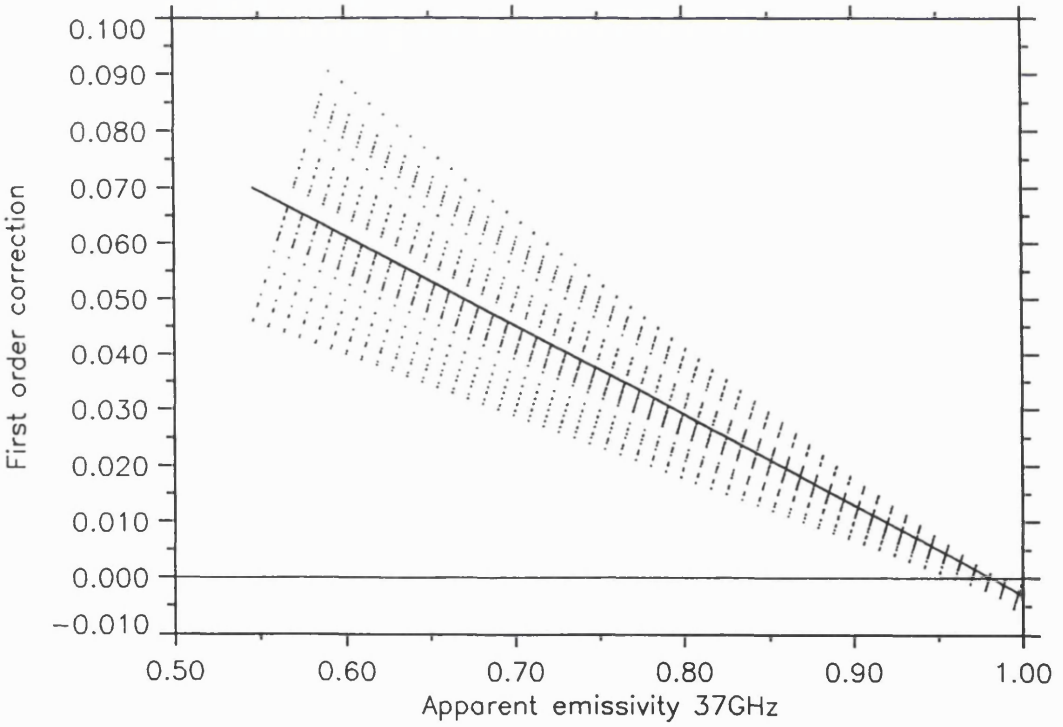

Figure 4.15b A first order correction plot against apparent emissivity at 37 GHz (TOPEX channel) for Alice Springs radiosondes.

Second order correction

The coefficients for the second correction were generated for the following two cases :

1) 37 GHz and 21 GHz
2) 18 GHz and 21 GHz

Tables 4.11(a) to 4.11(d) show the coefficients of the second correction for different ranges of emissivities and for the two possible differences between the two channels under consideration (i.e. 0.0 and 0.02, see section 4.4).

The slopes are the same for the 0.0 and 0.02 possible cases. However, the intercepts differ up to 0.013 in emissivity for the 0.5-0.6 range of emissivity for the 18 GHz frequency (the worst case) and by 0.002 for the 0.9-1.0 emissivity range (the best case). The uncertainty caused by not knowing the true difference in microwave surface emissivity between the two channels is discussed in section 4.5.

The r.m.s. residuals achieved in the worst case is 0.004 (0.4%) at 0.5-0.6 emissivity range at 18 GHz. This is 3.25 times better than the residual after the first correction. For the 37 GHz case the r.m.s residuals achieved in the worst case is 0.005 (0.5%) at 0.5-0.6 emissivity range. This is 2.6 times better than the residual after the first correction. The r.m.s residuals at 0.5 to 0.7 for the 18 GHz channel are less than 37 GHz channel. This is because the 37 GHz channel is more affected by the oxygen than the 18 GHz channel (see figure 3.1).

Alice Springs second order correction coefficients & r.m.s. residuals

Table 4.11a For TOPEX channels, assuming no difference in emissivity between 18 GHz and 21 GHz.

Case	Emissivity range	Intercept	Slope	r.m.s.
1	0.5 - 0.6	-0.033	-0.002	0.004
2	0.6 - 0.7	-0.025	-0.002	0.003
3	0.7 - 0.8	-0.016	-0.002	0.003
4	0.8 - 0.9	-0.009	-0.002	0.002
5	0.9 - 1.0	-0.001	-0.001	0.001

Alice Springs second order correction coefficients & r.m.s. residuals

Table 4.11b For TOPEX channels, assuming 0.02 difference in emissivity between 18 GHz and 21 GHz.

Case	Emissivity range	Intercept	Slope	r.m.s.
1	0.5 - 0.6	-0.046	-0.002	0.004
2	0.6 - 0.7	-0.037	-0.002	0.004
3	0.7 - 0.8	-0.029	-0.002	0.003
4	0.8 - 0.9	-0.018	-0.002	0.003
5	0.9 - 1.0	-0.003	-0.001	0.001

Alice Springs second order correction coefficients & r.m.s. residuals

Table 4.11c For TOPEX channels, assuming no difference in emissivity between 37 GHz and 21 GHz.

Case	Emissivity range	Intercept	Slope	r.m.s.
1	0.5 - 0.6	-0.022	-0.002	0.005
2	0.6 - 0.7	-0.017	-0.002	0.004
3	0.7 - 0.8	-0.012	-0.002	0.003
4	0.8 - 0.9	-0.006	-0.002	0.002
5	0.9 - 1.0	-0.001	-0.001	0.001

Alice Springs second order correction coefficients & r.m.s. residuals

Table 4.11d For TOPEX channels, assuming 0.02 difference in emissivity between 37 GHz and 21 GHz.

Case	Emissivity range	Intercept	Slope	r.m.s.
1	0.5 - 0.6	-0.013	-0.002	0.005
2	0.6 - 0.7	-0.008	-0.002	0.004
3	0.7 - 0.8	-0.003	-0.002	0.002
4	0.8 - 0.9	0.001	-0.002	0.002
5	0.9 - 1.0	0.003	-0.001	0.001

4.4.4 Comparison between results from Alice Springs and Saudi Arabia

A comparison between results from the Alice Springs and day and night Saudi Arabian radiosondes, for the ATSR/M channels are demonstrated in this section. The objectives of these comparisons were described in section 4.4.

The coefficients from the first corrections of the Alice Springs (8 a.m.) were calculated for 36.5 GHz. These coefficients were compared with the night and day Saudi Arabian radiosondes coefficients (see table 4.12). The results show that the 3 a.m. Saudi coefficients are closer to the 8 a.m. Alice Springs ones. The difference in the intercept and slope at these two times will cause an error in emissivity ≤ 0.001 for the worst case (i.e. at low surface emissivity and high atmospheric water vapour). However, using the coefficients for Saudi day time at 3 p.m. instead will cause an error of 0.01 for the worst case. The residuals after the first order correction for the Saudi night and Alice Springs are shown in table 4.13. Since the night-time Saudi coefficients are similar to those for Alice Springs, the second order correction will be for these two.

The coefficients of the second correction are listed in tables 4.14 and 4.15 for Alice Springs and Saudi respectively. The coefficients from both these radiosondes are similar, and the difference in the intercepts will cause an error no greater than 0.001 in emissivity. A discussion of the differences in results due to different diurnal times and different desert atmospheres is given in the next section.

Table 4.12 Comparison between the first order correction coefficients for Alice Spring (8 a.m.) & Saudi (3 a.m.)and (3 p.m.).

Radiosonde	Emissivity	Intercept	slope
Alice Springs (8 a.m.)	0.5-1.0	0.156	-0.160
Saudi Arabia (3 a.m.)	0.5-1.0	0.153	-0.157
Saudi Arabia (3 p.m.)	0.5-1.0	0.136	-0.141

Table 4.13 R.M.S residual after first correction for different ranges of emissivities and for 36.5 GHz ATSR/M channel.

Emissivity range	r.m.s. Alice Springs (8 a.m.)	r.m.s. Saudi (3 a.m.)
0.5-0.6	0.013	0.016
0.6-0.7	0.010	0.012
0.7-0.8	0.007	0.008
0.8-0.9	0.004	0.005
0.9-1.0	0.002	0.002

Alice Springs (8 a.m.) second order correction coefficients & r.m.s. residuals

Table 4.14 For ATSR channels, assuming no difference in emissivity between 36.5 GHz and 23.8 GHz.

Case	Emissivity range	Intercept	Slope	r.m.s.
1	0.5 - 0.6	-0.022	-0.002	0.005
2	0.6 - 0.7	-0.017	-0.002	0.004
3	0.7 - 0.8	-0.012	-0.002	0.003
4	0.8 - 0.9	-0.006	-0.002	0.002
5	0.9 - 1.0	-0.001	-0.001	0.001

Saudi (3 a.m.) second order correction coefficients & r.m.s. residuals

Table 4.15 For ATSR channels, assuming no difference in emissivity between 36.5 GHz and 23.8 GHz.

Case	Emissivity range	Intercept	Slope	r.m.s.
1	0.5 - 0.6	-0.024	-0.002	0.006
2	0.6 - 0.7	-0.018	-0.002	0.005
3	0.7 - 0.8	-0.013	-0.002	0.004
4	0.8 - 0.9	-0.007	-0.002	0.003
5	0.9 - 1.0	-0.001	-0.001	0.002

4.5 Discussion of Results

The correction coefficients derived here give specific results which are valid only for regions with similar atmospheres (and the same microwave frequencies) as those used in these simulations.

In this section, the results from the simulations using the North Atlantic, Global, and Alice springs radiosondes are discussed as well as the results from the comparison of the desert radiosondes. The discussion covers the following different aspects:

1. The residual error after the application of the first and second order corrections and the dependence of the accuracy of the correction technique on total water vapour in the atmosphere at different surface microwave emissivity ranges. The discussion will include the limits of the new technique.

2. The dependence of the slope and intercept of the first and the second order corrections on water vapour and microwave surface emissivity. Also, the dependence of atmospheric effects on microwave frequency will be considered.

3. In chapter 5, the technique is validated over the ocean considering those data having wind speed $\leq$ 7m/s. This section will demonstrate how it is possible to get the second correction intercept for the ocean case from knowing the sea surface temperature. For soil, the choice of the correct intercept is complicated by the fact that difference between the true surface emissivities of the two microwave channels is not known. In chapter 6, the application of the technique is performed over Simpson Desert, therefore the choice of the correct intercept in the second correction for soil is discussed and the errors in not knowing the intercept are assessed in this section. It is important to note that the 2nd order slope remains constant in all scenarios.

4. The comparison between Alice Springs and day and night Saudi desert radiosondes.

1. Residuals

Tables 4.16(a) and 4.16(b) summarise the r.m.s. residual errors in the microwave surface emissivity after the first and second corrections. From these tables we can deduce the following:

1. As the water vapour content increases, the difference between the radiance received by the satellite and that emitted from Earth's surface increases, due to the increase of the downwelling and upwelling atmospheric emission. Therefore, the r.m.s. error after the first and second order correction increases. This can be seen from the comparison of North Atlantic with Alice Springs and Global radiosondes. Figure 4.16 shows this dependence of the r.m.s. residual on total water vapour from the comparison between North Atlantic and Global data sets.

2. The r.m.s residual error is inversely dependent on the surface microwave emissivity. High surface emissivities have small r.m.s. residuals, while low emissivities have larger r.m.s. residuals. This is due to the increased contribution from the downwelling atmospheric emission as emissivity decreases (i.e. reflectivity increases). The exception is the second r.m.s residuals of the North Atlantic radiosondes which have the lowest total water vapour atmospheres and do not show any dependence on surface emissivity. Figure 4.16 show this dependence of the r.m.s residual on surface emissivity from the comparison between North Atlantic and Global data set. From this figure and tables 4.16(a) and (b), it can be seen that the dependence on surface emissivity is greater after the first order correction than after the second order correction.

3. Figure 4.16 and tables 4.16(a) and (b) show that there is no need for the second correction at high emissivities (i.e. 0.9 to 1.0) as the atmospheric effects are small at higher emissivities. However, the second correction is necessary for lower values of surface emissivity . At high emissivities, the achievable accuracy in emissivity after the second correction is 0.001 for all cases, while at low emissivities it is 0.001 for North Atlantic, 0.005 for Global, and 0.004 for Alice Springs. In section 4.6, the effects of the measurement noise from the microwave radiometer and the surface temperature retrieval from the infrared radiometer are investigated.

Table 4.16a R.M.S residuals after first order correction for different radiosondes and radiometric frequencies

Radiosonde	Frequency GHz	r.m.s. 0.4-0.5	r.m.s. 0.5-0.6	r.m.s. 0.6-0.7	r.m.s. 0.7-0.8	r.m.s. 0.80-0.9	r.m.s. 0.9-1.0
N.Atlantic (ocean)	36.5 ATSR	0.007	0.006	0.005	0.003	0.002	0.001
Global (ocean)	36.5 ATSR	0.022	0.017	0.013	0.009	0.005	0.002
Alice Springs (desert)	18 TOPEX	****	0.013	0.010	0.007	0.004	0.001
Alice Springs (desert)	37 TOPEX	****	0.013	0.010	0.007	0.004	0.002

Table 4.16b R.M.S residuals after second order correction for different radiosondes and radiometric frequencies

Radiosonde	Frequency GHz	r.m.s. 0.4-0.5	r.m.s. 0.5-0.6	r.m.s. 0.6-0.7	r.m.s. 0.7-0.8	r.m.s. 0.80-0.9	r.m.s. 0.9-1.0
N.Atlantic (ocean)	36.5 ATSR	0.001	0.001	0.001	0.001	0.001	0.001
Global (ocean)	36.5 ATSR	0.005	0.004	0.004	0.003	0.003	0.001
Alice Springs (desert)	18 TOPEX	****	0.004	0.003	0.003	0.002	0.001
Alice Springs (desert)	37 TOPEX	****	0.005	0.004	0.003	0.002	0.001

**** not in the range of soil emissivities

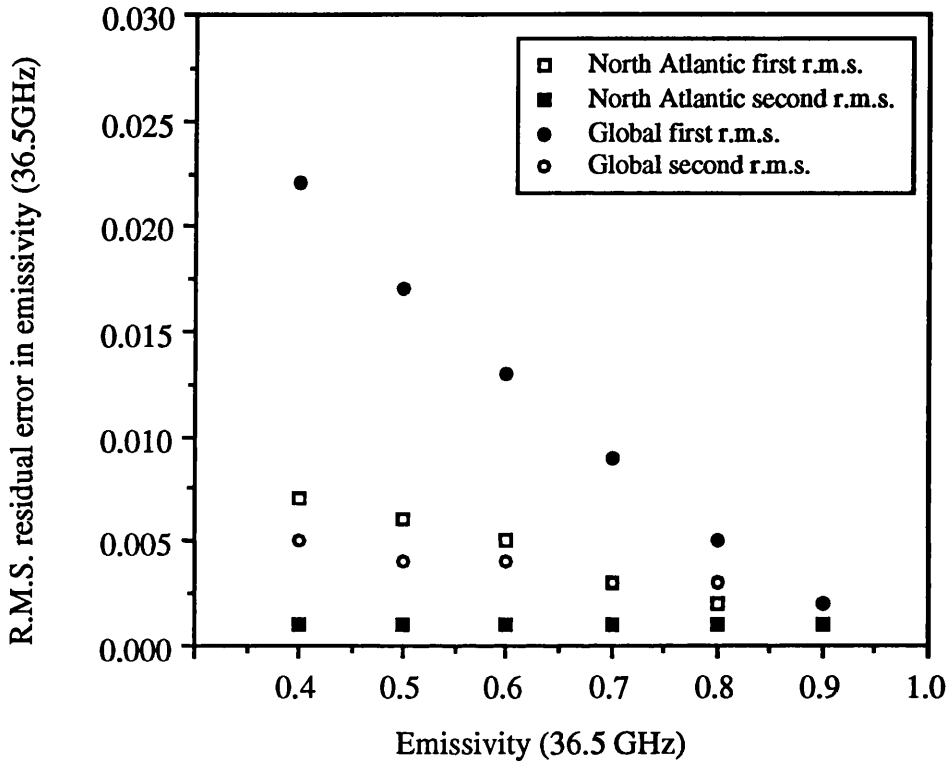

Figure 4.16 The r.m.s residual after first and second order correction against surface microwave emissivity at 36.5 GHz for North Atlantic (average total water vapour = 9.5 kg/m2) and Global (average total water vapour = 35 kg/m2). This diagram illustrates the dependence of r.m.s residual on total water vapour and surface emissivity.

Third order correction and the limits of the new technique

The possibility of a third order correction to refine the final estimate of the true surface emissivity is investigated here. This correction assumes that any intrinsic errors following the second order correction is due to a third order atmospheric effect (principally due to water vapour, or atmospheric temperature). Assuming that the intrinsic errors are due to water vapour variations, we perform the third order correction based on the same principle used in the second order correction.

The third correction is performed using the Global radiosondes as they have the highest water vapour atmospheres. The example given assumes that the surface emissivity is 0.4 and the difference in surface microwave emissivity between the two ATSR/M channels is 0.04 (e.g. the surface microwave emissivity at 36.5 GHz is 0.4 and at 23.8 GHz is 0.36). Since after the application of the second correction, the surface emissivity is known within 0.005 for all emissivities from 0.4 to 0.5, the third correction is performed at one surface microwave emissivity, which is 0.4, as an example.

By plotting the residuals left after the second order correction against the difference between TB36.5 and TB23.8, we obtain figure 4.17. The coefficients of the least squares fit are used to perform the third order correction following the same steps of the second correction described in section 4.3. Figure 4.18 shows the residuals left after the third correction against the difference between TB36.5 and TB23.8. It is clear that the slope in this figure is ≈ 0.0 which indicates the limit of this correction. Also, the r.m.s. left after the third correction which is 0.004, has not been significantly improved compared with r.m.s. residual after the second correction which is 0.005 and there is still some residual scatter around the zero line, after third correction (see figure 4.18).

The conclusion from this investigation is that the residuals are due to atmospheric temperature. Since the upwelling and downwelling atmospheric emission are dependent on air temperature as well as water vapour and oxygen. Also, and to a less extent, air temperature increases the strength of oxygen line absorption at 37 GHz due to line broadening. Therefore, there will be more of the atmospheric emission.

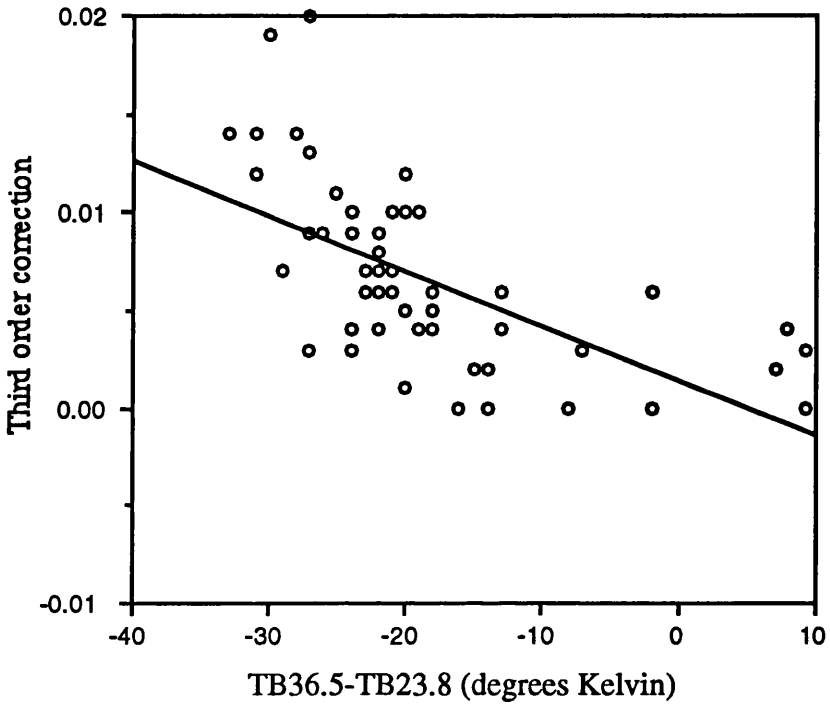

Figure 4.17 Plot of third order atmospheric correction for 36.5 GHz channel against the difference in microwave brightness temperature at 36.5 GHz and 23.8 GHz (ATSR/M channels).

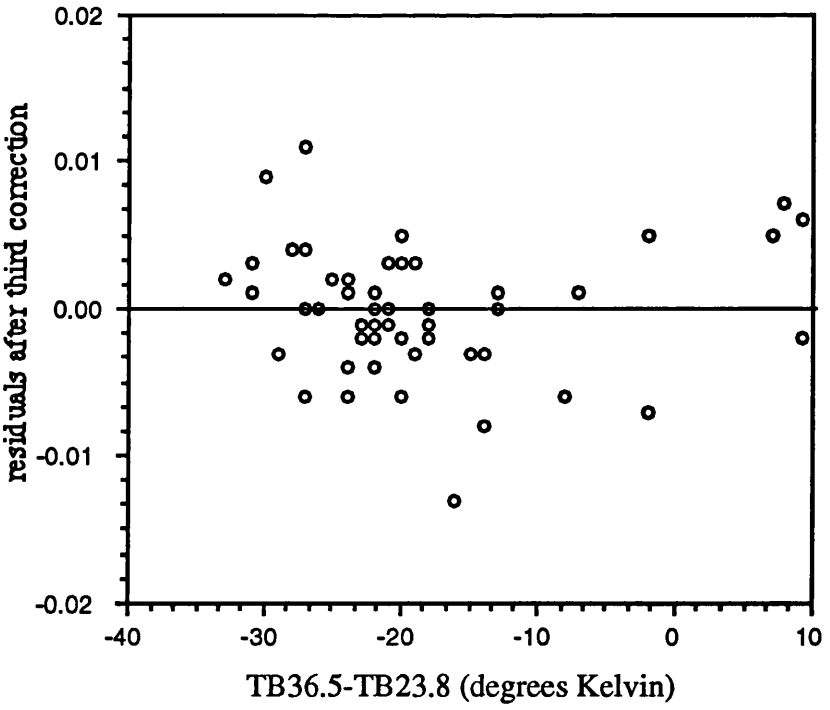

Figure 4.18 Showing the residuals after the third correction against the difference in microwave brightness temperature at 36.5 GHz and 23.8 GHz. This figure shows the limit to the atmospheric corrections. The example shown here is for the Global radiosonde.

2. Coefficients of first and second order corrections

The slope and the intercept of the first order correction do not depend on the surface emissivity. This is clear from equation (4.6) and the results described. The slope and the intercept of the first order correction depend principally on mean atmospheric parameters-chiefly due to variations in atmospheric water vapour (see figures 4.19 and 4.20). The two figures show the total water vapour against the slope and intercept from the first order correction for different atmospheres in the North Atlantic, Global, and Alice Springs radiosondes. The global atmospheres which have the highest total water vapour for most cases have the steeper gradients, while the North Atlantic atmospheres which have the lowest total water vapour contents for most of its atmospheres have the lower gradients. Similarly, the Global atmospheres (highest in total water vapour) have the highest intercepts, while the North Atlantic atmospheres (lowest in total water vapour) have the lowest intercepts. The majority of Alice Springs atmospheres lie between the Global and North Atlantic atmospheres. The dependence of the slopes and intercepts on total water vapour is expected, as the apparent microwave emissivity increases as water vapour increases due to the increase of upwelling atmospheric emission and the downwelling reflected atmospheric emission.

In the second order correction, the slope for all radiosondes and surface emissivities have the same value, which is 0.002. The intercept in the second correction becomes negative value as the water vapour increases. For example, comparing North Atlantic (low water vapour) with Global (high water vapour) in the 0.4 to 0.5 range of surface emissivity, the intercept coefficients are 0.012 and -0.038 respectively. This is because the 23.8 GHz is more sensitive to water vapour and therefore the brightness temperature at 23.8 GHz exceed that at 36.5 GHz due to the increase of both upwelling and reflected downwelling atmospheric emission. Therefore, (TB36.5 - TB23.8) becomes more negative with water vapour (see figure 4.7). As we go to global atmospheres (more water vapour content), figure 4.13 shows the difference (TB36.5 - TB23.8) for surface emissivities in the range 0.4 to 0.8 have higher negative values compared with the North Atlantic ones, and therefore the line of the least squares fit intercept the y-axis at higher negative intercept values.

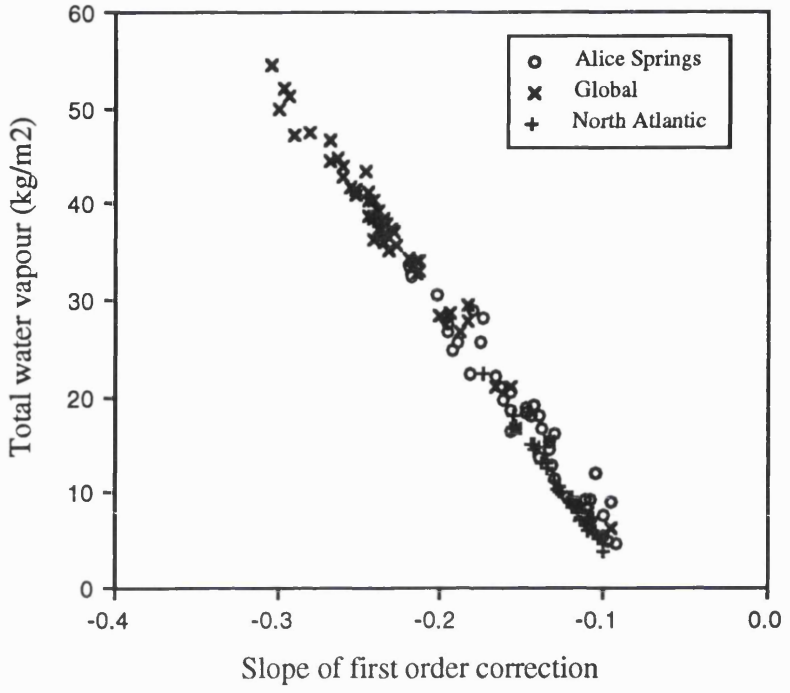

Figure 4.19 Showing the total water vapour (kg/m2) against the slope of first order correction for North Atlantic, Global, and Alice Springs radiosondes. Averaged total water vapour is 9.5 kg/m2, 35 kg/m2, and 18 kg/m2 for North Atlantic, Global, and Alice Springs respectively.

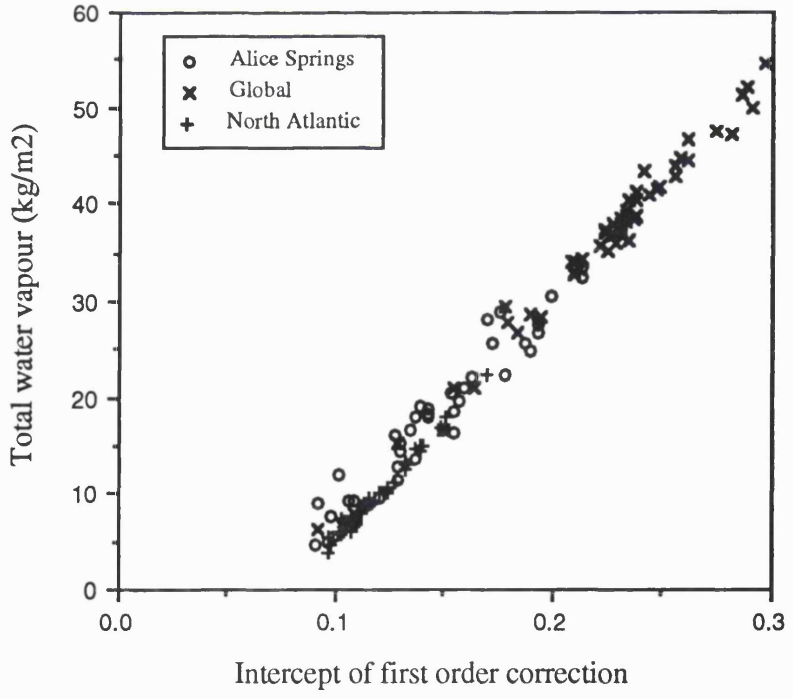

Figure 4.20 showing the same thing but this time it is the dependence of the intercept of the first order correction on total water vapour.

Simulations of Alice Springs radiosondes at 37 GHz and 18 GHz showed that the effect of the atmosphere at 37 GHz is more pronounced than at 18 GHz (see section 4.4.3). However, even if we go to low frequencies, the atmosphere is still affecting the apparent emissivity at low true surface emissivities. For example, figure 4.21 shows the first order correction for 1.4 GHz at 0.5-0.6 emissivity range. The figure shows that the apparent emissivity overestimates the true emissivity by more than 0.01 at emissivity = 0.5.

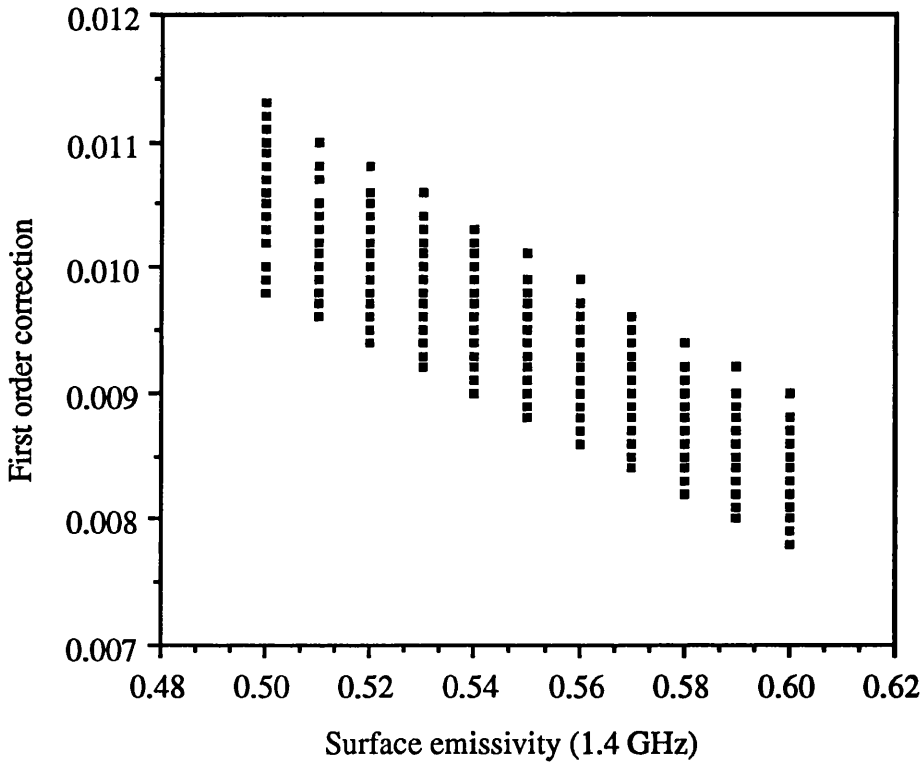

figure 4.21 A first order correction plot against apparent emissivity at 1.4 GHz for Alice Spring radiosondes and for 0.5 to 0.6 true surface emissivity range.

3. The choice of the correct intercept in the second order correction

After the first order correction, the microwave emissivity is corrected to within 0.007 in emissivity (worst case) for the North Atlantic, within ~ 0.022 (worst case) for Global and within 0.013 (worst case) for Alice Springs. Therefore it is possible to know what range the surface emissivity lies in to within 0.02. The remaining problem is the choice of the correct intercept of the second order correction as this depends on the difference in microwave surface emissivity between the two microwave channels. From previous results, the intercept increases as the difference in emissivity between the two frequencies increases. Figure 4.22 shows a plot of the intercept of the second correction against the emissivity difference from tables 4.4(a) to 4.4(d) for the North Atlantic radiosonde measurements for the 0.4 to 0.5 emissivity range.

Over the ocean, and for wind speeds less than 7m/s, the microwave emission depends primarily on sea surface temperature. Therefore it is possible to predict the difference in surface microwave emissivity between the 36.5 GHz and 23.8 GHz ATSR/M channels by knowing the sea surface temperature from IR data (figure 4.23). From figures 4.22 and 4.23, it is possible to predict the intercept of the second order correction by knowing the sea surface temperature. The coefficients which relate the sea surface temperature with the intercept of the second correction will be demonstrated in the validation of the new technique in chapter 5.

The question that arises is: what is the final uncertainty in determining the surface microwave emissivity if the difference in surface microwave emissivities between the two frequencies used in the second correction cannot be determined? The example given here is for soil surfaces (Alice Springs results) which will be used in chapter 6.

Uncertainty in the intercept of the second order correction for the Alice Springs

The maxima and minima in the emissivity difference between the two microwave frequencies (i.e. 21 and 37 GHz) used in the second correction are 0.02 and zero (see section 4.4). In the real case, as the statistical distribution between the difference in the true surface emissivities at the two frequencies is not known, we will assume a Gaussian distribution. Therefore the total error will include this uncertainty in the intercept of the second order correction together with the r.m.s. residuals after the second order correction for Alice Springs case is $\delta\varepsilon$:

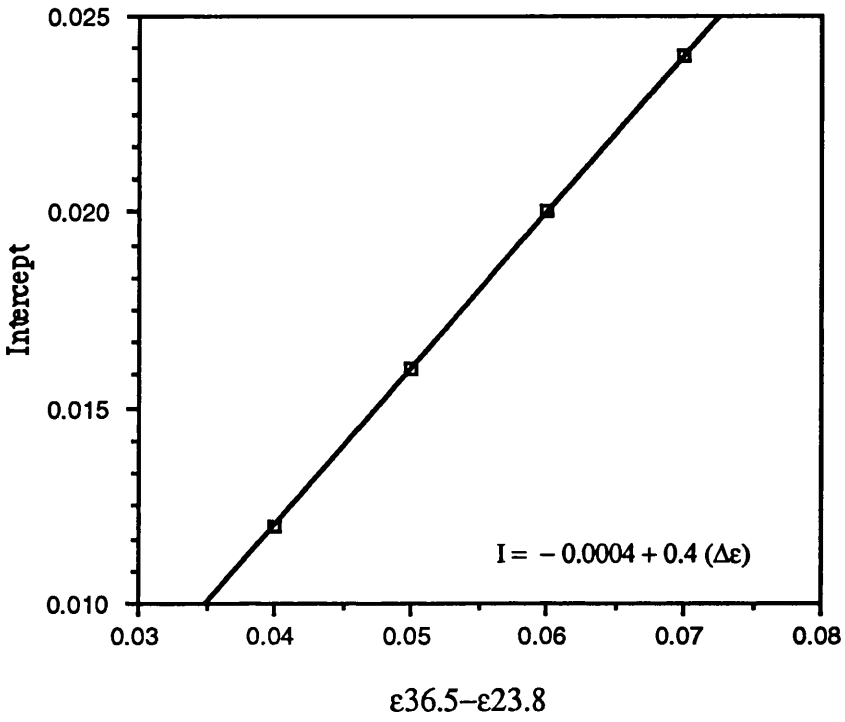

Figure 4.22 The dependence of the intercept of the second order correction on the surface microwave emissivity difference between 36.5 GHz and 23.8 GHz. (North Atlantic)

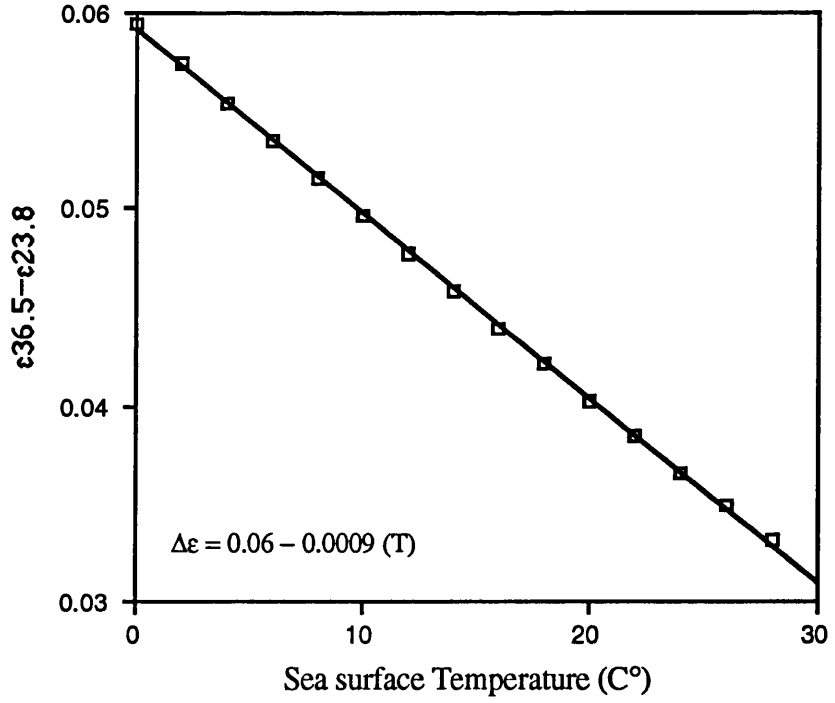

Figure 4.23 The dependence of the emissivity difference (ε36.5–ε23.8) on the sea surface temperature for wind speed around or less than 7m/s. The simulation is based on the Wilheit model (chapter 2).

$$\delta\varepsilon = \sqrt{(r.m.s.residual)^2 + (1/4\Delta)^2} \qquad (4.11)$$

where Δ = intercept coefficient (no emissivity difference) - intercept coefficient (0.02)

The uncertainties ($\delta\varepsilon$) for all possible ranges of microwave emissivities are shown in table 4.17 for the Simpson case and for TOPEX channels. This table shows that the effect of the uncertainty due to not knowing the intercept of the second order correction on the results is very small, and it is within ~0.001 or less compared to the r.m.s error after the second order correction (see table 4.11).

Table 4.17 The total error as described in equation 4.11 for Alice Springs at 18 and 37 GHz

Emissivity range	$\delta\varepsilon$ (18 GHz)	$\delta\varepsilon$ (37 GHz)
0.5-0.6	0.005	0.006
0.6-0.7	0.004	0.005
0.7-0.8	0.004	0.004
0.8-0.9	0.003	0.003
0.9-1.0	0.001	0.001

4. Desert radiosondes (Alice Springs & Saudi)

The results from the comparison of desert radiosondes show the following:

1. The comparison between Saudi night and day data, show that there is a significant difference in the coefficients of first order correction. This difference causes an error of 0.01 for the worst case. The difference in the coefficients of first order correction is due to the variation between day and night air temperatures over the desert. During the day the atmosphere tends to be cooler with respect to the surface temperature, while during the night the atmosphere tends to be warmer with respect to the surface temperature. As a result, the contribution from the atmospheric emission during the night is more than that during the day. Therefore it is not recommended to use coefficients of corrections of the night (around midnight) radiosonde to correct for day (around noon time) microwave satellite measurements or vice versa.

2. The first correction coefficients of Alice Springs are closer to Saudi night-time. The difference causes an error of less than 0.001 in emissivity. The comparison between the second order correction of Alice Springs and Saudi data show that the difference in the coefficients is small, and will cause an error less than 0.001 in emissivity. These results indicate that it is possible to use coefficients from Saudi radiosondes to correct for microwave measurements from the satellite over the Simpson desert or vice versa, provided that the radiosondes cover all different seasons and about the same diurnal time as for the satellite measurement.

4.6 Radiometric Limits on the Accuracy of the New technique

The r.m.s. residual errors quoted in the tables are derived solely from the atmospheric model and do not include any contribution from uncertainties in the satellite microwave radiometric measurements or the accuracy of surface temperature determination from the infrared radiometer . These r.m.s. errors were calculated for the perfect case where T_B and T_S in equation (4.7) do not have any errors. Actually, the microwave absolute radiometric error for ATSR/M is quite high ~ 3 K (Bernard et al.. 1993), and the radiometric noise is 0.4 K. For the TOPEX microwave radiometer, the net uncertainties in brightness temperature is also significant (0.79 to 0.88 K-Janseen et al. 1995) (see chapter 3). Also, the impact of the accuracy of surface temperature determination for ocean and land need to be considered (chapter 5 and 6).

In order to assess the total error in determining the surface microwave emissivity, we first propagate the errors due to microwave radiometer measurement and the accuracy of surface temperature determination from the following expressions:

The error in the apparent emissivity from equation (4.2a) is :

$$\delta\varepsilon^* = \sqrt{(\frac{\delta T_B}{T_S})^2+(\frac{T_B}{T^2_S}\times\delta T_S)^2} \tag{4.12}$$

Then the error in the emissivity after first order correction from equation (4.7) is:

$$\delta\varepsilon 1 = \sqrt{\delta\varepsilon^{*2}+(1-\frac{1}{(a-b)}\delta\varepsilon^*)^2} \tag{4.13}$$

The propagated error in the second order correction from equation (4.9) is:

$$\delta\varepsilon 2 = \sqrt{\delta\varepsilon 1^2+(m\delta TB_{V1})^2+(m\delta TB_{V2})^2} \tag{4.14}$$

In this section the expected total error in emissivity is investigated for the following two cases :

A. *The North Atlantic dataset* which is used in the validation of the technique over the ocean surface around the UK (see chapter 5). The ATSR/M microwave radiometer was used to measure TB, and the ATSR IR radiometer was used for determining the sea surface temperature over the ocean surface. In this case the contributions to the total error in emissivity are :

1. The r.m.s residual error left after the second order correction for the North Atlantic case.

2. The radiometric contribution to TB measurement error for ATSR/M. The absolute calibration error (~3 K) which is a bias and the radiometric resolution (0.4 K)which is a random error.

3. The accuracy of sea surface temperature SST from the ATSR product provided by RAL (see chapter 5). The expected error from these products is ± 0.4°C r.m.s. error with a bias up to 0.4°C due to the skin effect (Harris et al 1995).

The total error in surface emissivity for the ocean case (wind speed < 7m/s), including the r.m.s. residual from the technique and the propagated error from radiometric measurements which is calculated in equation (4.14) is:

$$\delta\varepsilon(total\text{-}ocean) = \sqrt{\delta\varepsilon_2^2+(\text{r.m.s.residual})^2} \qquad (4.15)$$

The calculated total error is 0.003 r.m.s. due to ATSR/M radiometric noise plus the error in SST measurement, while the anticipated bias due to the absolute calibration is 0.01. In chapter 5 this error will be considered in the validation of the new technique over the North Atlantic ocean.

B. The Alice Springs case, which is used in chapter 6 as an application of the technique for soil moisture measurements over the Simpson desert. The TOPEX microwave radiometer is used to measure TB, and the AVHRR radiometer is used in determining T_S for the Simpson desert. In this case the contributions to the total error in emissivity are :

1. The r.m.s residual error left after the second order correction for the Alice Springs dataset.

2. The radiometric contribution to TB measurement error for the TOPEX microwave radiometer. The net uncertainties in brightness temperature which range from 0.79 to 0.88K.

3. The accuracy of Ts determination over the Simpson desert from AVHRR infrared radiometer. The expected r.m.s. error in this case is ~1 K (see chapter 6).

4. The uncertainty in the intercept of the second order correction.

The total error in surface emissivity for the soil case including all the above contributions is:

$$\delta\varepsilon(total\text{-}soil) = \sqrt{\delta\varepsilon_2^2 + (\delta\varepsilon)^2} \qquad (4.16)$$

where $(\delta\varepsilon)$ is the from equation (4.11) and includes both contribution (1) and (4).

The results of the total expected error in surface microwave emissivity for the Alice Springs case and at 18GHz is shown in tables 4.18. The total error range from 0.003 for $0.9 \leq \varepsilon < 1.0$ to 0.006 for $0.5 \leq \varepsilon < 0.6$. The results in table 4.18 are very encouraging. These errors will be assessed in terms of the requirements for soil moisture measurements for the purpose of climate application in chapter 6.

Table 4.18 Showing total expected error in surface microwave emissivity for Alice Springs dataset at 18 GHz including the r.m.s. residual after the second order correction, radiometric noise from TOPEX microwave radiometer, the accuracy in determining the land surface temperature from AVHRR, and the uncertainty in the intercept of the second order correction.

Emissivity range	$\delta\varepsilon 2$	$\delta\varepsilon$	*Total*
0.5-0.6	0.003	0.005	0.006
0.6-0.7	0.003	0.004	0.005
0.7-0.8	0.003	0.004	0.005
0.8-0.9	0.003	0.003	0.004
0.9-1.0	0.003	0.001	0.003

4.7 Conclusions

We can summarise the results from this chapter as follows:

- A novel atmospheric correction technique is proposed in this work to retrieve the true surface microwave emissivity from satellite measurements. The method uses simultaneous measurements from microwave and infrared satellite radiometers.

- A radiative transfer model together with generic atmospheres covering all seasons have been used to investigate the effect of the atmosphere for a range covering all possible terrestrial emissivities. The atmospheric effect - mainly due to water vapour - increases as the true surface emissivity decreases due to the increase of the downwelling reflected atmospheric emission. This effect is more pronounced at higher water vapour atmospheres and at higher microwave frequencies. At 36.5 GHz (ATSR/M), the effect can be up to 0.14 in emissivity for tropical atmospheres.

- The technique corrects the apparent microwave emissivity as seen by the satellite radiometer for emissivity and water vapour effects by using first and second order corrections respectively. The essence of the first order correction is that the relationship between the apparent microwave emissivity and the true surface emissivity is linear and the difference between them is proportional to the apparent microwave emissivity. The essence of the second order correction is that any residuals following the first order correction are due principally to the absorptivity of the atmosphere - chiefly due to water vapour. Therefore the second order correction makes use of two microwave frequencies, one of which is more sensitive to the water vapour, to compensate for the dependence on water vapour content.

- The proposed technique has been demonstrated to correct the microwave emissivity for the effect of the atmosphere to an accuracy of 0.001 r.m.s for atmospheres with low to middle in water vapour content and for all emissivities in the 0.4-1.0 range. For atmospheres with higher water vapour contents up to 55 kg/m^2, the accuracy is expected to be between 0.001-0.005 depending on emissivity.

- The water vapour content and emissivity value affect the accuracy of surface emissivity retrieval. The higher the water vapour content and the lower the emissivity, the higher the r.m.s. error.

- The slope and intercept of the first order correction depend on mean atmospheric parameters-chiefly due to variations in atmospheric water vapour. The slope and intercept do not depend on surface emissivity. In the second order correction the slope for all atmospheres and surface emissivities have the same value, which is 0.002. The intercept of the second order correction go to higher negative values as we go to higher water vapour atmospheres. Also, the intercept depends on the difference between the true surface emissivities at two frequencies. For ocean and for wind speeds ≤ 7 m/s, it is possible to predict the intercept by knowing the sea surface temperature based on Wilheit model. For bare soil, the effect of the uncertainty in the intercept of the second order correction on the results is very small and it is with in ~0.001 or less.

- The residual scatter which are left after the third order correction are mainly due to atmospheric temperature effect. Since the upwelling and downwelling atmospheric emission are dependent on air temperature as well as water vapour and oxygen. To a lesser extent, higher air temperature increases the strength of oxygen absorption line at 37 GHz due to line broadening, leading to more atmospheric emission (and absorption).

- Over the deserts, the Alice Springs (8 a.m.) coefficients are very close to the Saudi (3 a.m.) coefficients and that the difference will cause an error in emissivity ≤ 0.001 for the worst case. However, the comparison between Saudi night and day data, show that there is a significant difference in the coefficients of first order correction. This difference causes an error ~ 0.01 for the worst case. The difference is due to the air temperature difference between night and day atmospheres. Therefore it is not recommended to use coefficients of corrections of the night radiosonde to correct for day microwave satellite measurements or the later to the former.

- Although low frequencies are little affected by the atmosphere, the simulations showed that the emissivity is affected by the atmosphere at low surface emissivities. For example, at 1.4 GHz and for surface emissivity at 0.5, the error in emissivity can be up to 0.01 in emissivity. This is due to the increase of reflected downwelling atmospheric emission. Although such error is still within the 0.02 soil moisture accuracy for climate studies (see chapter 1), it will be shown in chapter 6 that it is feasible to get better accuracy of soil moisture when atmospheric correction is considered and surface temperature is measured with an accuracy of ~ 1 K.

- For the North Atlantic dataset, the calculated total error is 0.003 r.m.s. due to ATSR/M radiometric noise plus the 0.4°C r.m.s. error in SST measurement from ATSR (Harris et al. 1995), while the anticipated bias due to the absolute calibration is 0.01. For the Alice Springs dataset, the total error range from 0.003 for $0.9 \leq \varepsilon < 1.0$ to 0.006 for $0.5 \leq \varepsilon < 0.6$ including the net radiometric noise from TOPEX, the error of surface temperature retrieval from AVHRR (~ 1 K) (chapter 6), and the uncertainty in the intercept of the second order correction.

- The advantages of the new atmospheric correction technique are:

  - The proposed technique is very straight-forward and provides an independent method in correcting microwave data from the knowledge of microwave and infrared satellite brightness temperatures alone without a priori-knowledge of any atmospheric parameters (e.g. simultaneous radiosondes).

  - The potential accuracies for this technique are very encouraging (see before), however it is likely that even better accuracies may be achieved if a correction for atmospheric temperature are considered is incorporated

  - The generated coefficients cover all terrestrial surface emissivities, and thus they can be applied on a global basis, using satellite microwave and infrared data, provided that the atmospheric conditions are similar to those used in generating the coefficient at the first time and at the same radiometric frequency.

- The disadvantages of the new atmospheric correction technique are:

  - The technique treat clear sky conditions only, as the surface temperatures retrieved from infrared radiometers are restricted for non cloudy surfaces.

Chapter 5

Validation of the New Atmospheric Technique

5.1 Introduction

The atmospheric technique described in chapter 4 shows great potential for atmospheric correction of microwave emission. The simulation study showed that if no correction is applied then estimates of the surface emissivity will have errors which depend on surface microwave emissivity and water vapour loading. For the worst case, at 36.5 GHz, when the water vapour is high and the true microwave surface emissivity is low, the technique is capable of reducing the error from bias of 0.1 to 0.001 r.m.s for atmospheres having water vapour less than 2.5 gm/cm^{-3}.

However, two important questions need to be answered: (1) Whether the new technique lines up to the expectations from the simulations in chapter 4? (2) How accurately it is possible to correct the microwave emission with ERS-1 passive microwave and infrared (ATSR) radiometers?

ERS-1 is the most suitable satellite at this time to be used to validate the technique as it provides simultaneous measurements from microwave and infrared radiometers. In this chapter the new atmospheric correction technique is validated using set of satellite microwave emission data from the ERS-1 microwave radiometer (ATSR/M) over the ocean surface around UK.

5.2 Methods

The validation of the new atmospheric correction technique was conducted by comparing the derived microwave emissivity from the ATSR/M (see chapter 3) with predictions from the model for ocean microwave emission of Wilheit (1979).

5.2.1 The Test Area

The ocean around British Isles was chosen for the validation. The region is between latitudes 45°and 60°N and longitudes 4°E and 14°W. Apart from the easy access to the ERS-1 data for this region, an ocean region was chosen as a case study in this validation for the following reasons:

- The ocean has a smaller numbers of surface parameters compared with the land surface (chapter 2). Therefore the computed surface microwave emissivity from any model used in comparison with the corrected satellite measurements, will have limited sources of errors.

- The ocean (not covered with foam) has low microwave emissivity compared with the land surface (see figure 2.15). Chapter 4 showed that this will result in more downwelling reflected microwave emission which will introduce more error to the apparent microwave emissivity. Therefore the ocean region presents a very good opportunity to test the performance of the new atmospheric technique.

5.2.2 Satellite Dataset

The satellite dataset consisted of microwave emission measurements from 123 ATSR/M footprints during the period April-June 1992, figure 5.1. The microwave brightness temperatures from ATSR/M (chapter 3) were normalised using corrected weighted sea surface temperatures from the (ATSR) (see later). The apparent surface emissivity was corrected by using the new atmospheric correction technique and compared with the computed microwave surface emissivity from the model (see next). The following conditions were met by the 123 measurements:

1. Averaged infrared data from ATSR over the ATSR/M footprint were clear from clouds (see later).
2. Data measurements were away from land to avoid land contamination.
3. Surface wind speeds were around or less than 7m/s (see chapter 4).

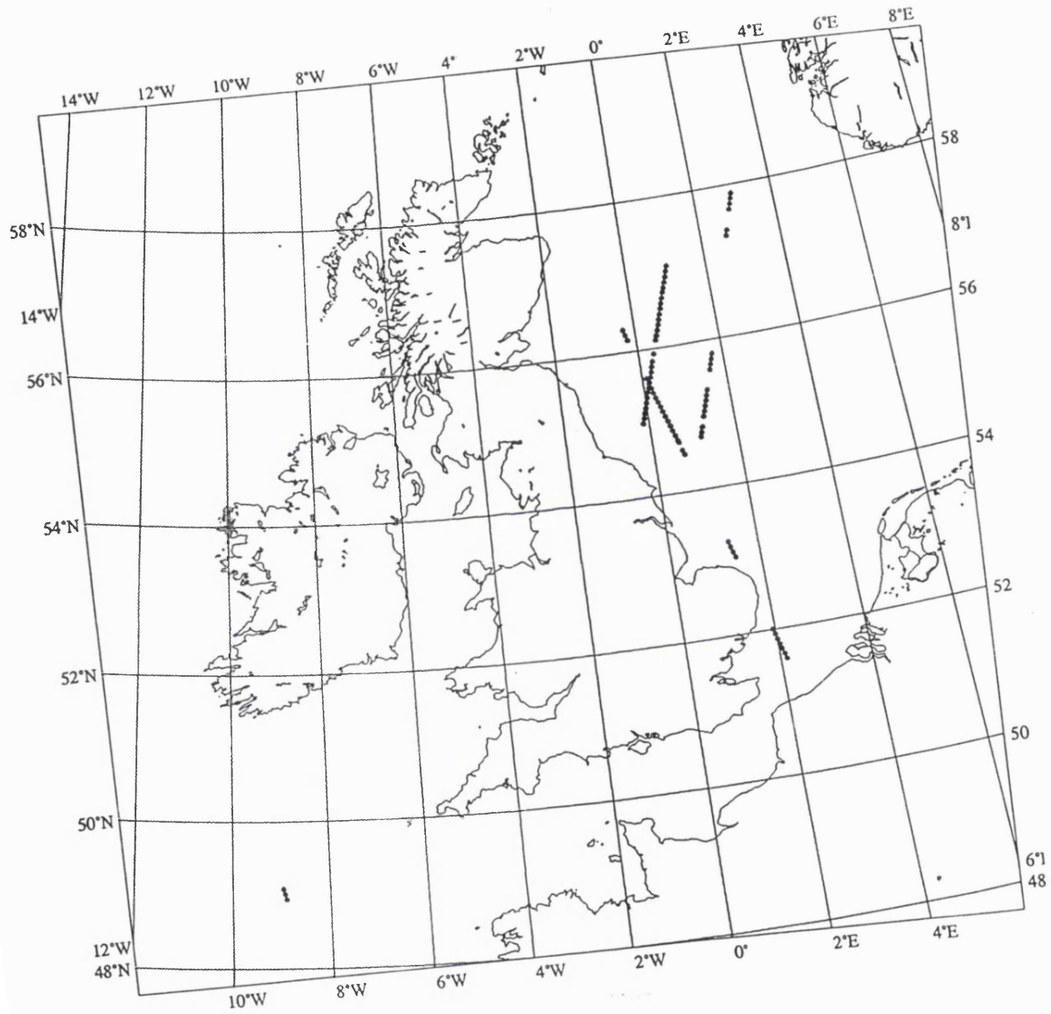

Figure 5.1 Map of British Isles showing the 123 location of ATSR/M footprints

5.2.3 Ocean Emissivity Model

The measured emissivities were compared with predictions from the ocean emissivity model of Wilheit (1979). The model requires input of wind speed and ocean surface temperature, which were obtained from the ERS-1 Altimeter and ATSR respectively.

The anticipated r.m.s error in the retrieval of emissivity from the model due to the wind speed and SST error is discussed in next section. The main reason for choosing satellite derived parameters to compute the emissivity rather than the direct ground measurements is that wind speed and the surface temperatures are from ERS-1 Altimeter and ATSR and are all coincident with the microwave emission data from ATSR/M radiometer.

5.3 Data Corrections and Analysis

This section describes the different processes and corrections applied to the data in order to retrieve the surface parameters. It then describes the sensitivity analysis used to determine the effect of the retrieval accuracies of wind speed and sea surface temperature on the error in the computed emissivity from the model.

5.3.1 Satellite data:

Sea surface temperature (SST)

Satellite infrared radiometry has been used to determine sea surface temperature (SST) for around two decades. This requires a consideration of the radiative properties of the atmosphere and to a lesser extent, the effect of surface emissivity. In the thermal infrared region, the emissivity of sea water is high and relatively constant and therefore is not a major problem. The major source of error in SST determination is the atmospheric absorption of infrared radiation which is partially compensated for by atmospheric emission (Harris and Mason, 1992). Various techniques have been used to account for the atmosphere for SST determination. These techniques were reviewed by Becker and Li (1990).

In this study the ocean surface temperatures were derived directly from the SST products provided by Rutherford Appleton Laboratory (RAL). These temperature were derived using a dual (nadir and forward) view algorithm. The ATSR SST products are validated to have an accuracy of 0.4K (Harris et al. 1995).

Averaging infrared pixels inside ATSR/M footprint

The ATSR pixels (1 km) are not the same size as the ATSR/M footprint (20 km). Therefore averaging is necessary in order to get the infrared values on a scale comparable with the microwave measurements. Such averaging is improved by introducing a weighting function to the ATSR pixels. This weighting function which takes into account the distance of the each pixel from the centre of the microwave footprint can be obtained from the antenna pattern. Assuming that the SST is homogeneous over the microwave footprint an averaging was performed using the mean of SST instead of the weighting function.

Declouding

The derivations of accurate SST from infrared data can only be achieved for areas that are cloud free as brightness temperatures are greatly affected by the presence of clouds. Therefore a computer program written by Dr. Andy Harris at MSSL for cloud clearance was used for this purpose. Only microwave footprints which were at least 90% cloud free were used in this study.

Correction of the sea surface microwave emissivity

The ATSR/M apparent microwave emissivity was then corrected to obtain the true ocean microwave emissivity by applying the coefficients of the first and second corrections using the North Atlantic atmosphere as described in chapter 4.

The first order correction was applied using the coefficients from table 4.2. The intercept of the second order correction depends linearly on the difference in true microwave surface emissivity between the two ATSR/M channels (36.5 GHz and 23.8 GHz) (see figure 4.22). In section 4.5 it was shown also that the difference in the true microwave surface emissivity between the two frequencies depends on sea surface temperature for wind speeds less than 7 m/s (see figure 4.23). Figures 4.22 and 4.23 suggest that it is possible to predict the intercept of the second order correction from the knowledge of the sea surface temperature. Figure 5.2 shows this relation for a range of sea surface emissivity of 0.4 to 0.5.

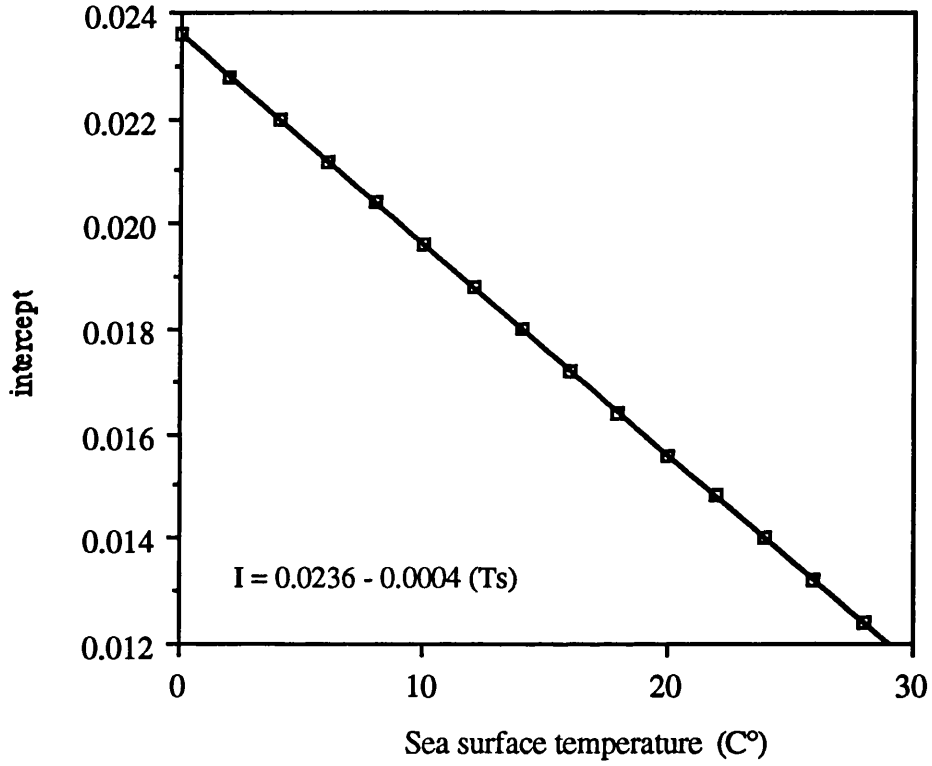

Figure 5.2 This figure shows the dependence of intercept of the second correction on the surface temperature. This dependence is valid for wind speeds around or less than 7m/s.

The correction to the microwave emissivity which is the difference of the apparent emissivity and the emissivity after the second order correction, is plotted against the computed emissivity from 123 measurements in figure 5.3. This figure shows that a substantial correction (0.08 to 0.05) is needed for the surface emissivity in the range of 0.47 to 0.5 as was predicted in the simulations of North Atlantic radiosondes in chapter 4.

5.3.2 Sensitivity analysis of Model Parameters

A stochastic approach was used in the evaluation of the response of microwave surface emissivity to wind speed and SST measurements errors. For wind speeds below 7 m/s the model predicts no emissivity dependence on wind speed (chapter 2). Therefore the model is expected to be mainly sensitive to the surface temperature error. The anticipated r.m.s error in the retrieval of emissivity from the model due to the 0.4 K r.m.s in the SST measurement is 0.002.

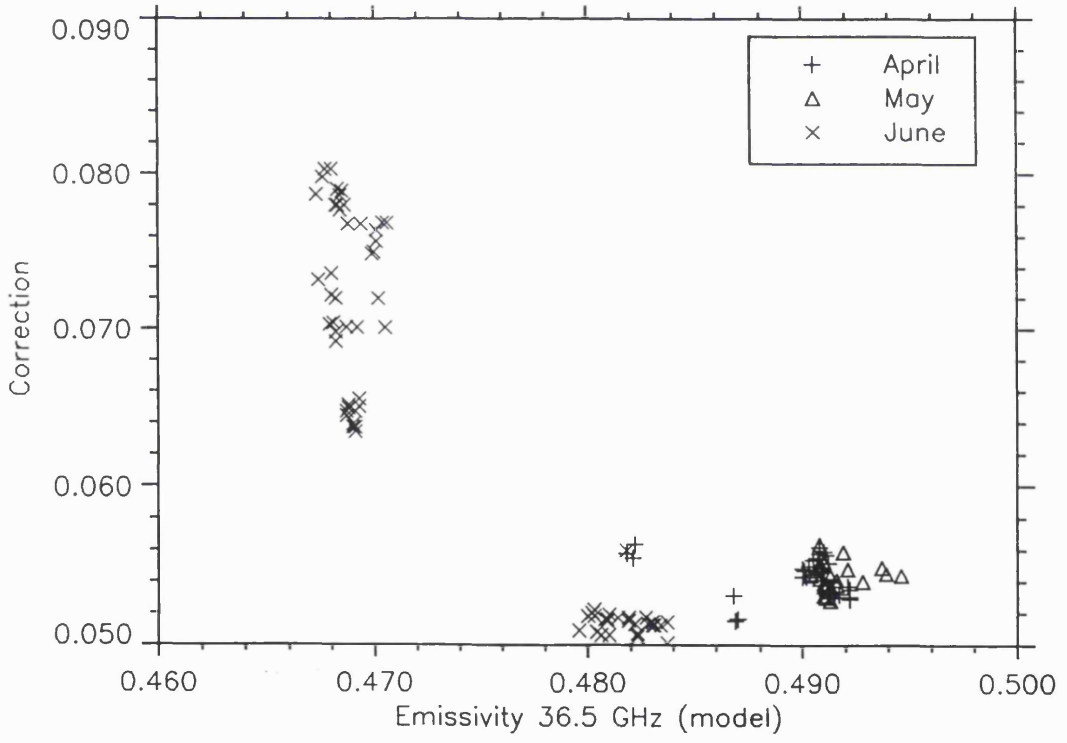

Figure 5.3 The correction of microwave emissivity (i.e. difference between apparent emissivity and emissivity after the second correction). This figure shows that a substantial correction of (0.08 to 0.05) was needed for the surface emissivity in the range of 0.47 to 0.5.

5.4 Results and Discussion

The ATSR/M corrected emissivity is plotted against the model prediction in figure 5.4. The results show that there is a general increase in the corrected emissivity with respect to the 1:1 line. This increase represents a bias rather than a scatter around the 1:1 line. The bias does not follow any temporal relationship as might be expected if it were due to a drift in the radiometer calibration.

The emissivity bias was investigated by plotting it against the surface temperature and wind speed, figures 5.5 and 5.6. Figure 5.5 reveals no dependence of the bias on sea surface temperature. In fact the dependence is upon the wind speed as figure 5.6 shows a general increase of the bias till wind speed of 7 m/s. This observation confirms that the Wilheit model which predicts a constant emissivity as a function of wind speed up to 7m/s, is a simplification (see chapter 2). It appears that there is a linear dependence of emissivity on wind speed below 7m/s.

The points in figure 5.6 show a mean bias of 0.010, but an overall r.m.s difference from the model of 0.003. However, although the predicted maximum bias in measured emissivity due to the 3K absolute calibration is 0.010 (chapter 4), the absolute calibration error in the measurements should not show any dependence on wind speed. The bias appears to be due to the model error rather than to the predicted bias due to the 3K absolute calibration error (see chapter 4). Therefore the absolute calibration error in the measurements in this study may be smaller than 3K .

The 0.003 r.m.s *difference from the model* is within the *predicted* 0.003 r.m.s. from chapter 4 due to the ATSR/M 0.4 K radiometric noise and ATSR 0.4 K r.m.s of SST measurement. Note that the 0.003 r.m.s. *difference from the model* includes both the anticipated 0.002 r.m.s. error in the retrieval of emissivity from the model (see section 5.3.2) due to the SST measurement and the r.m.s. technique error. On the other hand the *predicted* 0.003 r.m.s is the technique error including the radiometric noise (chapter 4).

This validation study has shown that correction of the microwave emissivity from ATSR/M produces a result within the 0.003 predicted r.m.s errors and 0.010 bias (see chapter 4), and is considerably better than that obtained by SSM/I (Fleming et al. 1991) which shows an r.m.s of 0.03 and bias of -0.017.

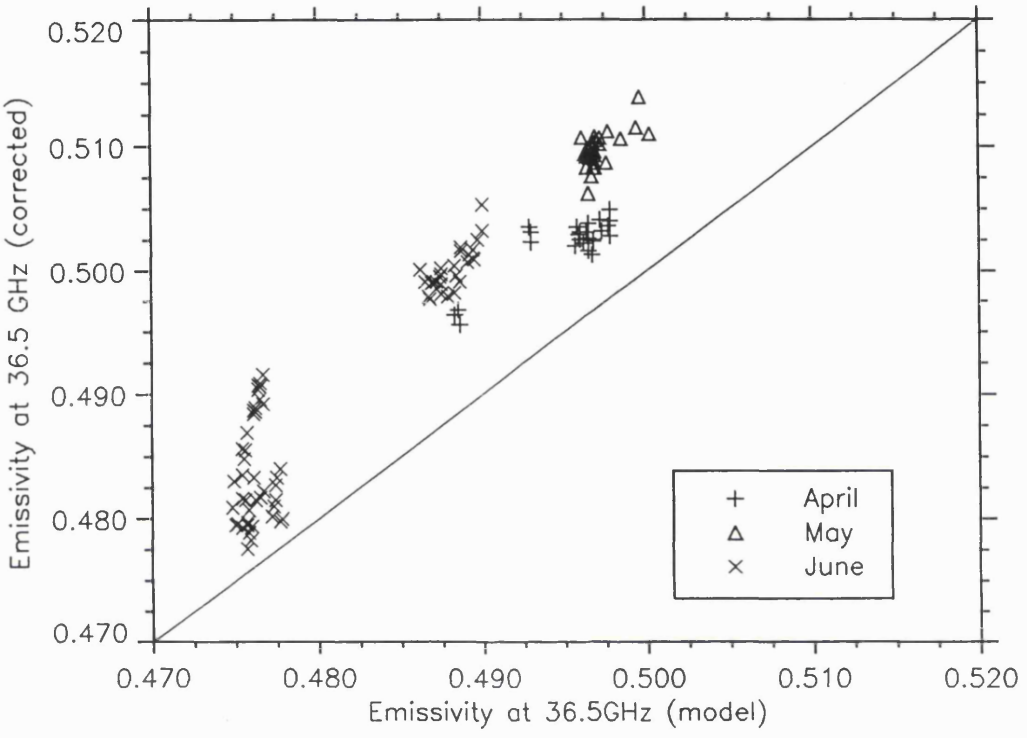

Figure 5.4 Showing the corrected emissivity against the predicted from model. This figure shows that there is a bias with respect to 1:1 line.

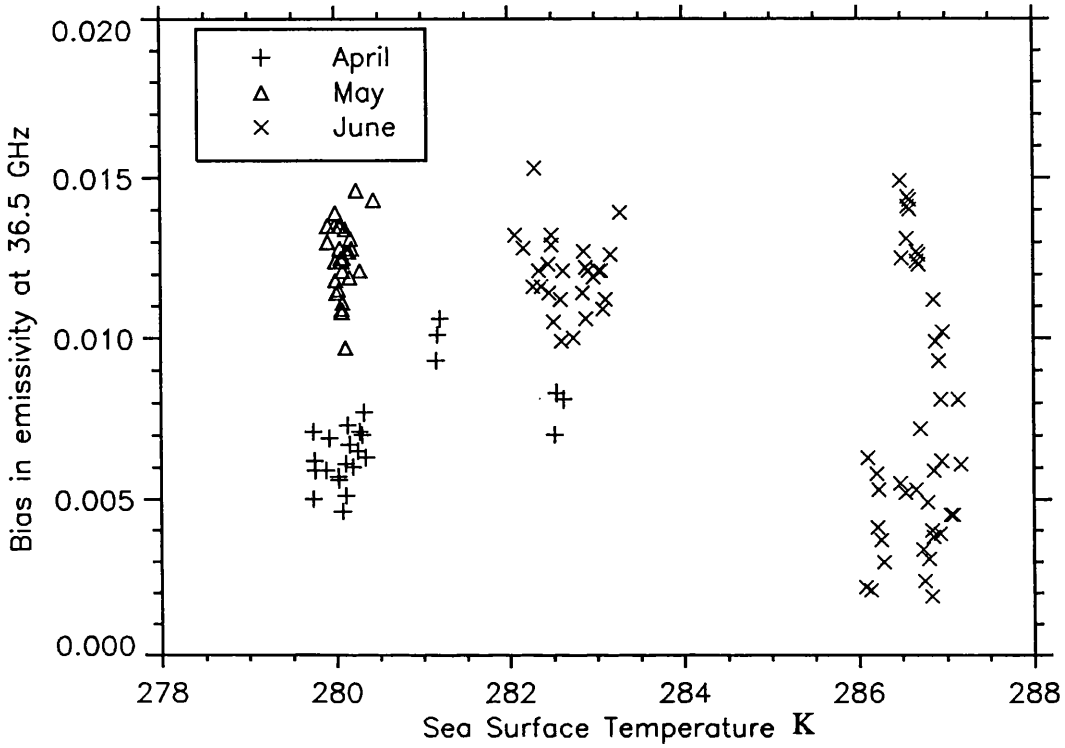

Figure 5.5 Showing that there is no dependence of the bias on surface temperatures.

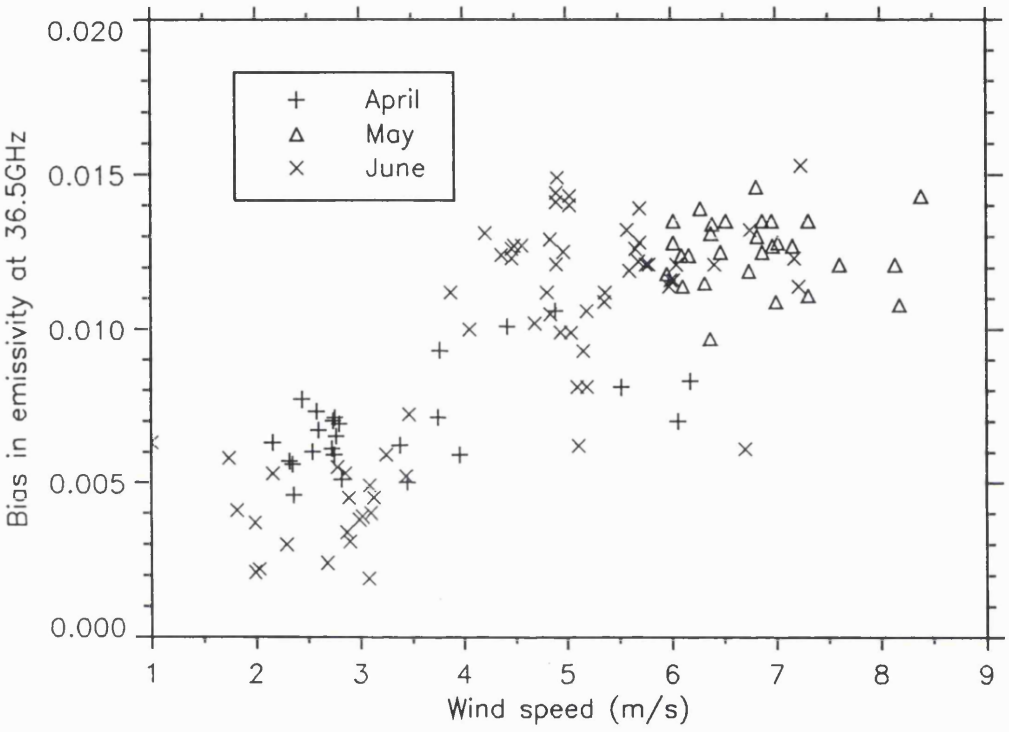

Figure 5.6 Showing that the bias in emissivity depends on wind speed. This is due to deficiency in the model for vertical looking angles.

5.5 Conclusions

- The application of the new atmospheric correction technique to real ATSR/M microwave data from ERS-1 is feasible and straightforward. This is because the apparent microwave emissivity was obtained by dividing the microwave brightness temperature from ATSR/M by coincident SST measurements from ATSR.

- The validation shows very encouraging results in correcting the microwave emissivity from ATSR/M with an r.m.s of 0.003 and bias of 0.010 for atmospheres with less than 2.5 gm/cm^3 water vapour content. These results represent an order of magnitude improvement in precision over those obtained by the SSM/I (Fleming et al. 1991) which show an r.m.s of 0.03 and bias of -0.017.

- Although the results are within the predicted errors, the 0.003 measured r.m.s in emissivity is not easy to explain as it includes both model (due to anticipated error from SST), and measurement noise (due to ATSR SST measurement and ATSR/M radiometric noise and r.m.s from the new technique).

- The emissivity bias of 0.01 which is a function of wind speed confirms that the ocean emission model (Wilheit 1979) is in error for vertical incidence measurements and low wind speeds.

- The benefits of the technique are more noticeable for lower emissivity surfaces.

- It would be useful to carry out further validation work on the new atmospheric correction with a better ocean surface model in order to assess the true precision attainable with ATSR/M data.

Chapter 6

Application of the New Atmospheric Correction Technique to Remote Sensing of Soil Moisture

6.1 Introduction

One of the applications of microwave radiometers over land is the retrieval of soil moisture. This chapter shows how the retrieval of soil moisture using passive microwave radiometers can be improved with the new atmospheric correction technique described in chapter 4.

There are numerous studies in the literature involving studies of passive microwave-soil moisture relationship from ground and airborne experiments (e.g. Newton and Rouse, 1980: Wang and Choudhury, 1981, Wang et al. 1982; Wang 1983; Dobson et al. 1985; Hallikanainen et al. 1985; Schmugge et al, 1986; Jackson and Schmugge; 1989; Roa et al. 1989; Jackson et al. 1993). These studies established a strong inverse correlation between microwave emission and soil moisture. This is due to the unique dielectric properties of water in this region of electromagnetic radiation (chapter 2). Although these studies revealed strong relationship between soil moisture and microwave emission, they were conducted under a controlled environment with homogeneous surface conditions and high spatial resolution.

Studies of the measurement of soil moisture from satellite's microwave radiometers have been less numerous (e.g. Wilke and McFarland, 1986; Choudhury et al, 1987; Choudhury and Golus, 1988; Owe et al, 1988; Choudhury et al, 1990; Choudhury et al, 1992, England et al, 1992, Choudhury 1993). Most of the previous satellite investigations have used highly empirical Antecedent Precipitation Index (API) methods (e.g. Wilke and McFarland, 1986; Choudhury et al, 1987; Choudhury and

Golus, 1988; Owe et al, 1988). The API model provides a daily measure of soil wetness based on average air temperature and precipitation combined with the API measurements from the previous day. This method does not accurately reflect daily soil moisture (Owe et al 1992). England et al (1992) proposed the Radiobrightness Thermal Inertia (RTI) method which is based on using the day-night differences in satellite sensed radiobrightness to monitor soil moisture.

The coarse spatial resolution of satellite microwave radiometer presents some difficulties in interpreting the microwave emission data in terms of soil moisture. This difficulty increases as the spatial heterogeneity in surface conditions increases. For example, highly variable precipitation and subsequent surface soil moisture distribution within the resolution area is one contribution factor (Owe et al. 1988). Another example is the temporal variation of vegetation within the resolution area which will contribute to the difficulty in interpreting the microwave emission from the footprint. This should not be a problem over desert regions with sparse vegetation.

There are a number of factors, such as roughness and vegetation which must be considered in the interpretation of soil moisture from microwave emission (chapter 2) Few studies have considered the atmospheric effect on the microwave emission as observed by the satellite radiometer (see chapter 1).

The simulations in chapter 4 showed that the atmospheric emission and absorption by water vapour may cause significant errors in the retrieval of surface microwave emissivity. These errors in emissivity depend on the surface emissivity and water vapour content and can be more than 0.1 for high water vapour content and low microwave emissivities (smooth and wet surfaces). This would make the fractional accuracy of soil moisture retrieval (i.e. 0.02) as impossible. Even in the case of high microwave emissivities (dry soil), the simulation from Alice Springs radiosondes in chapter 4 showed that there will be an error of 0.02 to 0.01 in emissivity which will affect the accuracy of soil moisture retrieval (see later) if a correction is not applied.

In this chapter, the new microwave atmospheric correction effect is applied prior to solving the inverse problem of soil moisture retrieval from the satellite microwave emission data. A multi sensor approach demonstrated by schematic diagram in figure (6.1) shows the steps used for soil moisture retrieval. The multi-sensor approach described in the figure can be applied over areas with few and sparse vegetation (deserts).

The first step is to compute the microwave surface emissivity by dividing the brightness temperature received by the satellite microwave radiometer from the footprint (microwave resolution element) by the corrected surface temperature determined by the satellite infrared radiometer, averaged over the microwave footprint. The second step is to correct the microwave emissivity for atmospheric emission and absorption by water vapour. The third step is to eliminate the ambiguity caused by the surface roughness through the use of additional data. The Radar Altimeter is used as shown by Ridley and Strawbridge (1995), to retrieve the surface roughness. Correction for the effect of surface roughness is then possible using an appropriate roughness model (e.g. Mo and Schmugge 1987). The fourth and the final step requires information on the physical properties of the soil (e.g. bulk density, grain density, sand fraction) which are fitted into a smooth surface emission model (e.g. Dobson et al. 1985) to compute the soil moisture.

A sensitivity analysis to estimate the surface temperature and infrared emissivity measurement accuracies needed in order to satisfy the 0.02 accuracy requirement for soil moisture is demonstrated in section 6.2. Following the steps described above, soil moisture is retrieved over the Simpson desert from TOPEX 18 GHz and 37 GHz apparent emissivities (after normalising the brightness temperatures with corrected surface temperatures from the AVHRR). The results are then compared with field measurements of soil moisture collected during the Simpson 93 campaign (section 6.3).

The approach described in this chapter provides an opportunity for operational satellite remote sensing of soil moisture measurement over arid and semi-arid regions for climate studies.

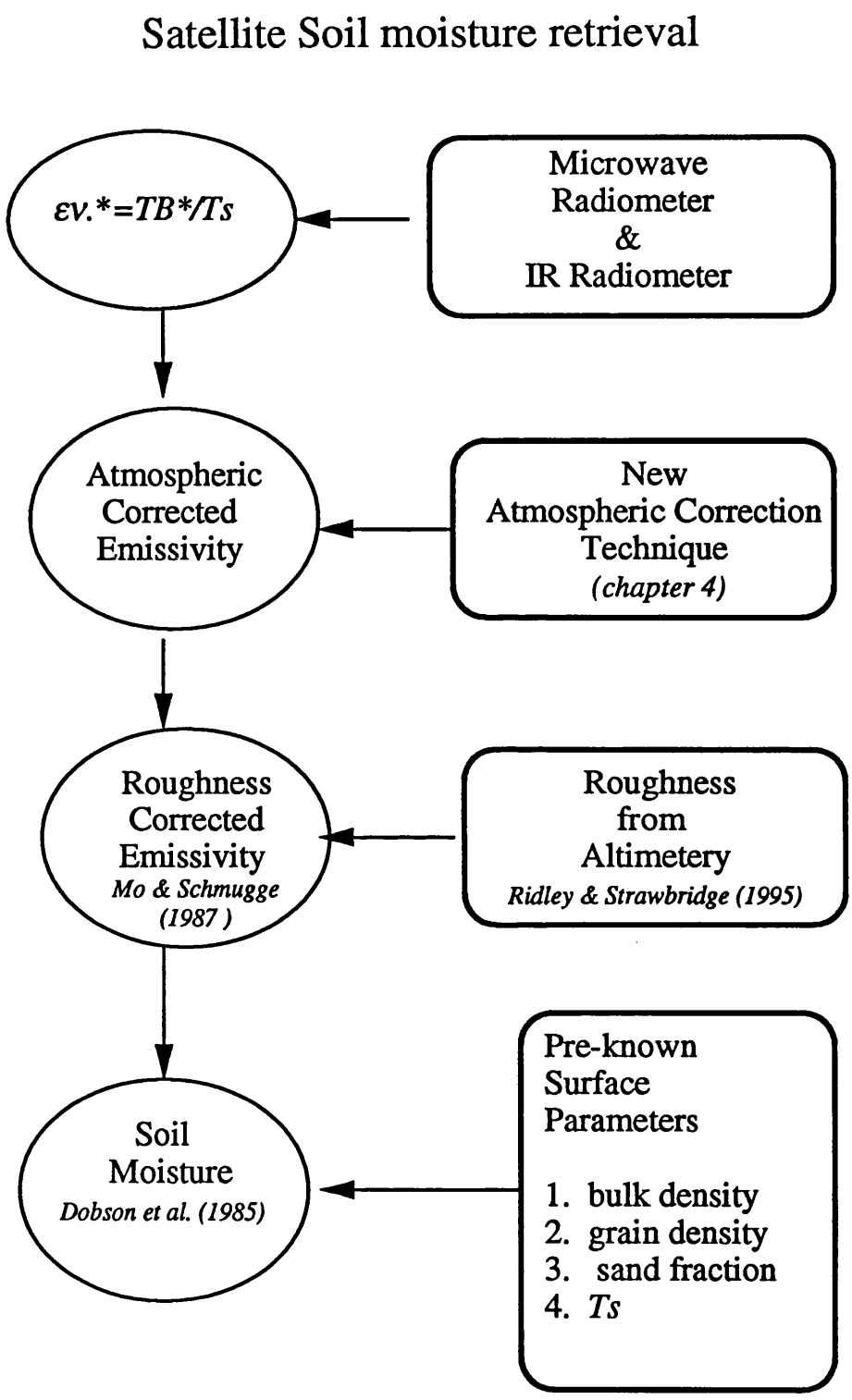

Figure 6.1 Showing a schematic diagram for retrieving soil moisture for bare soils

6.2 Sensitivity Analysis to determine accuracy

The approach described in this chapter for measuring soil moisture from space uses a multisensor technique (see figure 6.1) in which the uncertainty in the soil moisture is dependent upon the uncertainties in numerous input parameters. The variation in each parameter is expressed in terms of standard deviation.

The sources of errors are:

a. Instrumental effects.
b. Technique uncertainty.
c. Uncertainty in the surface properties.

The effect of the following parameter variations (shown in figure 6.1) on soil moisture accuracy need to be assessed:

1. The radiometric noise determines the accuracy with which the microwave brightness temperature is measured. The instrumental noise is known from the specifications of the microwave radiometer (see chapter 3).

2. The accuracy of the land surface temperature retrieval from the IR radiometer depends on the method used and the uncertainty in the land emissivity (see later). The land infrared emissivity is dependent on spectral and spatial variations of the surface roughness and other physical parameters of the surface (Becker and Li, 1990).

3. Accuracy of the atmospheric correction technique (see chapter 4).

4. Accuracy of roughness retrieval from the Altimeter which is 20% (Ridley and Strawbridge, 1995).

5. Uncertainties in the soil properties (e.g. bulk density, sand fraction). In this study, since the investigation is restricted to Simpson desert, these properties my be estimated with little uncertainty (Strawbridge et al. 1994).

The errors in the estimation of all the above parameters are defined, except the land surface temperature accuracy from IR radiometer which depends in principle on the error in the estimate of the surface infrared emissivity. A sensitivity analysis is conducted to measure the rate of change of one parameter on another parameter. In this

case of the error of soil moisture on the error of surface temperature. There are two approaches to sensitivity analysis: stochastic and deterministic.

A *stochastic sensitivity analysis* is a measure of the effect of the variations of all parameters on an output parameter by running the model with input parameters values selected according to their statistical distributions. The model is run many times, each time using slightly different input parameter values across their probability distribution. Then the standard deviation of the output parameter (the one we are interested in) is calculated from its statistical distribution around the mean. A *deterministic approach* determines the effect of variations in each of the model parameters individually upon the output from the model. A detailed description of the sensitivity analysis using the two approaches is found in Strawbridge (1992).

6.2.1 The Accuracy requirement in the Land Surface Temperature measurement

A stochastic approach was used in the evaluation of the response of the microwave surface emissivity to realistic variations of input surface parameters of Dobson et al. (1985) and Mo and Schmugge (1987) models. The values of all the input parameters with their standard deviations are shown in table (6.1). The surface emission model including roughness was run 500 times in order to evaluate the probability distribution of the microwave surface emissivity at TOPEX 18 GHz frequency. Then the mean value of this distribution and its standard deviation were computed.

Three different cases were considered based on three values of soil moisture over deserts: case (A) when soil moisture is 0.1, case (B) when soil moisture is 0.05, and case (C) when soil moisture is 0.02. The surface roughness (0.014) and its standard deviation (0.003) over Simpson 93 were calculated by Ridley and Strawbridge (1995) using TOPEX altimeter data. The likely values of surface parameters and their standard deviations are based on Simpson 93 field observations (Strawbridge et al. 1994). As the surface emission model is not very sensitive to surface temperature (chapter 2), the value of its standard deviation will not affect the result. Therefore a 2 degrees standard deviation of surface temperature is given as an arbitrary choice. The results of the standard deviation of the microwave surface emissivity for the three different cases of soil moisture ranges from 0.021 to 0.017 as shown in table (6.1).

By running the stochastic model again using the computed microwave emissivity and its standard deviation from the previous stochastic analysis and the brightness temperature with radiometric noise of ~ 0.9 degree (TOPEX) as input parameters to TB/ε_V we can evaluating the mean surface temperature and its standard deviation. The

results of the three cases are shown in table (6.2). As the soil moisture decreases from the 0.1 to the 0.02 the acceptable error in the measurement of surface temperature falls from 7.5 K to 5.8 K.

Table 6.1 Input parameter mean values and standard deviation for each, for the stochastic sensitivity analysis. The ouput is the microwave surface emissivity mean value and standard deviation for three different cases of soil moisture values. Case A, soil moisture is 0.1 ± 0.02, case B, soil moisture is 0.05 ± 0.02, and case C, soil moisture is 0.02 ± 0.02. Note that Ts is used here in Dobson model.

Input	roughness	Ts	bulk density	grain density	sand fraction
value	0.014	24.0	1.2	2.65	0.9
r.m.s.	0.003	2.0	0.1	0.1	0.02
Output	Microwave Surface Emissivity (ε_V)				
case	A		B	C	
value	0.85		0.90	0.93	
r.m.s.	0.022		0.023	0.019	

Table 6.2 Input parameter mean values of ε_V and TB with their standard deviation, for the stochastic sensitivity analysis. The output is the microwave surface emissivity mean value and standard deviation for three different cases of soil moisture values. Note Ts is obtained here from TB/ε_V.

case	A		B		C	
Input	ε_V	TB	ε_V	TB	ε_V	TB
value	0.85	0.021	0.9	266.7	0.93	276.4
r.m.s.	0.022	0.9	0.023	0.9	0.019	0.9
Output	Ts (K degrees)					
value	297.5		296.3		297.8	
r.m.s.	7.5		7.1		5.8	

6.2.2 Sensitivity of surface temperature to uncertainty in infrared emissivity

The greatest unknown when measuring the land surface temperature from thermal infrared is the emissivity over land. The thermal infrared emissivity will change as a function of chemistry, particle size, moisture, and vegetation (Nerry et al. 1988). One way to solve this problem is to assume a mean emissivity with an uncertainty, and to evaluate how much this uncertainty will affect the retrieval of surface temperature.

By allowing the thermal infrared emissivity to vary within the range 0.88 to 0.98 and by using the radiative transmission model provided by RAL together with a set of 40 Alice springs radiosonde data, it is possible to estimate the sensitivity of surface temperature measurements to variations in surface emissivity. The results showed that $\delta T \approx 50 \times \delta\varepsilon$, or in another words, the error in temperature is 50 times the error in surface emissivity. For example an uncertainty of 0.02 in infrared emissivity causes an error of 1 K in surface temperature.

These results are approximately comparable to the estimates predicted by Mansor and Cracknell 1992; Becker 1987 and Ottle and Stoll 1993). Mansor and Cracknell (1992) estimated a 1.5 K error in land surface temperature for an error of 0.02 in infrared land emissivity. More recently Ottle and Stoll (1993) observed that this error depend on atmospheric water vapour. For example they found for one atmosphere an error of 0.02 on emissivity leads to an error of 1.5 K in surface temperature while for another atmosphere it is about 1K per 0.02 of emissivity error. Ottle and Stoll (1993) concluded that the more transparent the atmosphere is, the larger is the effect of an error in ε.

The results of the stochastic analysis in section 6.2.1 showed that the maximum permissible error in Ts is 7 K. Using $\delta\varepsilon = \delta T/50$, we can see that an estimate of thermal infrared emissivity with 0.14 accuracy might be quite enough for the purpose of our study. Later in section (6.3.4) we will show that it is possible to get better than 0.02 accuracy of soil moisture as long as the surface temperature is known better than 7 K.

6.3 Simpson 93 As a Case Study

The work in this section investigates the performance of the new technique and the feasibility of measuring soil moisture from space. The physical model used in the retrieval of soil moisture is based on the Dobson et al. (1985) semi-empirical model for the dielectric constant and an empirical model for Mo and Schmugge (1987) for surface roughness. Strawbridge (1992) compared these models with satellite data and found that they are adequate.

As microwave radiometers have large footprints (in tens of kilometres), a large area with uniform characteristics is needed if sub-footprint scale variability is to be avoided. This is necessary when point field measurements are used for comparison with satellite averaged footprint emissivities.

A valuable opportunity to measure the soil moisture was afforded by a field campaign conducted by a team of scientists from Mullard Space Science Laboratory (MSSL) and University of New South Wales (UNSW) in the Simpson Desert in Australia in September 1993. MSSL has an interest in the Simpson Desert with campaigns taking place in 1988, 1992, and 1993 (Guzkowska et al. 1990; Cudlip et al. 1995; Strawbridge et al. 1994). Test sites in these campaigns were characterised by spatially constant radar backscatter (Rapley et al. 1987; Wielogorski 1988). These were identified from a study of radar altimeter measurements which are sensitive to variations in dielectric characteristics as well as topography and morphology. The homogeneity of these test sites permits the approximation of point measurements, such as roughness, in representing large averaged microwave footprints (see later).

A rain event occurred during the Simpson 93 field campaign, allowing the change in soil moisture to be monitored as the soil dried over the following few days. As the microwave surface emissivity decreased with increased soil moisture following the rain event, more of the downwelling atmospheric emission would be reflected. Therefore the apparent microwave emissivity as seen by the satellite will overestimate the actual surface emissivity (see chapter 4). This provides a valuable opportunity to use the Simpson 93 field campaign as a first case study in the application of the new atmospheric correction technique and for the validation of the soil moisture retrieval methodology.

6.3.1 Methods

6.3.1.1 The Simpson Desert Study Area

The Simpson Desert lies in the centre of the Australian continent between the McDonnell mountains to the north-west and Lake Eyre to the south-east, occupying the area between latitude 23° S and 27° S, and longitudes 135° E to 139° E, see figure 6.2. This region is classified as an arid zone. Arid regions are defined as regions receiving less than 250 mm of rainfall annually. Although the Simpson Desert is characterised by low rainfall, it is not classified as extreme arid like the Sahara. Maximum temperatures during the summer day reach as high as 46° C. The mean monthly maxima and minima are 19° C and 4° C in July ranging to 35° C and 21° C in January (Strawbridge et al. 1994). The landscape of Simpson Desert is dominated by NNW-SSE trending longitudinal sand dunes whose parallel ridges may extend up to 100 km in length. The dunes in the survey region are continuous for tens of kilometres, and are separated by 200 to 500 metres.

The test site which is located at 23° 50' 14" S latitude and 136° 4' 6" E longitude, is considered homogeneous with respect to vegetation cover and temperature within a 50 Km footprint. The soil moisture shows variability on a scale around 10 km (Strawbridge et al. 1994). This is mainly due to: (a) the rainfall distribution pattern; (b) the depth of the bedrock under the sand varies and the nearer the bedrock to the surface, the greater the soil moisture. This may produce a small difference between a point measurement and the averaged soil moisture over the microwave footprint (Strawbridge et al. 1994).

The vegetation covers 30 % of the surface (Strawbridge et al. 1994). This is regarded as a sparse vegetation with considerable areas of sand between the individual plants. Therefore for a nadir looking microwave radiometer the effect of vegetation on the passive microwave footprint is regarded as small (Ridley and Strawbridge, 1995).

6.3.1.2 Satellite Sensors and Data

Satellite sensors

Two satellites systems were used in this study as they overpassed the test sites during the field campaign: TOPEX /Poseidon (TP) and AVHRR (chapter 3). The microwave brightness temperatures at 18 GHz, 21 GHz, and 37 GHz footprints were extracted from TP, while the surface temperatures were corrected from AVHRR data. Also, TP carries

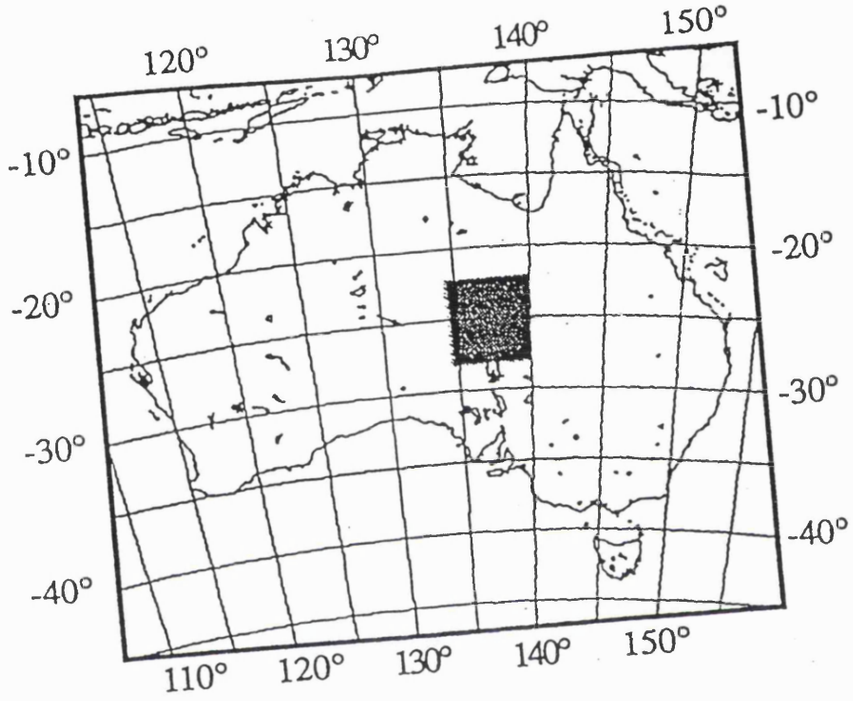

Figure 6.2 Map of Australia showing location of Simpson desert. The shaded area corresponds to the area in figure 6.3 (Strawbridge et al. 1994).

an altimeter which is an active microwave sensor. The altimeter data were used to provide the roughness measurements over the test sites (Ridley and Strawbridge, 1995). TP overpassed the survey region twice (see figure 6.3). The first one was at midnight on the 10th of September (ascending) and the second one was at 10.30 am of the 15th of September (descending). The first overpass was twenty eight hours after the rain while the second overpass was around four and a half days afterwards.

The AVHRR overpasses the same location once every day. Data from two NOAA satellites were extracted: NOAA-11 and NOAA-12. NOAA-11 has a pre-dawn overpass and covers the survey region between 0430 - 0600 local time while NOAA-12 has an evening overpass between 1930 - 2130 local time. A total of 8 AVHRR images were available for the period of the field campaign (9th of September till the 15th of September). Details of the images are shown in table 6.3.

The raw AVHRR data were not geolocated. Geolocation of images was necessary to locate the field sites, therefore a geolocation program was written to georeference the pixels and correct the geometric distortion. The geolocation program is based on an orbital model adopted from (Ho and Asem 1986) using ephemeris data provided in the header of each file. Figure 6.4 shows a geolocated AVHRR image projected on an equicylindrical map. Note that the land has cooler temperature (darker colour) compared to sea (white colour) as this is a night image. Part of the sea is covered by cloud which are cooler than the sea. The predicted geolocation error is around 2-5 km. This should not affect our results as we are interested in an averaged temperature over the microwave footprint (~ 45 km at 18 GHz and ~ 24 km at 37 GHz).

Data from field measurements

The Simpson 93 campaign lasted from the 8th of September till the 15th of September. Beside the many field measurements conducted, principally in support of radar altimeter measurements, soil moisture and surface temperature were measured and they are used in the comparison with the satellite measurements in this study.

Soil moisture

On the first day of the campaign (i.e. 8th of September) a thunderstorm occurred with heavy rain fall at the test site (-23° 50' 14", 136° 2' 8") at 8 p.m. This presented a good opportunity to measure the change of soil moisture over the following days. Measurements of soil moisture started three hours and half after the rain event.

Table 6.3 The date and time of the eight files of AVHRR data used in this study.

File	Date (LT)	Hour (LT)	Satellite
1	9-Sep-93	21:03	NOAA-12
2	10-Sep-93	04:49	NOAA-11
3	10-Sep-93	20:30	NOAA-12
4	11-Sep-93	04:36	NOAA-11
5	13-Sep-93	21:18	NOAA-12
6	14-Sep-93	05:41	NOAA-11
7	14-Sep-93	20:55	NOAA-12
8	15-Sep-93	05:28	NOAA-11

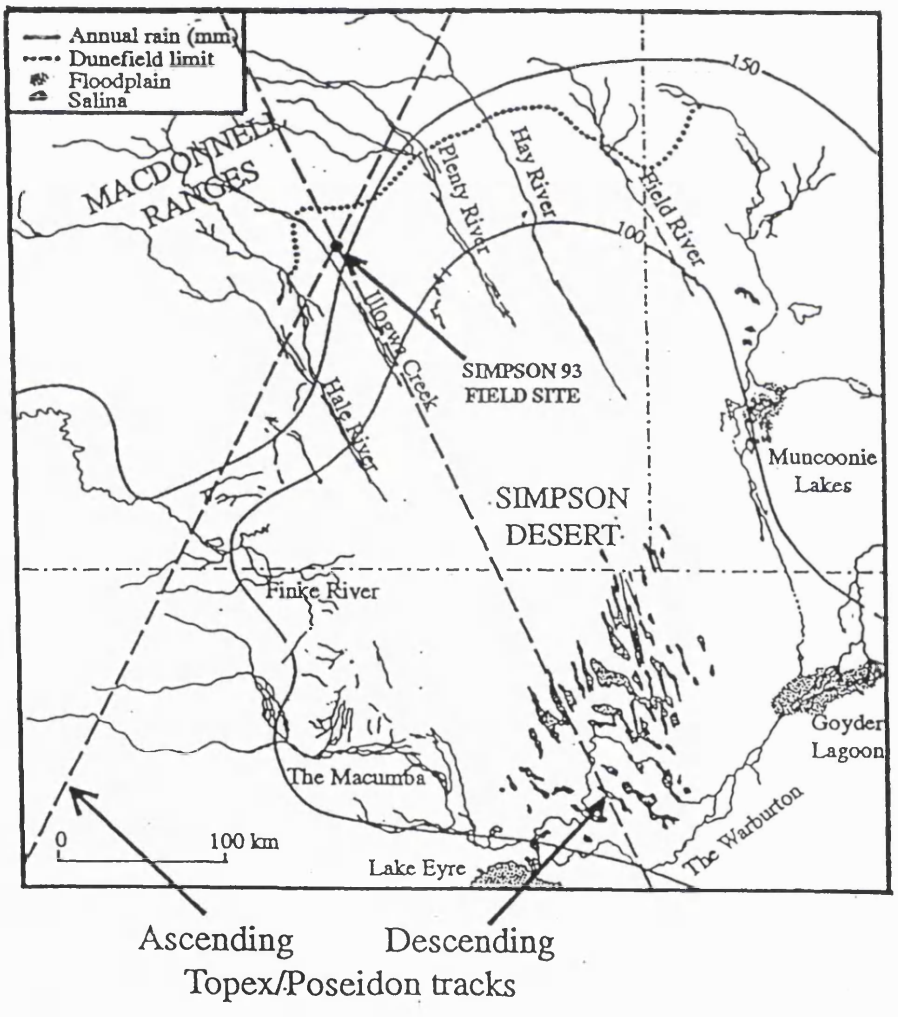

Figure 6.3 TOPEX overpasses Simpson desert twice during field campaign (Strawbridge et al. 1994)..

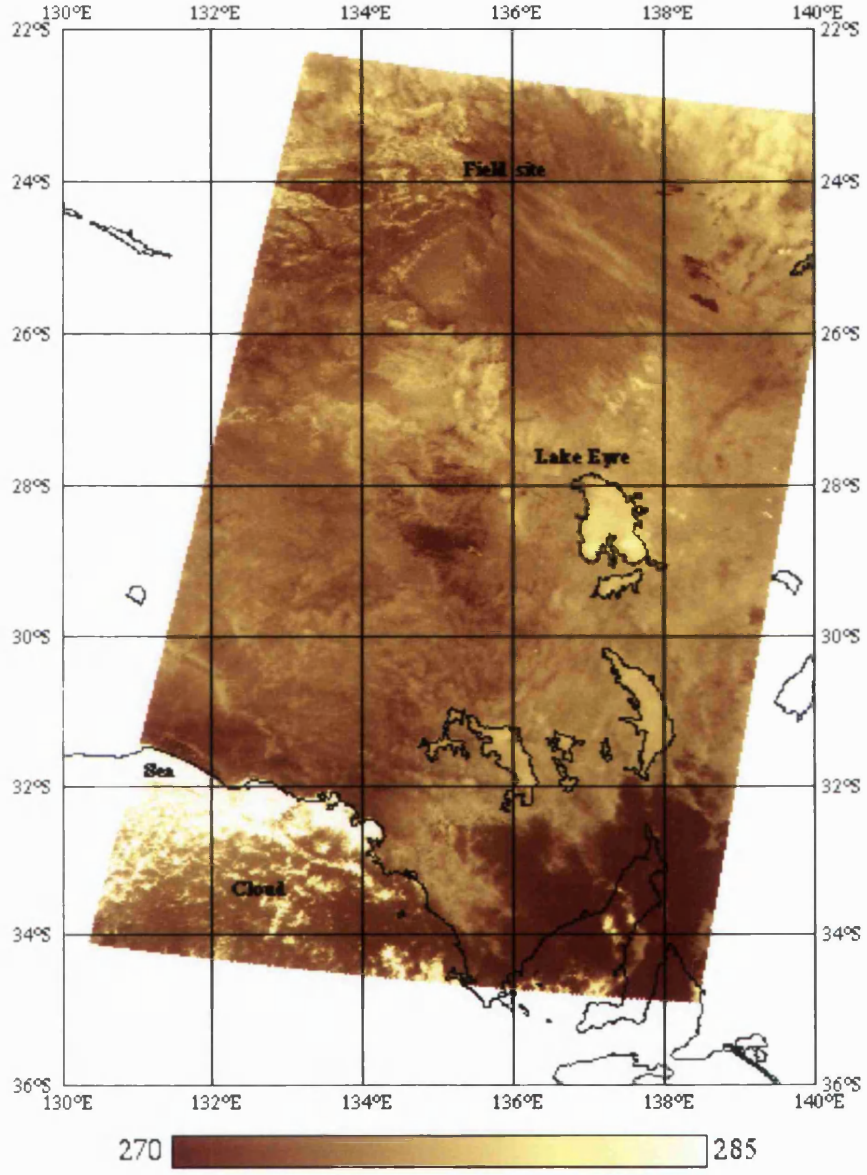

Figure 6.4 Geolocated image of central Australia projected on an equicylindrical map.

Four samples of soil were collected from the swale or interdune at different depths. They were collected in sealed aluminium containers. The soil moisture was measured by weighing them first then weighing them again after they are baked in the oven (see Strawbridge et al. (1994) for more details). Table 6.4 shows 4 profiles of soil moisture field measurements which were taken from depth between 1 cm to 70 cm. Note that samples 3 and 4 were taken closest to the TP overpass.

Soil surface temperature

Soil surface temperature measurements were taken with a thermocouple at the test site on the 11th of September and during the TP overpasses of the 10th and 15th of September. These data were taken every five minutes on these dates and are compared with the corrected surface temperature from AVHRR data in the next section.

Data from Alice Spring met office

Meteorological data from the Alice Spring Met. station were also used in this study. Air surface temperatures from the 8th to 16th of September were compared with the corrected surface temperature from AVHRR data at the Alice Springs station (see later). A radiosonde set (40 profiles) for Alice Springs for the year 1992 was used in the simulation of the surface temperature correction (see later).

Table 6.4 The soil moisture profiles in volumetric percentage (Mv %) at four different dates after the rain event together with TP overpass time (adapted from Strawbridge et al. 1994).

Date& Hour	8-Sep-93 23:30	9-Sep-93 13:00	10-Sep-93 11:00	14-Sep-93 11:00
Depth (cm)	Sample 1 (Mv %)	Sample 2 (Mv %)	Sample 3 (Mv %)	Sample 4 (Mv %)
1.0	18.6	6.2	2.8	0.9
2.5	6.6	9.9	4.7	4.8
3.5	4.6	3.1	3.9	3.5
7.5	3.1	2.2	3.8	5.1
10.0	-	5.0	5.3	-
20.0	5.4	5.5	6.4	7.0
40.0	7.7	8.9	8.2	9.7
70.0	12.2	10.9	-	-
TP overpass	-	-	10-9-93 midnight	15-9-93 10:30

6.3.2 Analysis of Data

6.3.2.1 Surface temperature measurement from AVHRR

AVHRR Infrared data were used to determine land surface temperatures over the test site after the application of an atmospheric correction. There are various methods for correcting the atmospheric effect in the infrared (see chapter 5). The method which will be employed here is the split window method.

The split window method has been used successfully to retrieve the temperature over the sea surface as the emissivity is almost spatially constant and is close to one. Over the land the situation is quite different as the surface emissivity is generally unknown and different from unity, and is spectrally and spatially variable (Becker and Li, 1990). There are different studies in the literature which investigated the use of the split window over the land (e.g. Becker and Li, 1990; Sobrino et al. 1994; Franca and Cracknell, 1994).

Becker and Li (1990) showed that accurate land surface temperatures can be retrieved using the local split window method once the emissivities in the two adjacent channels are known with sufficient accuracy. They used the term local which indicates that the coefficients relating the retrieved surface temperatures in the two adjacent channels depend on actual land surface emissivities, which may vary from pixel to pixel. Becker and Li (1990) contributed the difficulty in measuring the land surface temperatures from space to three main causes: 1. Not knowing the land surface infrared emissivity. 2. Land surfaces are usually inhomogeneous within a pixel and this makes the definition of effective surface temperatures and emissivities difficult. 3. Air temperatures just above the surface over land are usually different from the actual land surface temperatures.

Sobrino et al. (1994) compared r.m.s accuracy for retrieving the land surface temperature from five different split-window algorithms (see Sobrino et al. 1994, and references therein). These r.m.s accuracy range from 0.36 r.m.s K for Becker and Li (1990) to 2 r.m.s K for Sobrino et al. (1994).

Three assumptions are made before coefficients of the split window are derived in this study:

1. Prior knowledge of the approximate spectral emissivity at AVHRR bands 4 and 5. It is possible to estimate the emissivity based on the sand structure and percentage of

vegetation from the observations of the survey site of Simpson 93 field work. As the sand fraction is around 90% and vegetation is around 25-30% of the senryegrass species (spinifix), the approximate spectral emissivity at the AVHRR band 4 and 5 is 0.95 based on Salisbury and D'Aria (1992 a&b) and Labed and Stoll (1991). However, the sensitivity analysis in section 6.2 indicated that an accurate knowledge of surface temperatures is not critical and an estimate of thermal infrared emissivity within 0.14 accuracy is quite enough for the purpose of this study

2. Homogeneity of the Simpson Desert with respect to surface temperature and properties (Strawbridge et al. 1994). The surface properties at the test site may be considered homogeneous over the pixel size (1.1km). Soil moisture variations of 10% are not expected to affect the spectral emissivity in bands 4 and 5 by more than 1% (see Salisbury and D'Aria 1992b).

3. Air temperature just above the land surface is close to the physical surface temperature. This is true for deserts at night (Choudhury 1993). In this study, the AVHRR data are at night and early morning time (see table 6.3).

In this work, a radiative transfer model of RAL (see chapter 5) is used together with 40 sets of radiosonde profiles from Alice Springs to simulate both the AVHRR-11 and AVHRR-12 brightness temperatures. Then a linear regression is applied on the difference between band 4 and band 5 versus the atmospheric correction to obtain the coefficient of the split window. Figure 6.5a shows the variations in atmospheric correction with the difference in brightness temperature at channels 11 and 12μm for NOAA-11. The same thing is shown for NOAA-12 in figure 6.5b. The coefficients are generated for nadir angle or near nadir angle as the coefficients of the split window technique will depends not only on the atmospheric water vapour but also on the viewing angle (Franca and Cracknell 1994).

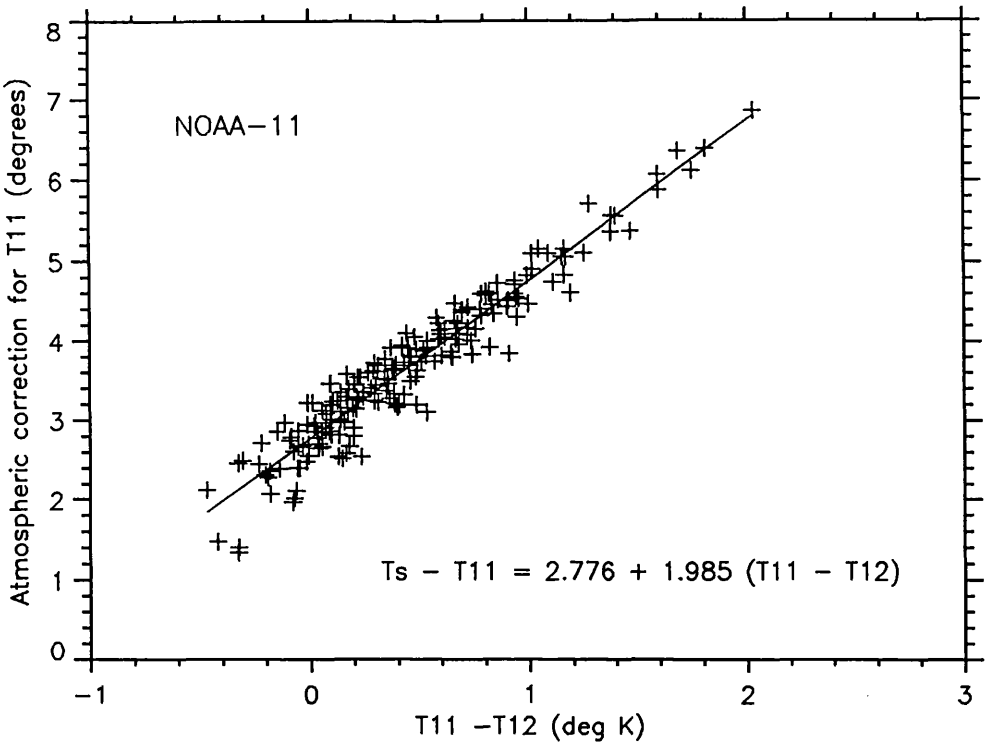

Figure 6.5a Infrared atmospheric correction at 11μm against the difference between bands 11 and 12μm for NOAA-11. The simulation for 40 Alice Springs atmospheres (radiosondes data).

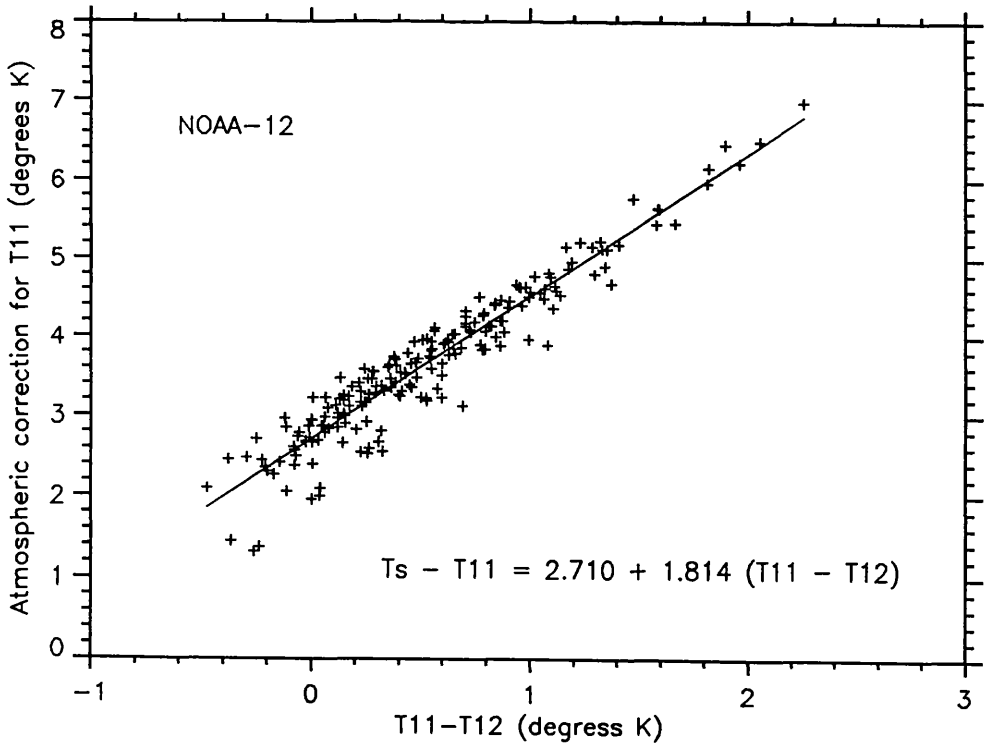

Figure 6.5b Infrared atmospheric correction at 11μm against the difference between bands 11 and 12μm for NOAA-12. The simulation for 40 Alice Springs atmospheres (radiosondes data).

6.3.2.2 Comparison between surface temperatures (AVHRR) and ground measurements

Under the assumptions 1, 2, and 3 in the previous section and using the coefficients of corrections for both NOAA-11 and NOAA-12, surface temperatures were corrected at two locations in the AVHRR images. The first location is at the Simpson 93 test site (latitude 23° 50' 14" S and longitude 136° 4' 6" E) where the field measurements were taken. The second location is at Alice Springs (latitude 23° 40' 2.45" S and longitude 133° 53' 7.84" E) where meteorological data are available. Data from the geolocated AVHRR images (section 6.3.1.2) were corrected and compared with the ground and meteorological measurements using the following two approaches:

1. Applying the derived split window coefficient to the *averaged* IR brightness temperatures inside the TP microwave footprint. Then the corrected AVHRR surface temperatures were compared with the point ground surface temperature measurements to investigate the spatial uniformity of surface temperature inside the TP microwave footprint.

2. By applying the derived split window coefficient to the AVHRR *pixel* which has the closest location (i.e. within 1-2 kilometres) to the latitude and longitude of the ground measurement. The objective of this approach is to test the validity of the derived coefficients of the split window which depend on the estimated infrared surface emissivity of the Simpson desert and on the atmospheric conditions derived from the Alice Spring radiosodes, which cover all seasons.

The AVHRR corrected surface temperatures for the Simpson 93 test site and the ground measurements are shown in table 6.5. Measurements from AVHRR files 1 to 8 from table 6.3 were compared with field measurements.

The AVHRR data local time corresponds to the time of the scan line of the test site. The field surface measurements were taken every 5 minutes using the thermocouple and there was no need for interpolation. This is because surface temperatures are not expected to change significantly over 5 minutes

The corrected and averaged surface temperatures from AVHRR data in table 6.5 agree very well with the ground measurements for the first three days. After the 13th of September 1993 the thermocouple reading started to give a large positive bias. Therefore measurements from the nearest meteorological station (Alice Springs) were used in the comparison for files 6, 7 and 8. Alice Springs is 300 km to the west of Simpson test site but has the same latitude. Therefore it is expected that surface

temperatures at these two locations would not differ greatly. However the error analysis is performed only for the first 4 measurements.

The standard deviation of the difference between field surface temperatures and AVHRR *averaged* and *pixel* corrected surface temperatures are 1.12 K and 1.2 K degrees respectively. The bias of the difference between field surface temperatures and AVHRR *averaged* and *pixel* corrected surface temperatures are -0.78 K and -0.81 K respectively. Although it is difficult to draw conclusions from only 4 measurements, the results are encouraging in terms of the standard deviations. The interpretation of the bias is difficult as there are only 4 measurements.

The result of the AVHRR corrected surface temperatures and the meteorological near surface air temperatures from Alice Springs are shown in table 6.6. All eight AVHRR files are used in this comparison as meteorological data were available every day.

Alice Springs near surface air temperature data exist only at times within one hour from the highest and lowest temperatures, therefore interpolation was necessarily to get the temperature which corresponds to the AVHRR time. A linear interpolation was used for this purpose.

There was no corrected averaged temperature for file 7 as most of the pixels inside the microwave size footprint were covered with clouds. Therefore surface temperature was corrected for the nearest non cloudy pixel to the Alice Springs site at file 7. The comparison in table 6.6 shows that the corrected average surface temperatures always have a positive bias compared to the meteorological data. This might be due to errors in estimating the effective infrared emissivity for Alice Springs, as the average footprint might contain pixels other than sand (e.g. Alice Springs airport). The comparison in table 6.6 also shows that the corrected pixel surface temperature seem to have a positive bias compared with to the meteorological data except for files 3 , 7 and 8.

The 0.70 K standard deviation of the difference between Alice Springs temperatures and AVHRR corrected averaged surface temperatures, is smaller than the AVHRR corrected surface temperatures at the pixel nearest to the location of Alice Spring which is 1.69 K This might be due to the fact that the averaged 30 × 30 pixels footprint reduces the effect of having non sandy pixels (e.g. airport) and therefore the actual effective emissivity is closer to the estimated one (i.e. 0.95). On the other hand the corrected surface temperature from that pixel which is at the Alice Springs location might contain some emission from Alice Springs Airport. The bias of the difference

between Alice Springs temperatures and AVHRR *averaged* and *pixel* corrected surface temperatures are 1.6 K and 0.95 K respectively.

The standard deviation of Alice Springs looks better than that at the test site in Simpson desert. This is most likely due to performance of the thermocouple which started to give large bias at file 5. Also we can not make a conclusion of these results as the standard deviation from the test site are for 4 measurements only. Figures 6.6 and 6.7 show plots of the AVHRR averaged corrected surface temperature compared to the measurements from Simpson 93 test site and Alice Spring meteorological data respectively. Note the large errors at later time in figure 6.6 are due to the failure in the thermocouple reading.

6.3.3 Results of soil moisture retrieval from TOPEX

In this section, the volumetric soil moisture measurements from TP microwave emission at 18 GHz and 37 GHz were retrieved over the Simpson Desert test site. The retrieved soil moisture measurements were compared with the field measurements during the Simpson 93 campaign.

Following the approach described in figure 6.1, the soil moisture retrieval from microwave emission measurements using the TP radiometer was undertaken as following:

1. The apparent microwave emissivity as seen the TP radiometer (or the normalised brightness temperature) was computed by dividing the microwave brightness temperature by the surface temperature. As there were only two passes of TP over the test site, there are only four measurements; two at 18 GHz and two at 37, GHz on the 10th and the 15th of September 1993. Surface temperatures from field measurements were used instead of the corrected surface temperatures from AVHRR radiometer. This is because there was a difference in time between the AVHRR and TP overpass. On the 10th of September TP passes the test site at midnight (LT) while the AVHRR overpass was at 20:30. On the 15 of September TP passes the test site at 10:30 while AVHRR, at 05:28.

2. The second step is to apply the coefficients which were derived from the Alice Springs radiosondes in chapter 4 to correct the microwave emission for atmospheric effects. A summary of results are shown in table 6.7.

Table 6.5 Field measurements of Ts in comparison with retrieved Ts from AVHRR pixel and averaged pixel over the TP footprint. Note the Italic numbers are from Alice Springs due to measurement bias in the thermocouple. The std and bias here are for the first 4 files.

AVHRR file	Ts (field)	Ts(AVHRR) averaged	Ts(AVHRR) pixel	ΔTs(std) (avr)	bias	ΔTs(std) pixel	bias
1	15.32	15.84	16.43				
2	8.84	8.44	7.82				
4	8.30	7.62	7.22				
5	14.18	11.62	11.93	1.12	-0.78	1.2	-0.81
6	*2.60*	1.92	2.99				
7	*13.70*	10.18	11.03				
8	*5.20*	3.39	3.95				

Table 6.6 Same as table 6.5, but for Alice Springs meteorological measurements.

AVHRR file	Ts (Alice)	Ts(AVHRR) averaged	Ts(AVHRR) pixel	ΔTs(std) (avr)	bias	ΔTs(std) pixel	bias
1	15.6	17.1	17.7				
2	7.5	9.4	9.1				
3	14.8	15.2	14.5				
4	6.9	8.8	9.5				
5	11.0	14.0	14.5	0.70	1.6	1.69	0.95
6	2.8	4.4	3.5				
7	15.7	cloudy	14.4				
8	4.6	5.5	3.3				

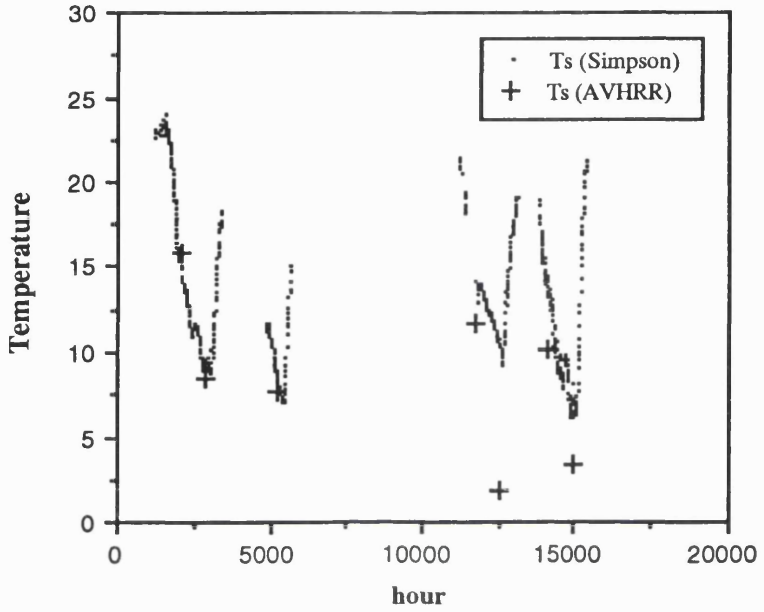

figure 6.6 Comparison between AVHRR averaged corrected temperatures and Simpson field measurement. The large error at later times are due to the failure in the reading of the field thermocouple.

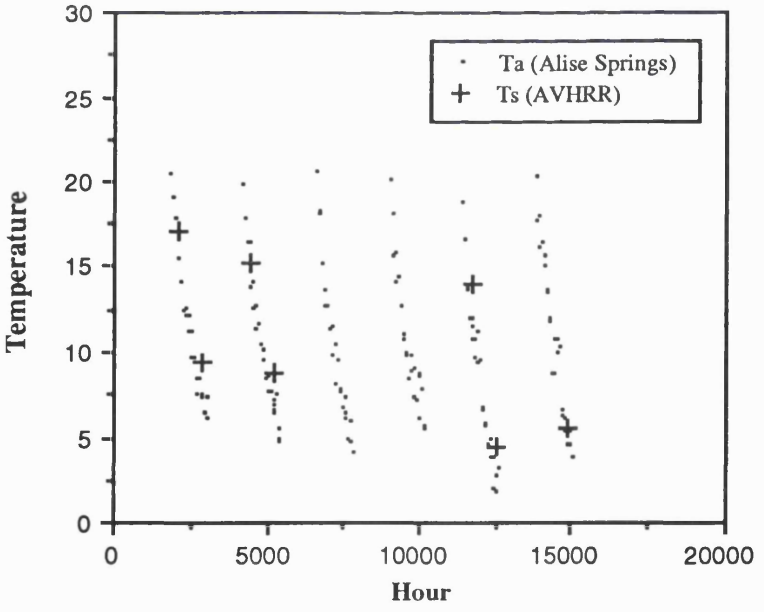

figure 6.7 Comparison between AVHRR averaged corrected temperatures and Alice Springs meteorological measurements. Note that the measurements of Alice meteorological temperatures shown in this figure are from 6p.m. to 6 a.m and therefore they always decrease within this time range.

3. As the surface roughness over the Simpson Desert test site is very small, with an r.m.s. slope of 0.014, it was found that after applying the roughness correction the emissivity is essentially the same as before.

4. From the corrected microwave emissivity at 18 GHz and 37 GHz, soil moisture were retrieved from the Dobson model for the 10th and 15th of September. The following values were used in Dobson model for surface parameters on the 10th of September: bulk density = 1.2, grain density = 2.65, sand fraction = 0.9, and surface temperature = 12° C. The same surface parameters values are considered on the 15th of September except that the surface temperature was 24°C. Field soil moisture at 18 GHz were averaged over the 3.5 cm depth and at 37 GHz the first measurements of soil moisture at the 1 cm depth was taken (see table 6.4). The effective depth of microwave emission at the 18 and 37 GHz are based on Ulaby et al. (1986). Results of the soil moisture retrieval TP were compared with those from the field in table 6.8. Note that the field measurements of day 14th of September were used in the comparison with soil moisture retrieved from TOPEX on day 15th (see table 6.4) as there were no field measurements on day 15th of September.

The standard deviation in soil moisture from these four measurement differences is 0.008, while the bias is 0.011. A discussion of these results is found in the next section.

Table 6.7 Comparison in emissivities at 18 GHz and 37 GHz before and after correction.

	10-9-93		15-9-93	
Emissivity	ε (18GHz)	ε (37GHz)	ε (18GHz)	ε (37GHz)
Before Correction	0.92	0.94	0.93	0.93
After Correction	0.91	0.93	0.92	0.92

Table 6.8 Comparison of soil moisture measured from field site with that retrieved from TOPEX.

	10-9-93		15-9-93	
Soil Moisture	Mv (18GHz)	Mv (37GHz)	Mv (18GHz)	Mv (37GHz)
Field	0.038	0.028	0.030	0.010
TOPEX	0.048	0.040	0.035	0.032
Difference	0.007	0.012	0.005	0.022
STD		0.008		
Bias		0.011		

6.3.4 Discussion of Results

The discussion in this section is devoted to the two main and important results in this chapter. First, the r.m.s. accuracy of land surface temperature retrieval from AVHRR and the implication of these results upon the accuracy of soil moisture retrieval. Second, the comparison between the field soil moisture measurements and retrieved soil moisture from TP.

The accuracy of LST and its implications for soil moisture retrieval

The results of section (6.3.2.2) show that the actual standard deviation in surface temperature from AVHRR data (~ 1 degree or less) are much better than the predicted accuracy (7 to 5 degrees) which is needed if we want to retrieve soil moisture with 0.02 accuracy (section 6.2.1). This implies that is possible to retrieve soil moisture from space with better than 0.02 accuracy. Note that the bias was calculated from very few measurement (4 data only in table 6.5) and the actual bias might be very small (i.e. ~ zero) when more field data are available for comparison.

The first step is to perform a stochastic sensitivity analysis with a 1 degree uncertainty in surface temperature from AVHRR (see section 6.3.2.2) and a 1 degree uncertainty in the microwave brightness from TP (Janseen et al. 1995). Thus, the predicted error in the microwave emissivity is ~ 0.005. This is achieved by running the stochastic code many times using the relation: emissivity = TB/Ts. The second step is to consider the error in surface microwave emissivity after applying the new atmospheric correction technique. This is by taking the root mean square of the sum of the squares of the predicted r.m.s in microwave emissivity which is ~ 0.005 and the r.m.s in surface microwave emissivity after applying the new atmospheric correction technique. The r.m.s results is within 0.007 to 0.005 depending on the surface microwave emissivity (chapter 4). The third step is to run a stochastic code again using the microwave surface emission model and assuming the same standard deviations of surface parameters as shown in table (6.1), the predicted r.m.s in soil moisture was found to be within 0.005.

So, theoretically it is possible to retrieve soil moisture from satellite microwave radiometer with accuracy four times better than 0.02. Although this accuracy might be controlled by different factors. For example the heterogeneity of the surface which might affect the effective infrared emissivity and therefore the retrieved surface temperature.

Discussion on results of soil moisture retrieval from TOPEX

The microwave surface emissivities in table (6.8) look quite high as these measurements were measured after 36 hours and 5 days after the rain event 10th and 15th of September respectively. By that time most of the soil moisture has dried out very quickly as expected in such a desert environment (see table 6.4), resulting in an increase in surface microwave emissivity.

The new atmospheric correction technique has corrected the surface emissivity by 0.01 which correspond to around 0.01 soil moisture. Although it is difficult to draw firm conclusion from only four measurements (i.e. two at 18 GHz and two 37 GHz), the result of the error in soil moisture retrieval from TP looks very encouraging, table 6.8. A crucial estimate of 0.008 standard deviation from the difference between field measurements and TP retrieval of soil moisture, shows it is close to the predicted error of 0.005 from the stochastic analysis if the surface temperature is known with an error of one degree (see before in this section). The bias in the difference between field measurements and TP retrieval of soil moisture is + 0.011. This indicate that the soil moisture retrieved from TP always overestimate the field measurement.

The bias in soil moisture measurements can be attributed to the following factors:

1. The difference in time between field measurement at day 10 which was taken at 11 am in the morning, while the TP overpassed at midnight at day 10. As soil moisture during the night is expected to be higher than the day time (Owe et al. 1992), therefore TP measurement (night) gives higher soil moisture measurement compared with the field measurement (day).

2. As soil dries out it might be that the effective depth of emission at 18 and 37 GHz is greater than expected. In this study it was assumed that the effective depth is 3.5 cm at 18 GHz and 1 cm at 37GHz (e.g. Ulaby et al 1986). This might explain why soil moisture from TP is always greater than the those calculated from field measurement

3. The difference might be because we are comparing point measurements of soil moisture with averaged measurements over 30 km footprint in which the soil moisture is not really homogeneous.

6.4 Conclusions and recommendations

The following conclusions can be summarised from this chapter:

- It has been demonstrated that the application of the atmospheric correction technique over land can improve the accuracy of soil moisture retrieval. If an atmospheric correction is not applied to the microwave emission, there may be considerable error in the soil moisture retrieval. Although in this study the error without atmospheric correction is ~0.01 in soil moisture which is still within the 0.02 accuracy needed for climate application, however, such error increases as soil moisture increases (and emissivity decreases) and the retrieval of soil moisture within 0.02 accuracy becomes difficult, if not impossible. Therefore the benefits of applying the new atmospheric correction technique to soil moisture retrieval are more noticeable for wet and smooth surfaces when the microwave surface emissivities have low values and the atmospheric contributions are proportionally greater.

- Although the accuracy needed for soil moisture in climate application is 0.02, it is feasible to do better than this. It has been shown that, in the absence of vegetation cover, it is possible to measure the land surface temperature to 1°K uncertainty error at night with AVHRR. Therefore, achieving the 0.005 accuracy of soil moisture or better is possible but will be limited to the accuracy of the soil model used.

- Although it is difficult to draw firm conclusion from only four measurements of soil moisture, the result of soil moisture retrieval from TP are very encouraging. The comparison study between the differences from field soil moisture measurements and retrieved soil moisture from TP show a standard deviation of 0.008 which is close to the predicted error of 0.005 from the stochastic analysis.

- The approach described in this chapter will allow operational soil moisture retrieval over arid and semi-arid regions, provided that a nadir looking radiometer is used, minimising the effect of vegetation.

- Although the application of the new atmospheric technique in this study used high frequencies channels (i.e. 18 GHz and 37 GHz) which are more affected by the atmosphere, the application of this technique should also be useful for low frequencies which are more desired for soil moisture applications. As simulations

of chapter 4 showed that even for 1.4 GHz, there is an error of 0.01 for wet and smooth surfaces when the surface emissivities are low. Although such error is still within the 0.02 soil moisture accuracy for climate studies, it is feasible to get a 0.005 accuracy of soil moisture when atmospheric correction is considered and surface temperature is measured with an accuracy ~ 1 K.

- The field data was limited in scope with few night time measurement of soil moisture and only limited measurements of surface temperatures. More measurements of field data are required to test the method fully. However, a more complete field program to test the technique faces the difficulties of the long period between satellite passes and hence few data points simultaneous with satellite overpasses.

- Although AVHRR can measure land surface temperature to within 1K, the large temperature gradients, in desert regions mean that the IR and microwave measurements must be within 30 minutes. NOAA satellite lack a microwave radiometer so ATSR is the only instrument that can do this. Unfortunately the ATSR/M radiometer does not have an 18 GHz or lower frequency channel. However, Earth Observation System (EOS) planned in the late 1990s will provide both infrared and microwave radiometers (see table 1.1). The EOS microwave radiometers have low frequencies channels which are important for soil moisture retrieval (see table 1.2).

Chapter 7

Conclusions

7.1 Introduction

The nature of the climate system has been reviewed (chapter 1). The importance and unique role of remote sensing towards climate studies has been discussed. The surface microwave emissivity has been identified as a valuable parameter for the climate research, as it depends on several important geophysical parameters (notably soil moisture, Rowntree, 1993). The effect of the atmosphere on surface microwave emission as measured by satellite radiometer is addressed. The few previous studies investigating this problem has been reviewed.

A necessary understanding of the physics of microwave emission, including assumptions made and constraints applied, were described (chapter 2). The microwave surface emission models for ocean and soil used in the validation and application of the atmospheric correction technique have been reviewed and examined. The effect of the atmosphere on the satellite measurement of microwave emission has been demonstrated through the radiative transfer process for clear sky conditions.

The characteristics of the satellite microwave and infrared radiometers used in this research have been reviewed. The implication of these characteristics for the technique described in this thesis were addressed in chapter 3.

A novel atmospheric correction technique to correct for atmospheric effect (clear sky conditions) and retrieve microwave surface emissivity using simultaneous

measurements from passive and infrared radiometers has been proposed in chapter 4 (Al Jassar et al. 1995). A simulation study using an atmospheric radiative transfer model, together with generic atmospheres covering all seasons, have been used to investigate the atmospheric contribution to the microwave signal from space for a range of all possible terrestrial emissivities. It was found that the atmospheric effect, in particular, at lower surface emissivities contribute to a major source of errors.

Predictions from an ocean surface emission model were compared with corrected microwave emissivities in order to validate the atmospheric correction technique (chapter 5). The application of the atmospheric correction technique over land to improve the accuracy of soil moisture retrieval has been demonstrated, and soil moisture measurements retrieved from satellite were compared with contemporaneous ground data (chapter 6).

In this chapter, the achievements of this research are summarised, and the contributions towards climate studies are addressed. Finally, recommendations for future work are made.

7.2 Results and Achievements

In this section we summarise the results from this research into different aspects as follows:

(i) The new technique

- *Performance and characteristics*

1. A new technique has been developed to correct the surface microwave emissivity for both atmospheric absorption and direct and reflected emission. The technique makes use of radiometer data in the infrared as well as the microwave region.

2. An atmospheric radiative transfer model, together with generic atmospheres covering all seasons, have been used to investigate the effect of the atmosphere for a range covering all possible terrestrial emissivities. The atmospheric effect - mainly due to water vapour - is found to increase as the true surface emissivity decreases due to the increase of the reflected downwelling atmospheric emission. This effect is more pronounced at higher water vapour atmospheres

and at higher microwave frequencies. At 36.5 GHz (ATSR/M), the effect can be up to 0.14 in emissivity for moist tropical atmospheres.

3. The technique corrects the apparent microwave emissivity as seen by the satellite radiometer for emissivity and water vapour effects by using first and second order corrections respectively. The essence of the first order correction is that the relationship between the apparent microwave emissivity and the true surface emissivity is linear and the difference between them is proportional to the apparent microwave emissivity. The essence of the second order correction is that any residuals following the first order correction are due principally to variations in the absorptivity of the atmosphere - chiefly due to changes in water vapour. Therefore the second order correction makes use of two microwave frequencies, one of which is more sensitive to the water vapour, to compensate for the dependence on water vapour content.

4. The proposed technique has been demonstrated to correct the microwave emissivity for the effect of the atmosphere to an accuracy of 0.001 r.m.s for atmospheres with low to middle in water vapour content and for all emissivities in the 0.4-1.0 range. For atmospheres with higher water vapour contents up to 55 kg/m^2, the accuracy is expected to be between 0.001-0.005 depending on emissivity.

5. The slope and intercept of the first order correction depend on mean atmospheric parameters chiefly due to variations in atmospheric water vapour. The slope and intercept do not depend on surface emissivity. In the second order correction the slope for all atmospheres and surface emissivities have the same value, which is 0.002. Also, the intercept depends on the difference between the true surface emissivities at two frequencies. For bare soil, the effect of the uncertainty in the intercept of the second order correction on the results is very small and it is within ~0.001.

6. The residual scatter after the second order correction is mainly due to the atmospheric temperature effect. The upwelling and downwelling atmospheric emission are dependent on air temperature as well as water vapour and oxygen. To a lesser extent, higher air temperature increases the strength of oxygen absorption at 37 GHz due to broadening of the line centred at 60 GHz, leading to more atmospheric emission (and absorption).

7. Although low frequencies are little affected by the atmosphere, simulations show that this effect can still be significant at low surface emissivities. For example, at 1.4 GHz and for surface emissivity at 0.5, the error in emissivity can be up to 0.01 in emissivity. This is due to the increase of reflected downwelling atmospheric emission. Although such error is still within the 0.02 soil moisture accuracy for climate studies, it is feasible to get a 0.005 accuracy of soil moisture when atmospheric correction is considered and surface temperature is measured with an accuracy ~ 1 K (chapter 6).

8. Over the deserts, the Alice Springs (8 a.m.) coefficients are very close to the Saudi (3 a.m.) coefficients and that the difference will cause an error in emissivity ≤ 0.001 for the worst case. However, the comparison between Saudi night and day data, show that there is a significant difference in the coefficients of first order correction. This difference causes an error ~ 0.01 for the worst case. The difference is due to the air temperature difference between night and day atmospheres. Therefore it is not recommended to use coefficients of corrections of the night radiosonde to correct for day microwave satellite measurements or the later to the former.

9. The accuracy in surface emissivity from the technique is limited by measurements noise. For the North Atlantic dataset, the calculated total error is 0.003 r.m.s. due to ATSR/M radiometric noise and the error in SST measurement, while the anticipated bias due to the absolute calibration is 0.01. For the Alice Springs dataset, the total error ranges from 0.003 for $0.9 \leq \varepsilon < 1.0$ to 0.006 for $0.5 \leq \varepsilon < 0.6$ including the net radiometric noise from TOPEX.

- *Advantages*

1. The proposed technique is very straightforward and provides an independent method for correcting microwave emission using satellite data alone without a *priori* knowledge of atmospheric parameters (e.g. simultaneous radiosondes).

2. The potential accuracies for this technique are very encouraging (see before), however it is likely that even better accuracies may be achieved if a correction for atmospheric temperature is incorporated.

3. The generated coefficients cover all terrestrial surfaces. Thus they can be applied on a global basis using satellite microwave and infrared data provided that the atmospheric conditions are similar to those used in generating the correction coefficients.

- *Disadvantages*

1. The technique is restricted to cloud-free conditions, since it requires the use of infrared data.
2. Although the technique is valid for day and night over the ocean, for soil (especially deserts) it is restricted to night measurements for the following reasons:

a. Air temperature just above the surface over land are usually quite different from the actual surface temperature during the day, especially over desert regions (Choudhury 1993). This will weaken the Planck function linearity assumption of the split window technique, and will therefore produce some errors in retrieving the surface temperature from the infrared radiometer.

b. Infrared radiometers retrieve the surface temperature (see chapters 3) and not the effective temperature. Therefore, the approximation of constant temperature profile is necessary when most of the microwave emission from soil comes from 1 to 50 cm (see chapter 2). The assumption of uniformity of the temperature profiles is a good approximation from 6 p.m. to 6 a.m. for cool months (England, 1990).

c. More critically, the high surface temperatures reached in deserts during the daytime can cause infrared radiometers to saturate, thus no valid data are returned.

(ii) The validation of the new technique

- The validation shows very encouraging results in correcting the microwave emissivity from ATSR/M with an r.m.s of 0.003 and bias of 0.010 for atmospheres with less than 2.5 gm/cm^3 water vapour content. These results represent an order of magnitude improvement in precision over those obtained by the SSM/I (Fleming et al. 1991) which show an r.m.s of 0.03 and bias of -0.017.

- The emissivity bias of 0.01 which is a function of wind speed suggests that the ocean emission model (Wilheit 1979) is in error for vertical incidence measurements and low wind speeds.

(iii) The application of the technique to improve the accuracy of soil moisture retrieval

- It has been demonstrated that the application of the atmospheric correction technique over land can improve the accuracy of soil moisture retrieval. If an atmospheric correction is not applied to the microwave emission, there may be considerable error in the soil moisture retrieval. Although in this study the error without atmospheric correction is ~0.01 in soil moisture which is still within the 0.02 accuracy needed for climate application, however, such error increases as soil moisture increases (and emissivity decreases) and the retrieval of soil moisture within 0.02 accuracy becomes difficult, if not impossible. Therefore the benefits of applying the new atmospheric correction technique to soil moisture retrieval are more noticeable for wet and smooth surfaces when the microwave surface emissivities have low values and the atmospheric contributions are proportionally greater.

- Although the accuracy needed for soil moisture in climate application is 0.02, it is feasible to do better than this. It has been shown that, in the absence of vegetation cover, it is possible to measure the land surface temperature to 1 K uncertainty error at night with AVHRR. Therefore, achieving the 0.005 accuracy of soil moisture or better is possible but will limited to the accuracy of the soil model used.

- The comparison study between the difference from field soil moisture measurements and retrieved soil moisture from TP show a standard deviation of 0.008. Although it is difficult to draw a firm conclusion from four measurements, the results are encouraging as the calculated 0.008 error is close to the predicted error of 0.005 from the stochastic analysis.

7.3 Assessment of Contributions with Respect to Climate Studies

In this section we relate the results stated in section 7.2 to climate studies with regard to the original aims outlined in chapter 1.

- Although the new atmospheric correction technique is limited to cloud-free conditions, it is potentially useful for soil moisture retrieval over arid and semi-arid regions (where cloud-free conditions prevail), provided that a nadir-looking

radiometer is used, thus minimising the effect of vegetation. Arid and semi-arid regions, which are about one-quarter of total land surface, are one of the most sensitive regions to climate change (Rowntree and Bolton, 1983).

- The technique should have a significant impact on the accuracy of the retrieval of important geophysical parameters from microwave remote sensing data. In chapter 4, the proposed technique has been shown to give very encouraging results in terms of the accuracy can be achieved in correcting the surface emissivity. In chapter 6, it has been shown that, in the absence of vegetation cover, it is possible to measure the land surface temperature to better than 1K r.m.s. at night with an infrared satellite radiometer. Therefore it should be possible to achieve an accuracy of 0.005 in soil moisture which is better than the recommended soil moisture accuracy of 0.02 for the validation of climate models.

7.4 Directions for Future Work

Further development of the technique is recommended to improve the accuracy in correcting the apparent microwave emissivity by including the atmospheric temperature effect.

It would be useful to carry out further validation work on the new atmospheric correction with a better ocean surface model in order to assess the true precision attainable with ATSR/M data.

The field data was limited in scope with few night-time measurement of soil moisture and only limited measurements of surface temperatures. More field data measurements are required to test the method fully. However, a more complete field program to test the technique faces the difficulties of the long period between satellite passes and hence few data points simultaneous with satellite overpasses. NOAA satellites lack a suitable microwave radiometer, so ATSR is the most convenient instrument that can do this currently. Unfortunately the ATSR/M radiometer does not have an 18 GHz (or lower) channel. However, Earth Observation System (EOS) planned in the late 1990s will provide both infrared and microwave radiometers (see table 1.1). The microwave radiometers on EOS have low frequencies channels (18.7 GHz, 10.65 GHz, 6.6 GHz, and 1.4 GHz) which are useful for soil moisture retrieval (see table 1.2). Although the 1.4 GHz and the 6 GHz are the best frequencies for soil moisture as they are less sensitive to vegetation

and surface roughness (see chapter 1&2), the exact frequency is not particular important as it is usually determined by considerations other than soil physics, such as the requirements of antenna size.

Hence, the higher frequencies (e.g. 18 GHz, 10 GHz and 6 GHz) are still useful for soil moisture retrieval over arid and semi-arid regions (i.e. regions with low vegetation cover) as they provide finer spatial resolution and require smaller antenna size. The application of the new atmospheric correction technique for such frequencies will improve the accuracy of soil moisture retrieval.

Finally, the potential for using the technique for other important geophysical parameters such as snow, and sea ice should be investigated.

References

Al Jassar, H. K., Harris, A., and Ridley, J. 1995. Retrieval of microwave surface emissivities using multi-sensor satellite sensing. *in proceedings International Geoscience and Remote Sensing Symposium , IGARSS`95* . Florence, Italy, in press.

Barrett, E. C., and Curtis, L. F. 1992. Introduction to Environmental Remote Sensing. Chapman and Hall.

Becker, F. 1987. The impact of spectral emissivity on the measurement of land surface temperature from a satellite. *Int. J. Remote Sensing*, vol. **8**, no. 10, 1509-1522.

Becker, F., & Li, Z. L. 1990. Towards a local split window method over land surface. *Int. J. Remote Sensing*, vol. **11**, no. 3, 369-393.

Bernard, R., Cornec, A. L., Eymard, L., and Tabary, L. 1993. The microwave radiometer aboard ERS-1: Part 1-characteristics and performances. *IEEE Trans. Geosci. Remote Sensing*, vol. **31**, no. 6, 1186-1198.

Blume, H.-J. C., Love, A. W., Van Melle, M. J., and Ho, W. W. 1977. Radiometric observations of sea temperature at 2.65 GHz over the Chesapeake Bay. *IEEE Trans. Antennas Propagat.*, **AP-25**, 121-128.

Chandrasekhar, S. 1960. Radiative Transfer. Dover Publications, inc.

Chang, A. T. C., & Wilheit, T. T. 1979. Remote sensing of atmospheric water vapour, liquid water, and wind speed at the ocean surface by passive microwave techniques from Nimbus-5 satellite. *Radio Sci.*, **14**, 793-802.

Choudhury, B. J., Schmugge, T. J., Chang, A., and Newton, R. W. 1979. Effect of surface roughness on the microwave emission from soils. *J. Geophys. Res.*, vol. **84**, no. C9, 5699-5706.

Choudhury, B. J. 1987. Estimation of primary productivity over the Thar desert based upon Nimbus-7 37 GHz data: 1979-1985. *Int. J. Remote Sensing*, vol. **8**, no. 12, 1885-1890.

Choudhury, B. J., and Golus, R. E. 1988. Estimating soil wetness using satellite data. *Int. J. Remote Sensing*, vol. **9**, no. 7, 1251-1257.

Choudhury, B. J., Wang, J. R., Hsu, A. Y., and Chien, Y. L. 1990. Simulation and observed 37 GHz emission over Africa. *Int. J. Remote Sensing*, vol. **11**, no. 10, 1837-1868.

Choudhury, B. J., Major, E. R., Smith, E. A., and Becker, F. 1992. Atmospheric effects on SMMR and SSM/I 37 GHz polarization difference over Sahel. *Int. J. Remote Sensing*, vol. **13**, no. 18, 3443-3463.

Choudhury, B. J. 1993. Reflectivities of selected land surfaces types at 19 and 37 GHz SSM/I observations. *Remote. Sens. Environ.*, vol. **46**, 1-17.

Colwell, R. N. E. 1983. Manual of Remote Sensing. Chapter 5, Passive microwave radiometry. Virginia: American Society of Photogrammetry, Falls Church.

Comiso, J. C. 1983. Sea Ice Effective microwave emissivities from satellite passive microwave and infrared observations. *J. Geophys. Res.*, vol. **88**, no. C12, 7686-7704.

Coppo, P., Luzi, G., Palocia, S., and Pampaloni, P. 1991. Effect of soil roughness on microwave emission : comparison between Experimental data and models. *in proceedings International Geoscience and Remote Sensing Symposium , IGARSS`91,* Finland, Helsinki University of Technology, 1991, vol. 3, 1167-1170.

Cox, C., and Munk, W. 1955. Some problems in optical oceanography. *J. Marine Res.*, **4**, 63-78.

Cracknell, A. P., and Hayes, L. W. B. 1991. Introduction to Remote Sensing. Taylor and Francis.

Cudlip, W., Phillips, H. A., Ridley, J., and Kearsley, A. W. K. 1995. A comparison of altimeter, GPS and bench-mark heights in the Simpson Desert, Australia. In preparation.

Deschamps, P. Y., and Phulpin, T. 1980. Atmospheric correction of infrared measurements of sea surface temperature using channels at 3.7, 11, 12μm. *Boundary-layer Meteorology*, **18**, 131-143.

Dobson, M. C., Ulaby, F. T., Hallikainen, M. T., and El-Rayes, M. A. 1985. Microwave dielectric behaviour of wet soil- Part II: Dielectric mixing models. *IEEE Trans. on Geosci. Remote Sensing*, vol. **GE-23**, no. 1, 35-46.

England, A. W. 1990. Radiobrightness of diurnally heated, freezing soil. *IEEE Trans. Geosci. Remote Sensing*, vol. **28**, no. 4, 464-476.

England, A. W., Galntowicz, J. F., and Schretter, M. S. 1992. The radiobrightness thermal inertia measure of soil moisture. *IEEE Trans. Geosci. Remote Sensing,* vol. **30**, no. 1, 132-139.

Eymard, L., Tabary, L., and Le Cornec, A. 1994. The microwave radiometer aboard ERS-1. Part II: validation of the geophysical products. submitted to *IEEE Trans. Geosci. Remote Sensing.*

Ferraro, R. R., Grody, N. C., and Kogut, J. A. 1986. Classification of geophysical parameters using passive microwave satellite measurements. *IEEE Trans. Geosci. Remote Sensing*, vol. **GE-24**, no. 6, 1008-1013.

Ferrazzoli, P., Palocia, S., Pampaloni, P., Schiavon, G., Solimini, D., and Coppo, P. 1992. Sensitivity of microwave measurements to vegetation biomass and soil moisture content: a case study. *IEEE Trans. Geosci. Remote Sensing*, vol. **30**, no. 4, 750-756.

Fleming, H. E., Grody, N. C., and Kratz, E. J. 1991. The forward problem and corrections for the SSM/T satellite microwave temperature sounder. *IEEE Trans. Geosci. Remote Sensing*, vol. **29**, no. 4, 571-583.

Franca, G. B., and Cracknell, A. P. 1994. Retrieval of land and sea surface temperature using NOAA-11 AVHRR data in north-eastern Brazil. *Int. J. Remote Sensing*, vol. **15**, no. 8, 1695-1712.

Grody, N. C. 1988. Surface Identification using satellite microwave radiometers. *IEEE Trans. Geosci. Electron.*, vol. **26**, no. 6, 850-859.

Gruber, A., and Arkin, P. A. 1992. Satellite data in climate diagnostic. In Reviews of Modern Climate Diagnostic Techniques, World Meteorological Organization (WMO), Commission for Atmospheric Sciences.

Guzkowska, M. A. J., Rapley, C. G., Ridley, J. K., Cudlip, W., Birkett, C. M., and Scott, R. F. 1990. Developments in Inland Water and Land Altimetry No. ESA report no. CR-7839/88/F/FL.

Hallikainen, M. T., Ulaby, F. T., Dobson, M. C., El-Rayes, M. A., and Wu, L.-K. 1985. Microwave dielectric behaviour of wet soil Part I: Empirical models and experimental observations. *IEEE Trans. Geosci. Electron.* vol. **GE-23**, no. 1, 25-34.

Harris, A. R., and Mason, I. M. 1992. An extension to the split-window technique giving improved atmospheric correction and total water vapour. *Int. J. Remote Sensing*, vol. **13**, no. 5, 881-892.

Harris, A. R., Saunders, M. A., Foot, J. S., and Smith, K. F. 1995. Improved sea surface temperature measurements from space. *Geophys. Res. Lett.*, in press.

Ho, D., Asem, A., and Deschamps, P. Y. 1986. Atmospheric correction for the sea surface temperature using NOAA-7 AVHRR and METEOSAT-2 infrared data. *Int. J. Remote Sensing*, vol. **7**, no. 10, 1323-1333.

Ho, D., and Asem, A. 1986. NOAA AVHRR image referencing. *Int. J. Remote Sensing*, vol. **7**, no. 7, 895-904.

Houghton, J. T., and Morel, P. 1984. The world climate research programme. (ed. J. T. Houghton), The Global Climate, Cambridge University Press.

Intergovernmental Panel on Climate Change (IPCC), 1990, (ed. Houghton, J. T., Jenkins, G. J., and Ephraums, J. J.), Climate Change, The IPCC Scientific Assessment. Cambridge University Press.

Intergovernmental Panel on Climate Change (IPCC), 1992, (ed. Houghton, J. T., Callander, B. A., and Varney, S. K. V.), Climate Change, The IPCC Scientific Assessment. Cambridge University Press.

Jackson, T. J., and Schmugge, T. J. 1989. Passive microwave remote sensing system for soil moisture: Some supporting research. *IEEE Trans. Geosci. Remote Sensing*, vol. **27**, no. 2, 225-235.

Jackson, T. J., Kostov, K. G., and Saatchi, S. S. 1992. Rock fraction effects on the interpretation of microwave emission from soils. *IEEE Trans. Geosci. Remote Sensing*, vol. **30**, no. 3, 610-616.

Jackson, T. J., Le-vine, D. M., Griffis, A. J., Goodrich, D. C., Schmugge, T. J., Swift, C. T., and O'Neill, P. E. 1993. Soil moisture and rainfall estimation over semiarid environment with the ESTAR microwave radiometer. *IEEE Trans. Geosci. Remote Sensing*, vol. **31**, no. 4, 836-841.

Janseen, M. A., Ruf, C. S., and Keihm, S. J. 1995. TOPEX/Poseidon Microwave Radiometer (TMR): II. antenna pattern correction and brightness temperature algorithm. *IEEE Trans. Geosci. Remote Sensing*, vol. **33**, no. 1, 138-146.

Kerr, Y. H., and Njoku, E. G. 1990. A semi-empirical model for interpreting microwave emission from semiarid land surfaces as seen from space. *IEEE Trans. Geosci. Remote Sensing*, vol. **28**, no. 3, 384-393.

Labed, J., and Stoll, M. P. 1991. Angular variation of land surface spectral emissivity in the thermal infrared: laboratory investigations on bare soils. *Int. J. Remote Sensing*, vol. **12**, no. 11, 2299-2310.

Lauritson, L., Nelson, G. J., and Porto, F. W. 1979. Data Extraction and calibration of TIROS-N/NOAA radiometers. no. TM NESS 107. NOAA tech. memo.

Mo, T., and Schmugge, T. J. 1987. A parameterization of effect of surface roughness on microwave emission. *IEEE Trans. Geosci. Remote Sensing*, no. **GE-25**, no. 4, 481-486.

Mo, T., Schmugge, T. J., and Wang, J. R. 1987. Calculation of microwave brightness temperature of rough surfaces: bare field. *IEEE Trans. Geosci. Remote Sensing*, vol. **GE-25**, no. 1, 47-54.

Mansor, S. B., and Cracknell, A. P. 1992. Land surface temperature from NOAA-9 AVHRR data. In: Proceeding of the 18th Annual Conference of the Remote Sensing Society, Remote Sensing from Research to Operation (ed. Cracknell, A. P., Vaughan, R. A.), 274-286. University of Dundee.

Mason, I. M., Sheather, P. H., and Bowles, J. A. 1990. On-board calibration of infra-red radiometers. In: Earth Observation Satellites-The Technology Behind the Image (conference). Royal Aeronautical Society.

Mason, G. 1991. Test and Calibration of the Along Tack Scanning Radiometer, A Satellite Infrared Radiometer Designed to Measure Sea Surface Temperature. Ph.D., University of Oxford.

McIlveen, R. 1992. Fundamentals of Weather and Climate. Chapman and Hall.

McMillin, L. M. 1975. Estimation of sea surface temperature from two infrared window measurements with different absorption. *J. Geophys. Res.*, vol. **80**, no. 36, 5113-5117.

Minnett, P., J. 1986. A numerical study of the effects of anomalous north Atlantic atmospheric conditions on the infrared measurement of sea surface temperature from space. *J. Geophys Res*, vol. **91**, no. C7, 8509-8521.

National Aeronautics and Space Administration (NASA), 1987. High-Resolution Multifrequency Microwave Radiometer (HMMR) , Earth Observing System, V IIe.

Nerry, F., Labed, F., and Stoll, M. 1988. Emissivity signatures in the thermal IR band for remote sensing: calibration procedure and method of measurement. *Applied Optics*, vol. **27**, no. 4, 758-764.

Newton, R. W., and Rouse, J. W. 1980. Microwave radiometer measurements of moisture content. *IEEE Trans. Antennas Propagat,* **AP-28**, 680-686.

Newton, R. W., Black, Q. R., Makanvand, S., Blanchard, A. J., and Jean, B. R. 1982. Soil moisture information and thermal microwave emission. *IEEE Trans. Geosci. Remote Sensing*, vol. **GE-20**, no. 3, 275-281.

Ottle, C., and Stoll, M. 1993. Effect of atmospheric absorption and surface emissivity on the determination of land surface temperature from infrared satellite data. *Int. J. Remote Sensing*, vol. **14**, no. 10, 2025-2037.

Owe, M., Griend, V., and Chang, A. T. C. 1992. Surface soil moisture and satellite passive microwave observations in semi- arid southern Africa. *Water Resources Research.* vol. **28**, no. 3, 829-839.

Owe, M., Chang, A., and Golus, R. E. 1988. Estimating surface soil moisture from satellite microwave measurements and a satellite derived vegetation index. *Remote Sens. Environ.*, **24**, 331-345.

Paloscia, S., Pampaloni, P., Chiarantini, L., Coppo, P., Gagliani, S., and Luzi, G. 1993. Multifrequency passive microwave remote sensing of soil moisture and roughness. *Int. J. Remote Sensing*, vol. **14**, no. 3, 467-483.

Pederson, L. T. 1990. Microwave radiometers. (ed. R. A. Vaughan) , Microwave Remote Sensing for Oceanographic and Marine Weather-Forecast Models. Kluwer Academic Publishers.

Rao, K. S., Rao, P. V. N., Rao, Y. S., Chandra, G., Raju, C. S., and Bapat, M. V. 1989. A study on the effect of soil texture on the passive microwave remote sensing. (ed. P. Pampaloni) , Microwave radiomet. Remote Sens. Appl, 125-131.

Rao, K. S., Raju, S., and Wang, J. R. 1993. Estimation of soil moisture and surface roughness parameters from backscattering coefficient. *IEEE Trans. Geosci. Remote Sensing*, vol. **31**, no. 5, 1094-1099.

Rapley, C. G., M. A. J. Guzkowska., W. Cudlip., and I. M. Mason., 1987. An Exploratory Study of Inland Water and Land Altimetry using Seasat Data, ESA CR-6483/85/NL/BI.

Ridley, J., & Strawbridge, F. 1995. Measurement of arid land surface properties. *in proceedings International Geoscience and Remote Sensing Symposium , IGARSS`95* . Florence, Italy, in press.

Rosenkranz, P. W. 1988. Interference coefficients for overlapping oxygen lines in air. *J. Quan. Spectrosc. Radiat. Transfer*, vol. **39**, no. 4, 287-297.

Rowntree, P. W., & Bolton, J. A. 1983. Simulation of the atmospheric response to soil moisture anomalies over Europe. *Quart. J. R. Met. Soc.*, **109**, 501-526.

Rowntree, P. R. 1993. Large-scale land-atmospheric models and data needs. In: Proceeding of St. Lary workshop on Passive Microwave Remote Sensing and Land-Atmosphere models, France.

Salisbury, J. W., and D'Aria, D. M. 1992(a). Infrared (8-14μm) remote sensing of soil particle size. *Remote Sens. Environ*, **42**, 157-165.

Salisbury, J. W., and D'Aria, D. M. 1992(b). Emissivity of terrestrial materials in the 8-14 μm atmospheric window. *Remote Sens. Environ*, **42**, 83-106.

Schanda, E. 1986. Physical fundamentals of remote sensing. Springer-Verlag.

Schmugge, T. J. 1980. Effect of texture on microwave emission from soils. *IEEE Trans. Geosci.Remote Sensing*, vol. **GE-18**, no. 4, 353-361.

Schmugge, T., O'Neill, P. E., and Wang, J. R. 1986. Passive microwave soil moisture research. *IEEE Trans. Geosci. Remote Sensing*, vol. **GE-24**, no. 1, 12-22.

Schutko, A. M., and Reutov, E. M. 1982. Mixture formula applied in estimation of dielectric and radiative characteristics of soils and grounds at microwave frequencies. *IEEE Trans. Geosci. Remote Sensing*, vol. **GE-20**, no. 1, 29-32.

Sobrino, J. A., Li, Z. L., Stoll, M. P., and Becker, F. 1994. Improvements in the split-window technique for land surface temperature determination. *IEEE Trans. Geosci. Remote Sensing*, vol. **32**, no. 2, 243-253.

Strawbridge, F. 1992. Passive Microwave Remote Sensing of Vegetation. Ph.D., University of Bristol.

Strawbridge, F., Ridley, J., Card, R., Phillips, H., Tregoning, P., and Low, B. 1994. Report on the Simpson 93 field campaign. Mullard Space Science Laboratory.

Tsang, L., and Newton, R. W. 1982. Microwave Emission from Soils with Rough Surfaces. Journal of Geophys. Res., vol. **87**, no. 11, 9017-9024.

Ulaby, F., Moore, R., and Fung, A. 1981. Microwave remote sensing: active and passive. Artech House, MD.

Ulaby, F., Moore, R., and Fung, A. 1982. Microwave remote sensing: active and passive. Artech House, MD.

Ulaby, F. T., Razani, M., and Dobson, M. C. 1983. Effects of vegetation cover on the microwave radiometric sensitivity to soil moisture. *IEEE Trans. Geosci. Remote Sensing*, vol. **GE-21**, no. 1, 51-61.

Ulaby, F., Moore, R., and Fung, A. 1986. Microwave remote sensing: active and passive. Artech House, MD.

Vass, P., and Handoll, M. 1991. UK ERS-1 Reference Manual: UK EODC ERS-1 Documentation. DC-MA-EOS-ED-0001.

Vinnikov, K. Y., and Yeserkepova, I. B. 1991. Soil moisture: Empirical data and model results. *J. of Climate*, **4**, 66-79.

Wang, J. R., and Schmugge, T. J. 1980. An empirical model for the complex dielectric permittivity of soils as a function of water content. *IEEE Trans. on Geoscience and Remote Sensing,* **GE-18**, no. 4, 288-295.

Wang, J. R., and Choudhury, B. J. 1981. Remote sensing of soil moisture content over bare field at 1.4 GHz frequency. *J. Geophys. Res.*, vol. **86**, no. C6, 5277-5282.

Wang, J. R., McMurtrey, J. E., Engman, E. T., Jackson, T. J., Schmugge, T. J., Gould, W. J., Fuchs, J. E., and Glazar, W. S. 1982. Radiometric measurements over bare and vegetated fields at 1.4 GHz and 5 GHz frequencies. *Remote Sensing Environ.*, **12**, 295-311.

Wang, J. R. 1983. Passive microwave sensing of soil moisture content: The effect of soil bulk density and surface roughness. *Remote Sens. Environ.*, **13**, 329-344.

Wang, J. R., O'Neill, P. E., Jackson, T. J., and Engman, E. T. 1983. Multifrequency measurements of the effects of soil moisture, soil texture and surface roughness. *IEEE Trans. Geosci. Remote Sensing*, vol. **GE-21**, no. 1, 44-51.

Wang, J. R., Chang, A. T. C., and Sharma, A. K. 1992. On the estimation of snow depth from microwave radiometric measurements. *IEEE Trans. Geosci. Remote Sensing*, vol. **30**, no. 4, 785-792.

Webster, W. J., & Wilheit, T. T. 1976. Spectral characteristics of the microwave emission from a wind-driven foam covered sea. *J. Geophys. Res.*, vol. **81**, no. 18, 3095-099.

Wegmuller, U., Matzler, C., and Schanda, E. 1989. Microwave signatures of bare soil. *Advance Space Research*, vol. **9**, no. 1, 307-316.

Weinreb, M. P., Hamilton, G., and Brown, S. 1990. Nonlinearity Corrections in Calibration of Advanced Very High Resolution Radiometer Infrared Channels. *J. Geophys. Res.*, vol. **95**, no. C5, 7381-7388.

Wielogorski, A. L. 1988. The selection of desert test sites for ERS-1 and SIR-C radar altimeters. Unpublished M.Sc., University of London.

Wilheit, T. T. 1979. A model for the microwave emissivity of the Ocean's surface as a function of wind speed. *IEEE Trans. on Geosci. Electron.*, vol. **GE-17**, no. 4, 244-249.

Wilheit, T. T., and Chang, T. C. 1980. An algorithm of ocean surface and atmospheric parameters from the observations of the scanning multichannel microwave radiometer. *Radio Sci.*, vol. **15**, no. 3, 525-544.

Wilheit, T. T., Greaves, J. R., Gatlin, J. A., Han, D., Krupp, B. M., Milman, A. S., and Chang, E. S. 1984. Retrieval of ocean surface parameters from the scanning multifrequency microwave radiometer (SMMR) on the Nimbus-7 satellite. *IEEE Trans. on Geosci. Remote Sensing*, vol. **GE-22**, no. 2, 133-142.

Wilke, G. D., and McFarland, M. J. 1986. Correlations between Nimbus-7 Scanning Multichannel Microwave Radiometer data and an Antecedent Precipitation Index. *J. Climate Appl. Met.*, **25**, 227-238.